Sympathetic Influences on Articular Cartilage Regeneration Capacity and Osteoarthritis Manifestation

Dissertation

zur Erlangung des Doktorgrades

der Naturwissenschaften

vorgelegt beim Fachbereich Biowissenschaften (FB15)

der Johann Wolfgang Goethe-Universität

in Frankfurt am Main

von

Karima El Bagdadi

Geboren in Frankfurt am Main (Hessen)

Frankfurt am Main (2021)

(D 30)

Vom Fachbereich Biowissenschaften (FB15) der Goethe-Universität als Dissertation angenommen.

Dekan: Prof. Dr. Sven Klimpel

Gutachter: Prof. Dr. Enrico Schleiff, Prof. Dr. Andrea Meurer

Datum der Disputation:

Index of contents

Index of figures

Index of tables

Abbreviations

6-OHDA	6-hydroxydopamine
ACE	Angiotensin converting enzyme
Adrb2$^{-/-}$	β2-AR deficient
AEC	3-Amino-9-ethylcarbazole
AP	Alkaline phosphatase
AR	Adrenergic receptor
AT1	Angiotensin II type 1 receptor
BMD	Bone mineral density
BMP	Bone morphogenetic protein
BMSC	Bone marrow-derived MSC
BS	Bone surface
BSA	Bovine serum albumin
BV/TV	Bone volume/ total tissue volume
cAMP	Cyclic adenosine monophosphate
CCB	Calcium channel blockers
CC	Calcified cartilage
CD	Cluster of differentiation
cDNA	Complementary desoxy ribonucleic acid
COL10A1	Collagen type X alpha 1 chain
COL2A1	Collagen type II alpha 1 chain
CTX-II	C-telopeptide of type II collagen
D	Doxazosin
DA	Dopamine
dH$_2$O	Distilled water
DMEM	Dulbecco's modified eagle's medium
DMM	Destabilization of the medial meniscus
DMMB	1,9-Dimethyl-methylene blue
DPBS	Dulbeccos phosphate-buffered saline
dsDNA	Double stranded DNA
E	Epinephrine
ECL	Enhanced chemiluminescence
ECM	Extracellular matrix
EDTA	Ethylenediaminetetraacetic acid
ELISA	Enzyme-linked immunosorbent assay
ERK 1/2	Extracellular signal-regulated kinases 1/2
FACS	Fluorescence-activated cell sorting
FBS	Fetal bovine serum
FITC	Fluorescein
G-Protein	Guanine nucleotide-binding protein
GAG	Glycosaminoglycan
GAPDH	Glyceraldehyde-3-phosphate dehydrogenase
GSH	glutathione
HLA-DR	Human Leukocyte Antigen—DR
HPLC	High performance liquid chromatography
HRP	Horseradish peroxidase

IgG	Immunoglobulin G
ITS	Insulin, transferrin, and selenous acid
LDH	Lactate dehydrogenase
LM	Lateral meniscus
LMTL	Lateral meniscotibial ligament
MMTL	Medial meniscotibial ligament
MM	Medial meniscus
MAPK	Mitogen-activated protein kinase
MMP13	Matrix metallopeptidase 13
mRNA	Messenger ribonucleic acid
MSC	Mesenchymal stem cell
NAD	Nicotinamidadenindinukleotid
NE	Norepinephrine
NSAIDs	Nonsteroidal anti-inflammatory drugs
OA	Osteoarthritis
OARSI	Osteoarthritis Research Society International
P	Propranolol
P/S	Penicillin streptomycin
PBS	Phosphate-Buffered Saline
PCR	Polymerase chain reaction
PE	Phycoerythrin
PFA	Paraformaldehyde
PKA	Proteinkinase A
PVDF	Polyvinylidene difluoride
RT-PCR	Reverse-transcriptase PCR
RUNX2	Runt-related transcription factor 2
sASC	Synovial adipose tissue-derived MSC
SDS-Page	Sodium dodecyl sulfate polyacrylamide gel electrophoresis
Syx	Sympathectomized
sGAG	Sulphated Glycosaminoglycans
SOX9	SRY-box transcription factor 9
SCBP	Subchondral bone plate
TbN	Trabecular number
TBST	Tris buffered saline with Tween20
TbSp	Trabecular space
TbTh	Trabecular thickness
TEMED	Tetramethylethylendiamin
TGF-β	Transforming growth factor β
TH	Tyrosine hydroxylase
TRAP	Tartrate-resistant acid phosphatase
Tris	Tris(hydroxymethyl)aminomethan
VOI	Volume of interest
WT	Wildtype
Y	Yohimbine

Zusammenfassung

Osteoarthrose (OA) ist eine chronische degenerative Erkrankung des gesamten Gelenks, die mehr als 80% der Weltbevölkerung mit einem Alter von über 55 Jahren und vorwiegend das Kniegelenk betrifft (Palo et al. 2015). Die Erkrankung ist gekennzeichnet durch einen fortschreitenden Knorpelverschleiß, einer Entzündung der Synovialmembran und einer subchondralen Sklerose, einer Verdichtung des subchondralen Knochens (Loeser et al. 2012).

OA ist nicht heilbar, da Knorpel und Knochenschäden nicht rückgängig gemacht werden können. Bei Erwachsenen ist die Regenerationsfähigkeit des Knorpels sehr gering. Reichen die Defekte bereits bis zu der unter dem Knorpel liegenden Knochenschicht, reiben die Gelenkknochen aneinander, was zunehmend zu Schmerzen und zu Bewegungsstörungen führen kann (Loeser et al. 2012). Neben der Knorpeldegeneration, entsteht bei der OA eine Entzündung der Synovialmembran (Synovitis), die sehr schmerzhaft ist und welche die Bewegung des betroffenen Gelenks limitiert. Im Rahmen der OA kann es sowohl zu einer Verdickung und Verdichtung des unter dem Knorpel liegenden subchondralen Knochens kommen, sowie zu Auswüchsen des Knochens an den Gelenkrändern (Osteophyten) (Loeser et al. 2012). Eine ärztliche Behandlung wird von an OA erkrankten Menschen in den meisten Fällen erst beim Auftreten von starken Gelenkschmerzen und zu spät aufgesucht, sodass eine gelenkerhaltende Behandlung nicht mehr möglich ist. Die Behandlungsmöglichkeiten zielen darauf ab die Schmerzen zu lindern. Funktioniert die Symptomlinderung durch eine Schmerz- oder Physiotherapie nicht, bleibt bei einer fortgeschrittenen OA in der Regel nur der chirurgische Eingriff als letzte Option, bei der das geschädigte Kniegelenk durch ein künstliches ersetzt wird (Evans, Kraus, and Setton 2014). Die Erforschung neuer präventiver Maßnahmen zur Vorbeugung einer Erkrankung an OA und Möglichkeiten einer rechtzeitigen Behandlung sind ebenso relevant, wie die Erforschung weiterer Therapiemöglichkeiten bei fortgeschrittener OA. Chondrozyten haben nur eine begrenzte Regenerationskapazität, um Knorpelschäden zu regenerieren. Bei der Knorpelregeneration könnten weitere Zellen, nämlich mesenchymale Stammzellen (MSCs), welche im Knorpel oder in den Knorpel umliegenden Geweben vorliegen, eine Rolle spielen. Studien deuten darauf hin, dass vor allem MSCs aus dem adiposen Synovialgewebe (sASC) an der Knorpelregeneration beteiligt sein könnten (McGonagle, Baboolal, and Jones 2017) und wurden daher in der vorliegenden Arbeit für die experimentellen *in vitro*-Versuche genutzt. Interessanterweise ist bei der OA eine Zunahme von MSCs in den Gelenkgeweben wie im Knorpel (Fellows et al. 2017) zu beobachten, was auf einen Reparaturversuch von MSCs hindeutet (McGonagle, Baboolal und Jones 2017). Dennoch weisen diese Zellen nur ein unzureichendes chondrogenes Differenzierungspotential auf und können nur bedingt Knorpelschäden regenerieren. Die Faktoren, welche für die begrenzte Regenerationsfähigkeit verantwortlich sind, sind bisher nicht bekannt.

Das sympathische Nervensystem und Osteoarthrose

Das sympathische Nervensystem (SNS) zeigt eine Vielzahl von Funktionen in verschiedenen Geweben. In einem gesunden Organismus vermittelt das SNS seine Wirkung über Katecholamine wie Noradrenalin, Dopamin und Adrenalin. Das Schlüsselenzym für die Synthese der Katecholamine ist Tyrosinhydroxylase (TH), ein Enzym, das auch als Marker für sympathische Nerven eingesetzt wird.

Sympathische Nervenfasern, welche Katecholamine wie Noradrenalin freisetzen, innervieren verschiedene Gewebe des Kniegelenks wie die Synovialmembran und den subchondralen Knochen, was darauf hindeutet, dass diese auch bei der OA-Pathogenese beteiligt sein könnten (Hukkanen et al. 1992). Interessanterweise wurde in der Synovialflüssigkeit von OA- und Knie-Trauma-Patienten eine erhöhte Noradrenalin-Konzentration gemessen, während andere Katecholamine nicht nachgewiesen wurden. Diese weiterführenden Erkenntnisse führten in den letzten Jahrzehnten dazu, dass der Einfluss des SNS auf Erkrankungen des Bewegungsapparates und vor allem auf die OA zunehmend an Bedeutung gewann. Bisher ist allerdings unklar, wie Noradrenalin und das SNS die Manifestierung und Pathogenese der OA beeinflussen.

Ziel dieser Arbeit war es daher, den Einfluss des sympathischen Nervensystems sowohl auf das Regenerationspotential der sASC von OA-Patienten, als auch auf die Entwicklung der OA in einem Mausmodell zu untersuchen. Um den Forschungsverlauf nachvollziehbar zu machen, wurden *in vitro* und *in vivo* Experimente einzeln dargelegt. Zunächst befasst sich der erste *in vitro* Abschnitt mit der Wirkung von Noradrenalin auf die chondrogene Differenzierung (Chondrogenese) von sASC in einer dreidimensionalen Pellet-Kultur. Im zweiten *in vivo* Abschnitt wurde der OA Verlauf in chemisch sympathektomierten (Syx) und Wildtyp (WT) Mäusen untersucht. Um die Rolle spezifischer adrenerger Rezeptoren (AR) bei der OA-Pathogenese zu untersuchen, wurde außerdem OA in β2-AR-defizienten Mäusen induziert und analysiert.

Die Wirkung von Noradrenalin auf das chondrogene Differenzierungspotential von sASC

Vor dem Hintergrund der Erkenntnis, dass sympathische Nervenfasern verschiedene Gewebe im Kniegelenk innervieren und Noradrenalin in der in der Synovialflüssigkeit von OA-Patienten nachgewiesen wurde, war das konkrete Ziel dieser Arbeit die Noradrenalin-Effekte auf die Chondrogenese von sASC und damit auf eine mögliche sASC-abhängige Knorpelregeneration zu untersuchen. Hierzu wurden sASC aus dem Synovialgewebe von OA-Patienten isoliert. Die Expression verschiedener Subtypen von ARs in sASC wurde mittels PCR analysiert. sASC exprimierten α1A-, α1B-, α2A-, α2B-, α2C- und β2-AR in Monolayer Zellkultur und nach der chondrogenen Differenzierung. Immunhistologisch wurde der α2A-AR und der β2-AR nachgewiesen. Noradrenalin wirkt in niedrigen Konzentrationen ($\leq 10^{-7}$) hauptsächlich über den α-AR Signalweg, während es in hohen Konzentrationen ($\geq 10^{-7}$ M) den β-AR-basierten Signalweg aktiviert. Eine Aktivierung des α2-AR Signalweg führt meist zu einer Deaktivierung der Proteinkinase A (PKA) einer cAMP-abhängigen Proteinkinase, während der β2-AR Signalweg dieses Protein aktiviert. Alternativ führt eine Stimulierung des α2-AR und β2-AR zur Aktivierung einer Kinase, der extracellular signal-regulated kinase (ERK) 1/2 (Goldring and Marcu 2009; Prasadam et al. 2010). Bei der Untersuchung dieser beiden Signalwege konnte gezeigt werden, dass die Behandlung von ASC mit Noradrenalin in hohen Konzentrationen zu einer signifikant erhöhten Phosphorylierung von ERK1/2 führte.

Die Proliferation und die chondrogene Differenzierung in Gegenwart von Noradrenalin (10^{-9}-10^{-6} M) wurden analysiert. Die Untersuchung ergab, dass Noradrenalin weder einen Einfluss auf die Proliferation und auf die Zellvitalität von sASC in Monolayer Zellkultur, noch auf die Chondrogenese in Pelletkultur hatte. Jedoch reduzierte Noradrenalin das Pelletvolumen konzentrationsabhängig am Tag 21 der Chondrogenese. Zeitgleich wurden die Matrixproteine der Pellets mittels biochemischer Methoden und immunhistologisch untersucht. Die Analyse ergab, dass Noradrenalin konzentrationsabhängig die Synthese von sGAG und Kollagen II reduzierte. Vor allem die Behandlung mit Noradrenalin in hohen Konzentrationen wie 10^{-6} M, reduzierte signifikant das Pelletvolumen und die Matrixproteinkonzentration.

Diese Noradrenalin Effekte wurden durch die gleichzeitige Behandlung mit dem α2-AR Antagonisten Yohimbin vollständig und durch den β2-AR Antagonisten Propranolol teilweise rückgängig gemacht. Gleichzeitig konnte durch eine Behandlung der Pellets mit Yohimbin die durch Noradrenalin induzierte ERK1/2 Phosphorylierung aufgehoben werden. Die Behandlung mit Noradrenalin hatte keinen Einfluss auf die Genexpression hypertropher Marker wie *MMP-13*, *RUNX-2* oder *COL10*, die eine Knorpelkalzifizierung begünstigen und bei der Chondrogonese und Knorpelsynthese unerwünscht sind.

Die vorliegende Studie bestätigt, dass Noradrenalin die Differenzierungsfähigkeit von sASC über den α2-AR unterdrückte. Diese Noradrenalin Effekte können daher gleichzeitig bei einer sASC abhängigen Knorpelregeneration relevant sein und somit bei der Pathogenese der OA beteiligt sein. Eine Inhibierung des α2-AR Signalweges kann daher ein vielversprechender Ansatz für die Entwicklung neuer Therapiemöglichkeiten der OA darstellen.

Die Wirkung des SNS während der Arthroseentwicklung im Mausmodell

Der Einfluss des sympathischen Nervensystems auf die Entwicklung von OA im Knie wurde in einem Tiermodell bislang nicht untersucht. Anhand der gewonnenen Daten der vorliegenden Forschungsarbeit, soll diese Forschungslücke ausgefüllt werden. Hierzu wurde im zweiten experimentellen Abschnitt dieser Arbeit analysiert, ob eine unterdrückte Katecholamin-Freisetzung in peripheren Geweben die Manifestierung und Pathogenese der OA *in vivo* verlangsamt. Hierzu wurde eine chemische Sympathektomie unter Verwendung von 6-Hydroxydopamin in C57BL/6-Mäusen durchgeführt, bei der selektiv nur die peripheren Nerven des sympathischen Nervensystems zerstört wurden. Damit wurde die Signalübertragung über Katecholamine zu ca. 80% blockiert. Die Auswirkungen der Sympathektomie auf die OA-Pathogenese wurde in einem experimentellen OA-Modell durch die chirurgische Destabilisierung des medialen Meniskus (DMM) durchgeführt. Der Einfluss der Sympathektomie auf die OA-Pathogenese wurde im Gelenkknorpel, in der Synovialmembran und im subchondralen Knochen 2, 4, 8 und 12 Wochen nach der OA-Induktion analysiert.

Zunächst wurde die Effizienz der Sympathektomie durch die Analyse der Expression von TH-positiven Nervenfasern in der Synovialmembran und durch die Messung von Noradrenalin in der Milz bewertet. Immunhistologisch konnte gezeigt werden, dass die Sympathektomie zu einer signifikanten Reduktion der TH-positiven Nervenfasern im Gewebe der Synovialmembran führte. Außerdem wurde durch die Sympathektomie der Noradrenalingehalt in der Milz ab der 4. Woche um circa 70% signifikant reduziert, verglichen zu WT Mäusen. Interessanterweise führte die OA-Induktion mittels DMM zu einer erhöhten Noradrenalin-Konzentration in der Milz von WT Mäusen, was darauf hindeutet, dass die verstärkte OA und mechanische Belastung in WT Mäusen zu einer Steigerung der SNS Aktivität führt.

Um den OA-Grad in den Kniegelenken histologisch zu bestimmen, wurde die Arthrose-Klassifikation (Pritzker et al. 2006) der OARSI (Osteoarthritis Research Society International) verwendet. Die OA-Induktion löste eine OA in DMM-operierten WT und Syx Mäusen aus. Nach 8 und 12 Wochen konnte, im Vergleich zu Sham-operierten Mäusen, ein signifikant erhöhter

OA-Grad in DMM-operierten Mäusen beobachtet werden. Unter anderem ergab die Untersuchung, dass verglichen zu den WT DMM Mäusen, die Sympathektomie in Syx DMM Mäusen zu signifikant niedrigeren OARSI-Werten führte, also die Knorpeldegeneration verlangsamte.

Neben dem OARSI-Score wurde die Knorpeldegeneration durch die Analyse des Kollagen II -Abbaus im Knorpel untersucht. Kollagen II ist das vorwiegende Hauptkollagen in der Knorpelmatrix und dessen Abbau kann durch die Messung der Abbaufragmente wie z.B. CTX-II im Serum nachgewiesen werden (Lohmander et al. 2003). Die Analyse mittels ELISA ergab, dass das im Serum freigesetzte Kollagen II-Fragment CTX-II in Syx Mäusen zu keinem Zeitpunkt verändert war, während ein starker Anstieg nach 4 Wochen in WT DMM Mäusen gemessen worden ist. Dies bestärkt die Annahme, dass eine Sympathektomie knorpelprotektiv ist bzw. eine erhöhte SNS Aktivität die OA Knorpeldegeneration beschleunigt.

Eine Entzündung der Synovialmembran wurde durch ein etabliertes Synovitis-Score-System analysiert (Mathiessen and Conaghan 2017). Der Synovitis-Score in WT DMM Mäusen stieg im Verlauf der OA, von der 2. Woche bis zur 12. Woche an. Solch ein Anstieg wurde in Syx Mäusen nicht festgestellt. Demnach lag eine erhöhte Entzündung der Synovialmembran in WT DMM Mäusen verglichen zu Syx DMM Mäusen vor. Darüber hinaus wurde untersucht, ob der OARSI-Score mit dem Synovitis-Score korreliert. Die Analyse ergab, dass in WT DMM Mäusen eine Korrelation existierte, während in Syx Mäusen nur eine sehr schwache Korrelation bestimmt werden konnte. Die Sympathektomie konnte somit im Verlauf der OA nicht nur den Knorpelverschleiß, sondern auch die Synovitis abschwächen.

Chondrozyten können im Knorpel die Kollagenase MMP-13 exprimieren, welche beim Knorpelabbau beteiligt ist. Zahlreiche Studien haben bereits gezeigt, dass MMP-13 in einer entzündeten Synovialmembran exprimiert wird und dessen Freisetzung in die Synovialflüssigkeit zur Knorpeldegeneration beitragen kann (Charni-Ben Tabassi et al. 2008; Itoh et al. 2006). MMP-13 wurde daher immunhistologisch in der Synovialmembran gefärbt und die Analyse ergab, dass in Syx DMM Mäusen die MMP-13 Färbung deutlich schwächer war als in WT DMM Mäusen. Dieses Zwischenergebnis gibt Grund zur Annahme, dass die in der Synovialmembran exprimierten MMP-13 bei der Knorpeldegeneration beteiligt sind und diese beschleunigen. Zudem wurde immunhistologisch gezeigt, dass vereinzelte Zellen im Knorpel, Synovium und subchondralen Knochen den α2A-AR und β2-AR exprimierten.

In Forschungsarbeiten konnte gezeigt werden, dass Zellen in der Synovialmembran bei einer Entzündung des Synovialgewebes vermehrt TH exprimieren, um Noradrenalin zu produzieren, welches in erhöhter Konzentration über den β2-AR antiinflammatorisch wirkt (Capellino et al. 2010). Interessanterweise stieg nach DMM die TH Expression im Synovialgewebe der WT

Mäuse stark an, was die Annahme verstärkt, dass die Zellen selbst Noradrenalin produzieren, um der erhöhten Inflammation entgegenzuwirken.

Neben dem Knorpel und der Synovialmembran, wurde auch der subchondrale Knochen 8 Wochen nach der Operation analysiert. Typische OA bedingte Knochenveränderungen wie eine Kalzifizierung des Knorpelgewebes, eine Verdichtung des subchondralen Knochens, eine Verdickung der subchondralen Knochenplatte oder die Entstehung von Osteophyten, wurden mittels Micro-CT 8 Wochen nach der Operation analysiert. Die Analyse ergab, dass im Vergleich zu WT DMM Mäusen, bei Syx DMM Mäusen eine signifikant erhöhte kalzifizierte Knorpeldicke vorlag. Die Sympathektomie in Syx Mäusen führte im Vergleich zu WT DMM Mäusen, zu einer signifikanten Erhöhung des subchondralen Knochen-Volumenanteil (BV/TV), zu einer Verkleinerung des Trabekelabstands (Tb.Sp), sowie zu einer Verdickung der subchondralen Knochenplatte (SCBP). Die Bildung von Osteophyten wurde in beiden DMM Gruppen, WT und Syx Mäusen ohne Unterschiede nachgewiesen. Die Osteoklastenaktivität, die zu einem Knochenabbau führt, wurde histologisch im Bereich der Osteophyten und im subchondralen Knochen untersucht. Die Analyse ergab, dass eine stärkere Osteoklastenaktivität in WT DMM Mäusen zu Beginn der OA-Induktion vorlag, verglichen zu Syx DMM Mäusen. Dies könnte das erhöhte Knochenvolumen in Syx Mäusen erklären. Andere Studien haben gezeigt, dass das SNS die Osteoklastenaktivität im subchondralen Knochen über den β2-AR Signalweg verstärken kann (Elefteriou et al. 2005; Ducy et al. 2000). Zusammenfassend deuten diese Resultate darauf hin, dass eine Sympathektomie die Knochenveränderungen im Verlauf der OA verstärkt.

Da die Sympathektomie die Knorpeldegeneration verlangsamte, stellte sich die Frage, welcher Adrenerge Rezeptor dabei eine besondere Rolle spielt. Durch eine Sympathektomie ist zwar die Katecholaminfreisetzung teilweise blockiert, dennoch sind alle ARs intakt. Viele *in vitro* Studien weisen dem β2-AR eine bedeutende Rolle bei der Knorpeldegeneration zu. Als weiteres Untersuchungsziel wurde im Schlussteil dieser Arbeit daher der β2-AR Signalweg in Mäusen blockiert und die Auswirkung auf die OA Entwicklung analysiert. OA wurde in β2-AR-defizienten Mäusen 8 Wochen nach der Sham- oder DMM Operation untersucht. Die Behandlung und die Operationen der β2-AR-defizienten fanden unter den gleichen Bedingungen statt, wie bei den WT und Syx Mäusen. Ähnlich wie in den Syx Mäusen, ließ sich eine niedrige Noradrenalin-Konzentration in der Milz von β2-AR-defizienten Mäusen messen, was darauf hindeutet, dass nicht nur der β2-AR, sondern auch die reduzierte Noradrenalin-Konzentration diese Effekte induzierte.
Die OARSI-Scores in β2-AR-defizienten DMM Mäusen waren vergleichbar niedrig wie bei Syx DMM Mäusen und wiesen einen niedrigeren Knorpelverschleiß auf. Gleichzeitig wurden nach einer DMM-Operation in β2-AR-defizienten Mäusen, verstärkte OA charakteristische

Knochenveränderungen festgestellt, wie die Verdichtung des subchondralen Knochens und der Verdickung der subchondralen Knochenplatte. Auch hier waren diese Veränderungen noch ausgeprägter als bei den Syx Mäusen, was darauf hindeutet, dass der β2-AR einen Einfluss auf die Knochenveränderungen, während der Entwicklung OA aufweist. Im Hinblick auf die OA, spielt der β2-AR eine bedeutende Rolle bei der Knorpeldegeneration und den OA charakteristischen Knochenveränderungen und könnte daher ein attraktives Ziel für die Entwicklung neuer therapeutischer Ansätze sein.

Zusammenfassend hat die vorliegende Arbeit gezeigt, dass Noradrenalin das chondrogene Differenzierungspotential von sASC reduziert und somit eine mögliche Knorpelregeneration durch diese Zellen beeinträchtigt. Desweiteren konnte in dieser Arbeit erstmals die Wirkung des sympathischen Nervensystems im Verlauf der OA in verschiedenen Geweben des Kniegelenks nachgewiesen werden. Durch die Sympathektomie konnte eine Abschwächung der OA Progression im Knorpel und Synovium erzielt werden, obwohl gleichzeitig eine Verstärkung der OA charakteristischen subchondralen Knochenveränderungen zu beobachten waren. In Bezug auf das SNS bei der OA zeigte diese Studie, dass eine verringerte sympathische Aktivität das Kniegelenk insgesamt schützt, wenn man die Knochenveränderungen ignoriert. Die Untersuchung der OA im Knie von β2-AR-defizienten Mäusen zeigte erstmals, dass der β2-AR an der Knorpeldegeneration und den verstärkten subchondralen Knochenveränderungen beteiligt ist.

Abstract

The pathogenesis of osteoarthritis (OA) involves articular cartilage, synovial tissue and subchondral bone and is therefore a disease of the whole joint. OA is characterized by progressive degradation of cartilage, synovial inflammation, osteophyte formation and subchondral bone sclerosis. Cartilage-surrounding tissues are innervated by tyrosine hydroxylase (TH)-positive sympathetic nerve fibers with the most important sympathetic neurotransmitter norepinephrine (NE) detected in the synovial fluid of OA patients. Furthermore, adrenergic receptors are expressed in different knee joint tissues. Most *in vitro* studies indicate a potential role of the β2-adrenergic receptor, which has been not investigated during OA pathogenesis *in vivo*. The role of the sympathetic nervous system (SNS) in OA progression has not yet been studied. Therefore, the objective of this study was to analyze how the SNS and NE influence the MSC dependent cartilage regeneration *in vitro* and the OA pathogenesis and manifestation *in vivo.*

In the first part of this study, the effect of NE on the chondrogenesis of sASC, which are known to play an important role in cartilage regeneration was analyzed *in vitro.* In the second part of this study, the role of the SNS was studied *in vivo* in mice that were sympathectomized chemically followed by surgically induced OA. The specific focus was on the β2-adrenergic receptor effects on OA pathogenesis, which were analyzed in β2-adrenergic receptor-deficient mice.

The *in vitro* experiments have shown that NE reduced the chondrogenic potential of sASCs by decreasing the expression of type II collagen and sGAG. NE mediated these effects mainly by the α2-AR signalling. Furthermore, NE treatment led to activation of the ERK1/2 signal pathway. These findings suggested that the sympathetic neurotransmitter NE might suppress the chondrogenic capacity of MSC and their dependent cartilage regeneration and may also play a role in OA progression and manifestation.

The *in vivo* study has shown that sympathectomy reduced synovial TH-positive nerve fibers in the synovium and the NE concentration in the spleen significantly. In WT mice, DMM leads to increased NE concentrations in the spleen compared to sham mice indicating an increased SNS activity after mechanical stress or inflammation due to DMM. Sympathectomy leads to less pronounced cartilage degeneration (OARSI score) after DMM compared to DMM in WT mice. Furthermore, the release of the type II collagen degradation fragment CTX-II was abolished in Syx DMM mice compared to WT DMM mice, suggesting that less SNS activity due to sympathectomy reduced the cartilage degeneration during OA pathogenesis. Similarly, sympathectomy decreased the synovitis score significantly after DMM compared to DMM in

WT mice. Synovitis in WT mice was accompanied by increased MMP-13 expression in the synovium after DMM, compared to Syx mice. Cartilage degeneration seemed to be driven mainly by the increased synovial inflammation accompanied by an increased MMP13 expression in synoviocytes and not in chondrocytes. The pathological changes in synovium and cartilage might also be linked to each other, as indicated by the moderate correlation between the synovial inflammation (synovitis score) and cartilage degeneration (OARSI score). Subchondral bone volume as well the thickness of the subchondral bone plate (SCBP) and calcified cartilage (CC) were increased in Syx mice compared to WT after DMM. The data on DMM induction in β2-AR deficient mice revealed that the β2-AR signaling is involved in cartilage degeneration and the aggravated subchondral bone changes as these mice had less pronounced cartilage degeneration compared to WT mice. While the cartilage degeneration was similar, the subchondral bone changes were more pronounced in β2-AR deficient mice compared to the Syx mice.

Overall, the SNS had differential effects in cartilage, synovium and subchondral bone. A reduced SNS activity by sympathectomy attenuated cartilage degeneration and synovitis but aggravated the OA specific subchondral bone changes. These findings provide new insights into the development of novel therapeutic strategies for OA by targeting the SNS in a tissue-specific manner.

1 Introduction

1.1 Human knee anatomy

The knee joint is located between femur and the tibia and is the largest synovial joint in the body. The knee joint includes different tissues such as the articular cartilage, meniscus, anterior cruciate ligament, synovium and the subchondral bone (Stoker 1980), (Figure 1). These functional tissues are responsible for the complex activity. The knee joint includes ligaments such as the meniscotibial ligaments that attach the menisci to the tibial plateau and offer knee stability (DePhillipo et al. 2019). Articular cartilage is an avascular, aneural and alymphatic connective tissue located along the surface at the end of long bones in the joints. It is the key element of the knee joint that distributes the mechanical load equally and acts as a cushion, bearing a great amount of the bodyweight (D'Lima et al. 2012). As a consequence, the articular cartilage has a unique structure and extracellular matrix (ECM). Articular cartilage is characterized as hyaline cartilage, a smooth tissue that is abundant in type II collagen and proteoglycans (Fox, Bedi, and Rodeo 2009). Type II collagen consists of a central triple helix formed by three α-chains (Heinegård 2007). It constitutes 90% to 95% of total collagen in the matrix, while the minor collagen types are IX, X and XI (Aigner and Stöve 2003).

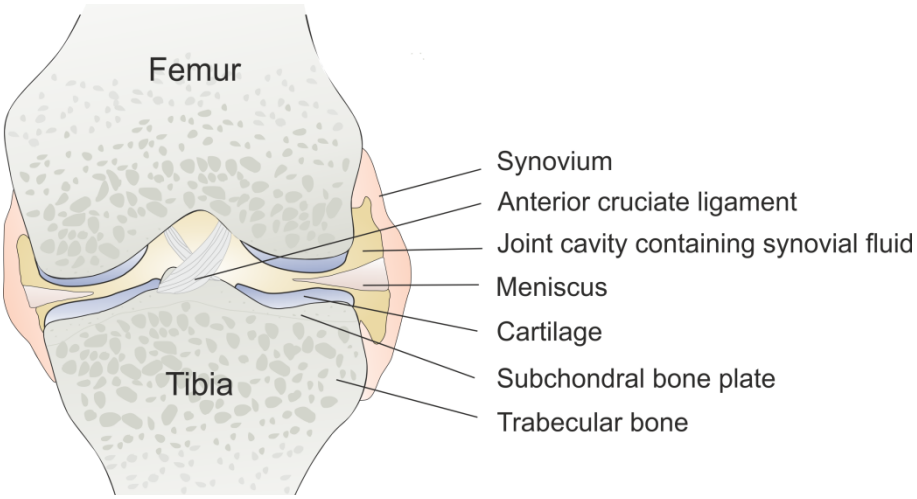

Figure 1 Knee joint anatomy.
The ends of femur and tibia are covered by articular cartilage. The synovium is a soft tissue that secretes synovial fluid and the menisci act as a shock absorber in the knee and adds stability to the knee joint. Subchondral bone plate and trabecular bone are located below the articular cartilage. Illustration was made using CorelDraw software.

Type II collagen forms a meshwork of fibers that is filled with proteoglycans such as aggrecan comprising over a hundred chondroitin sulfate or sulfated glycosaminoglycan (sGAG) chains, each made up of some 50 disaccharides of glucuronic acid and N-acetylgalactosamine with a sulfate group (Knudson and Knudson 2001). Due to the negative charge of sGAGs, aggrecan absorbs water which causes swelling and renders viscoelastic properties to the cartilage. This is limited by the collagen network, which provides tensile strength. Under loading, the matrix is compressed, and water is squeezed out of the cartilage, followed by the matrix rapidly regaining its previous shape as water molecules are drawn back after unloading (Heinegård 2007).

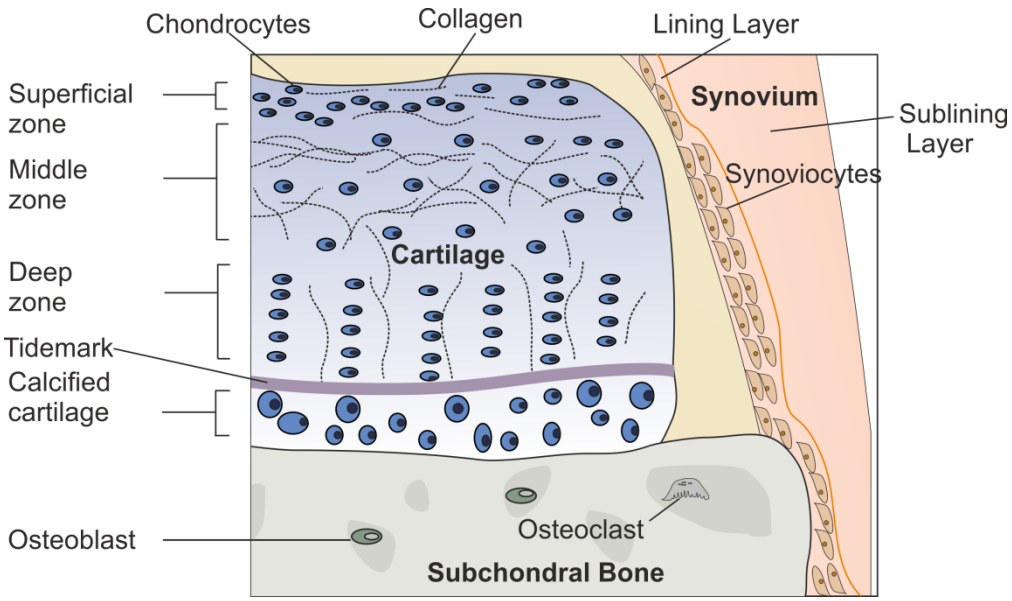

Figure 2 Schematic illustration of cells and structure in cartilage, subchondral bone and synovium.
Articular cartilage is divided into different zones beginning with the superficial, middle and deep zone, which are separated by the tidemark from the calcified zone and the subchondral bone. Synovium is divided into lining layer that includes lined synoviocytes and the sublining layer. Illustration was made using CorelDraw software.

Chondrocytes are the cell-type present in the articular cartilage. They have a limited ability to proliferate and make-up 3% of the cartilage mass (Aigner and Stöve 2003). They produce and maintain the articular matrix of cartilage by synthesizing and remodeling the ECM to preserve the functionality and the integrity of the cartilage. Chondrocytes are responsible for a delicate balance between anabolism and catabolism in the cartilage. Articular cartilage in the knees of human adults has a thickness of 1.3 to 2.6 mm (Hudelmaier et al. 2001; Eckstein et al. 2001; Shepherd and Seedhom 1999) and is organized into four different zones: superficial, middle (transitional zone), deep zone and the zone of calcified cartilage. Each zone possesses unique structural, functional and mechanical properties (Buckwalter, Mow, and Ratcliffe 1994; Becerra

et al. 2010), (Figure 2). The superficial zone makes up 10-20 % of the total cartilage thickness and contains a high number of flattened chondrocytes, compared to the other zones (Ulrich-Vinther et al. 2003). In this zone, collagen fibers, predominantly of type II collagen are packed tightly and aligned horizontally. The superficial zone is in direct contact with the synovial fluid, which is an essential source for the nutrition of the cartilage (Fox, Bedi, and Rodeo 2009). Due to its tensile properties, this zone resists the shear stress and protects deeper layers of cartilage. The middle zone represents 40-60% of the total cartilage and is therefore the thickest zone, with less organized, thick collagen fibers and rounded chondrocytes (Ulrich-Vinther et al. 2003). The main function of this zone is to resist the moderate compressive forces. The density of chondrocytes gradually decreases from the superficial zone to the deep zone respectively. In the deep zone, which makes up 30% of the cartilage thickness, chondrocytes and collagen fibrils are arranged in vertical columns to the articular surface and resist great compressive forces (Fox, Bedi, and Rodeo 2009). The tidemark is an interface between the articular cartilage and the calcified cartilage. The calcified cartilage connects the articular cartilage with the subchondral bone and consists of chondrocytes that are expressing hypertrophic markers such as type X collagen and alkaline phosphatase. These different zones provide articular cartilage mechanical properties that can absorb and transmits mechanical forces (Mikos et al. 2006). The chondrocytes in the different zones secrete different proteins in response to diverse stimuli such as growth factors and mechanical loads (Buckwalter and Mankin 1998).

The synovium seals the synovial cavity and fluid from surrounding tissues. The healthy synovium is known to have only a few cell types such as fibroblast-like synoviocytes (Figure 2). It consists of two layers: the inner layer with a thickness of 1-2 synoviocytes and the synovial sublining layer containing blood vessels and a low number of cells (Wenham and Conaghan 2010; Smith 2011). The synovium secretes synovial fluid found in the joint cavity. Synovial fluid is rich in lubricant macromolecules and cushions the joints during movement and reduces cartilage friction. The synovium mediates nutrient exchange between blood and synovial fluid (Mathiessen and Conaghan 2017).

The subchondral bone is located below the articular cartilage and supports it in distributing mechanical forces over the joint (Li et al. 2013), (Figure 2). It consists of the subchondral bone plate and subchondral trabecular bone. Osteoblasts and osteoclasts are cells that maintaining the integrity of the subchondral bone and the balance between synthesized and resorbed bone. Osteoblasts synthesize and secrete bone matrix and are responsible for the mineralization of bone, while osteoclasts degrade (resorb) bone tissue during bone remodeling (Intemann et al. 2020). The subchondral bone plate is invaded by channels that connect the articular cartilage and the underlying subchondral trabecular bone. The trabecular bone is

highly vascularized and provides another nutrition source for cartilage in addition to synovial fluid (Imhof et al. 2000). Interestingly, also sympathetic nerves innervate the subchondral bone; however, their role is poorly understood.

1.2 Osteoarthritis

Osteoarthritis (OA) is the most prevalent joint disease affecting more than 10% of the world population (Bijlsma, Berenbaum, and Lafeber 2011) and predominantly older adults (Cross et al. 2014). According to the Global Burden of Disease Study from 1990 to 2016, OA was ranked as the second rapidly rising condition associated with disability (Vos 2017). Symptoms of OA include chronic pain, joint instability, stiffness and reduced mobility (Felson 2006). Clinical features are progressive destruction of the articular cartilage, the formation of osteophytes, thicker subchondral bone and synovial inflammation (Loeser et al. 2012). Therefore, OA is considered to be a disease of the whole joint and can occur in any joint but most common in the knee (Hunter and Felson 2006). Osteoarthritis can be investigated by radiography showing the narrowing of the joint space because of cartilage loss (Hunter and Felson 2006). Incidence of knee OA increases steeply with age, overweight, and affects more frequently women than men (Magnusson, Turkiewicz, and Englund 2019). Knee OA is becoming globally a major problem due to the aging of the population and an increase in obesity around the world (Busija et al. 2010). The current treatments for OA are medications for pain relief such as nonsteroidal anti-inflammatory drugs (NSAIDs), opioids, intraarticular injections of cortisone and hyaluronic acid (Evans, Kraus, and Setton 2014). Nonetheless, there is only a limited healing potential of damaged cartilage and no treatment that can reverse the injury in the OA joint (Hermann, Lambova, and Muller-Ladner 2018). In most cases, prosthetic joint replacement is the major therapy option (Evans, Kraus, and Setton 2014).

1.3 Pathological changes in joint tissues during OA

1.3.1 Articular cartilage degradation

For an efficient gliding motion during joint movement, intact articular cartilage is necessary. Cartilage loss due to excessive mechanical loading is considered to be one hallmark of OA (Loeser et al. 2012). At an early OA stage, degradation of the articular cartilage such as cracks and mild abrasion within the cartilage can be detected by microscopy. Surprisingly, in OA, blood vessels and sympathetic nerves are invading the articular cartilage, which extends from the subchondral bone (Suri et al. 2007). However, the role of sympathetic nerves in OA is unclear.

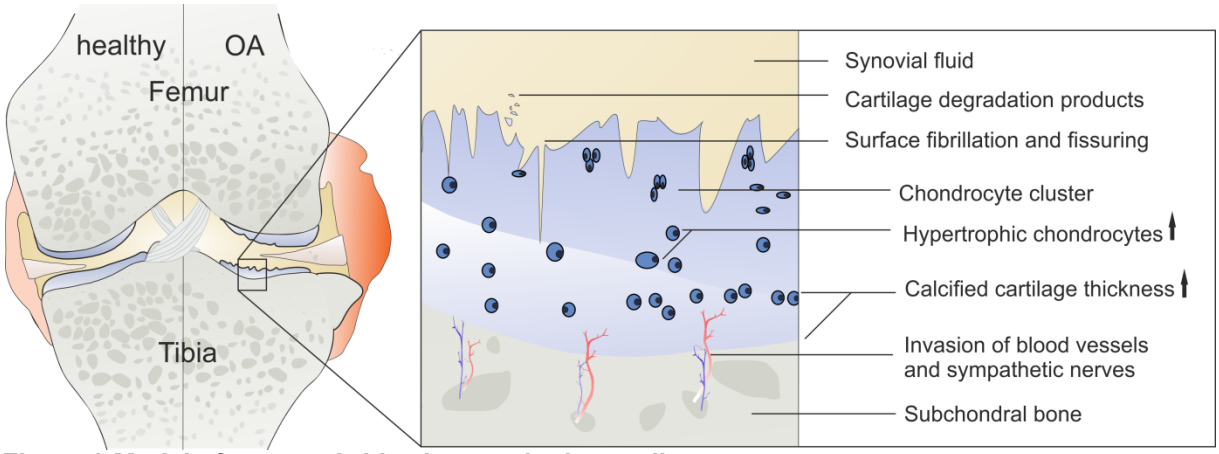

Figure 3 Model of osteoarthritic changes in the cartilage.
Cartilage changes are indicated by the formation of chondrocyte cluster and the differentiation into hypertrophic phenotype. In OA, the calcified cartilage thickness increase which is accompanied by nerves and blood vessels that invade the cartilage. Illustration was made using CorelDraw software.

In OA, chondrocytes proliferate, form cell clusters and have a low capacity to repair cartilage damage (Goldring and Marcu 2009). Furthermore, chondrocytes differentiate to a hypertrophic phenotype characterized by the big round shape and increased cytoplasm (Pritzker et al. 2006). Hypertrophic chondrocytes secrete type X collagen instead of type II collagen that promotes stiffness of the cartilage. The differentiation into hypertrophic chondrocytes can be a result of mechanical and inflammatory stimuli, involving mitogen-activated protein kinase (MAPK) pathways by activated extracellular signal-regulated kinases 1/2 (ERK1/2) (Goldring and Marcu 2009; Prasadam et al. 2010).

To detect and assess OA progression in the knee, a histopathological grading system has been established by the Osteoarthritis Research Society International (OARSI), which is widely used as a standard for histological cartilage damage in OA (Pritzker et al. 2006). The OARSI score grades the degeneration of the articular cartilage (grade 0-4) and the subchondral bone

(grade 5-6). At early stage of OA (Grade 1), the superficial zone is intact but uneven. The degradation of sGAG can be detected by a loss of matrix staining intensity by cationic stains such as dimethylmethylene blue (DMMB), safranin O, or toluidine blue (Pritzker et al. 2006; Becerra et al. 2010). With increased OA, deep fibrillation extends through the superficial zone (Grade 2), with vertical fissures in the middle zone (Grade 3), and may lead to cell death or proliferation. This is followed by the loss of the superficial zone (Grade 4) and the completely eroded hyaline cartilage (Grade 5) (Pritzker et al. 2006).

In healthy articular cartilage, anabolism and catabolism of the ECM molecules are in balance. This balance is maintained by chondrocytes and also controlled by the amount of cytokines and growth factors in the surrounding cartilage and synovial fluid. Chondrocytes respond to the structural changes in the surrounding cartilage matrix as well to external factors such as cytokines which are diffusing into the articular cartilage from the synovial fluid and subchondral bone (Stöve et al. 2007). OA leads to an imbalance between anabolic and catabolic activities in the cartilage. This imbalance causes destruction and failure of the extracellular matrix which is not able to fully resist mechanical loads leading to OA (Goldring, Tsuchimochi, and Ijiri 2006). Soluble factors, changes in oxygen levels and even mechanical stress can influence the synthesis and degradation of ECM molecules in the cartilage (Demoor et al. 2014).

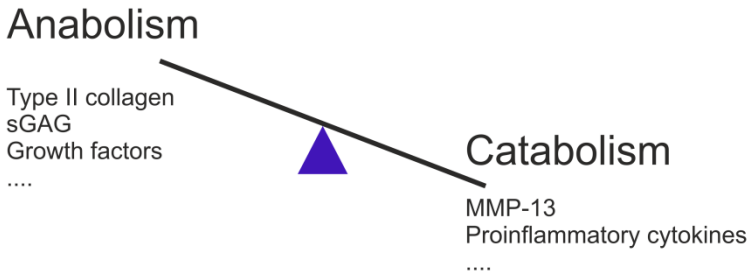

Figure 4 Key feature of OA is the imbalance in cartilage turnover.
Chondrocytes synthesize most of the ECM degrading proteases in particular MMP-13 and fully provide anabolic activity and the production of ECM molecules such as type II collagen and sGAG. The balance is regulated by growth factors and cytokines. Illustration was made using CorelDraw software.

In OA, the secretion of matrix metalloproteinases (MMPs) and aggrecan-degrading enzymes are increased in the cartilage, which is associated with the degradation of the ECM (Clements et al. 2011; Arner 2002). Cleavage of proteoglycans such as aggrecan results in enhanced release of aggrecan and sGAG from the cartilage (Roughley, Nguyen, and Mort 1991). MMPs (MMP-3, MMP-13 and MMP-14) have been detected in OA cartilage and synovium and are

considered to be the main enzymes responsible for the degradation of collagen in the ECM of articular cartilage (Tetlow, Adlam, and Woolley 2001; Dean et al. 1989). Out of these MMPs, MMP-13 is the most strongly expressed one in OA cartilage (Bau et al. 2002; Swingler et al. 2009). During cartilage breakdown, type II collagen is primarily cleaved by MMP-13 and released to the synovial fluid (Charni-Ben Tabassi et al. 2008; Itoh et al. 2006). The presence of cross-linked degradation fragment of collagen II (CTX-II), which is released by MMP-13 is widely used to determine the status of cartilage degradation (Lohmander et al. 2003).

In brief, cartilage degradation during OA is not reversible and chondrocytes have only a limited regeneration capacity to repair cartilage defects (Loeser et al. 2012). Other cells that might play a role in cartilage regeneration are mesenchymal stem cells (MSC). Cell-based therapies with MSC for OA have been evaluated in several pre-clinical studies (Diekman and Guilak 2013). The high proliferative capacity of cultured MSC and their ability to differentiate to the chondrocyte phenotype made them an attractive cell source for cartilage cell therapy (Gadjanski, Spiller, and Vunjak-Novakovic 2012).

During the past decades, the existence of highly regenerative mesenchymal stem cells was confirmed in cartilage-surrounding tissues (De Bari et al. 2001; McGonagle, Baboolal, and Jones 2017). Synovium-, synovial fluid-, bone marrow- and adipose tissue-resident MSC

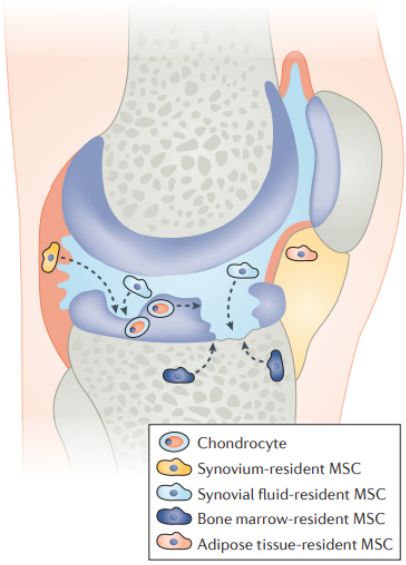

Figure 5 Schematic illustration of MSC involvement in an osteoarthritis knee joint. Sagital view of osteoarthritic knee joint and the contribution and migration of native MSC in to the cartilage defect area. Image adapted from (McGonagle, Baboolal, and Jones 2017).

supposedly migrate to the areas of damaged cartilage and differentiate to chondrocytes (McGonagle, Baboolal, and Jones 2017), (Figure 5). It has been proven, that synovial adipose tissue-derived MSC (sASCs) contribute to the repair of cartilage injuries (Sekiya et al. 2015; Li

et al. 2020; Zare et al. 2020) . Furthermore, the MSC numbers obtained from adipose tissue are much higher than from the bone marrow (Wolfstadt et al. 2015). Therefore, sASCs have been widely used including in the present study for the chondrogenesis model *in vitro*. Interestingly, OA is associated with an increase of MSC in the joint tissues such as cartilage (Fellows et al. 2017), bone marrow (Campbell et al. 2016) and synovial fluid (Sekiya et al. 2012), suggesting an attempt to repair cartilage (McGonagle, Baboolal, and Jones 2017).

Chondrogenesis is the process in which MSC differentiate into chondrocytes during cartilage development and occurs at the earliest phase of endochondral ossification during skeletal development *in vivo*. This process can be induced *in vitro* by incubating MSC in three-dimensional pellet culture with a defined cell culture medium. This method is widely used to analyse the process of chondrogenesis as it provides a three-dimensional environment that allows cell-cell interaction (Johnstone et al. 1998). This assay is also used for novel approaches focused on cartilage development and the research of certain substances that are relevant in OA or might influence OA pathogenesis. Differentiated chondrocytes produce hyaline cartilage ECM, which is rich in type II collagen and sGAGs (Medvedeva et al. 2018). The nuclear transcription factor Sox9 that regulates the expression of type II collagen (Ng et al. 1997; Lefebvre and Dvir-Ginzberg 2017) is essential for chondrocyte differentiation. Chondrocytes can differentiate to the hypertrophic phenotype at the end-stage of chondrogenesis, expressing more Runt-related transcription factor 2 (Runx2), MMP-13 and type X collagen (Mackie, Tatarczuch, and Mirams 2011). The transcription factor Runx2 is a pivotal regulator for hypertrophic maturation (Wuelling and Vortkamp 2011) while MMP-13 is

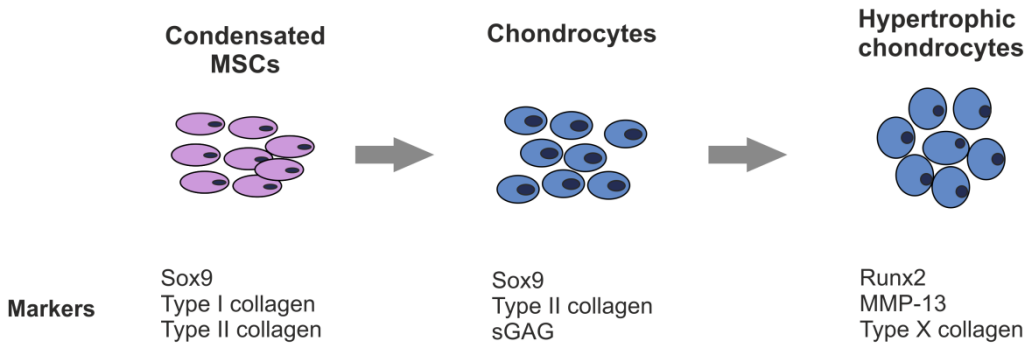

Figure 6 Chondrogenesis of MSC.
Chondrogenesis is initiated by condensation of MSC and expression of SOX9 and synthesis of type I and type II collagen. Differentiated chondrocytes secrete ECM molecules type II collagen and sGAG, while in hypertrophic chondrocytes the gene expression of Runx2 and synthesis of MMP-13 and type X collagen is elevated. Illustration was made using CorelDraw software.

a downstream target of Runx2 (Inada et al. 1999) and is more expressed in hypertrophic chondrocytes compared to mature chondrocytes. Elevated hypertrophic markers are associated with increased calcified cartilage thickness (Fuerst et al. 2009).

1.3.2 Synovial inflammation

The inflammation of synovium called synovitis causes pain, swelling of the joint and difficulties in moving (Scanzello and Goldring 2012). Synovitis, a common feature in OA (Mathiessen and Conaghan 2017) is also associated with cartilage degradation (Sellam and Berenbaum 2010). The synovium is increased in thickness during OA, which is caused by the thickening of the lining layer (Loeuille et al. 2005). Furthermore, the infiltration of mononuclear cells and the expression of inflammatory mediators are also increased in the synovium (Wenham and Conaghan 2010). These significant abnormalities in the synovium are visible even before excessive cartilage degeneration. Pathological scores for the evaluation of synovitis have been developed, which include the analysis of lining layer thickness, synovium thickness and cellular density of the synovial sublining layer (Mathiessen and Conaghan 2017).

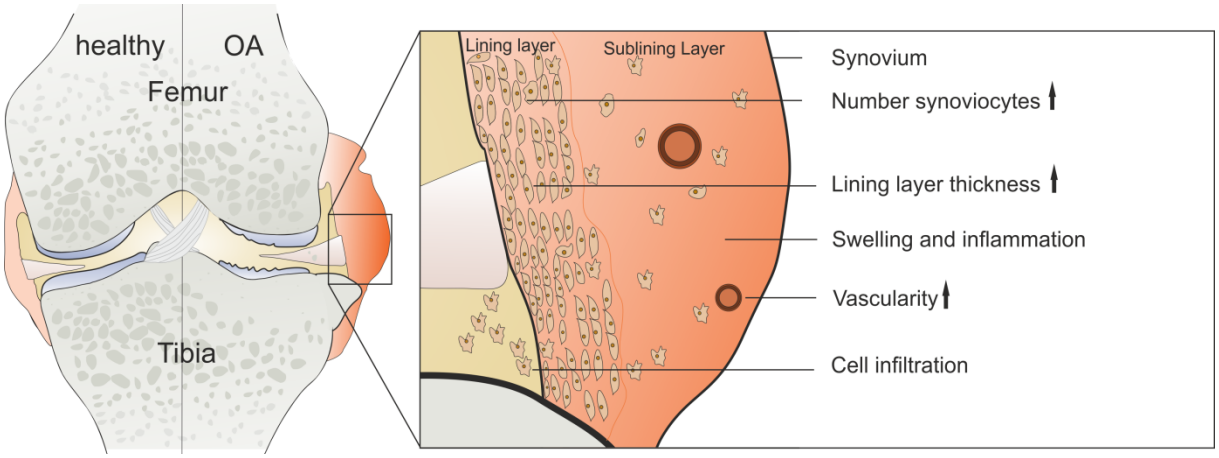

Figure 7 Model of synovitis in OA.
The inflammation of the synovial membrane is characterized by an increased number of fibroblast-like synoviocytes in the lining layer and the infiltration of cells in the sublining layer, which results in a thicker and swollen synovial membrane. Inflammation and vascularity were markedly increased in the OA synovium. Illustration was made using CorelDraw software.

It is not clear whether synovitis is a result of cartilage breakdown or initiate independently. Before excessive cartilage damage in OA, many catabolic factors are released from the cartilage into the synovial fluid, which are known to induce production of MMPs, which are also associated with initiation of synovitis (Bonnet and Walsh 2005; Pelletier, Martel-Pelletier, and Abramson 2001). Both chondrocytes in the cartilage and synoviocytes in the synovium secrete many types of MMPs (Li et al. 2017), of which MMP-13 protein expression is particularly enhanced in OA synovium (Marini et al. 2003). Furthermore, there is evidence that MMP-13 is released by synoviocytes to the synovial fluid (Blom and Berg 2007). Synovitis is not only implicated to be involved in cartilage degradation but also in the formation of osteophytes alongside inflamed synovial membrane, probably due to the secretion of several growth factors

from synovial cells (Blom et al. 2004). All these studies strongly indicate the contribution of the synovium to OA pathology.

1.3.3 Subchondral bone changes

There is a crosstalk between osteoblasts, the bone-forming cells and osteoclasts, the bone-resorbing cells that control bone remodelling (Intemann et al. 2020). Interestingly, numbers of blood vessels and sympathetic nerves increase in the subchondral bone during OA, which even invade the calcified cartilage (Suri et al. 2007). Several studies provide evidence that subchondral bone changes are involved in OA progression (Radin, Paul, and Tolkoff 1970; Adebayo et al. 2017). At the beginning of OA development, the subchondral bone loss increases, thus resulting in a thinner and porous subchondral bone plate. At a late OA stage, bone resorption is reduced while bone formation is increased which results in higher bone mass and bone mineral density in the subchondral bone (Sepriano et al. 2015; Findlay and Atkins 2014). Furthermore, increased mineralization of the subchondral bone and altered bone

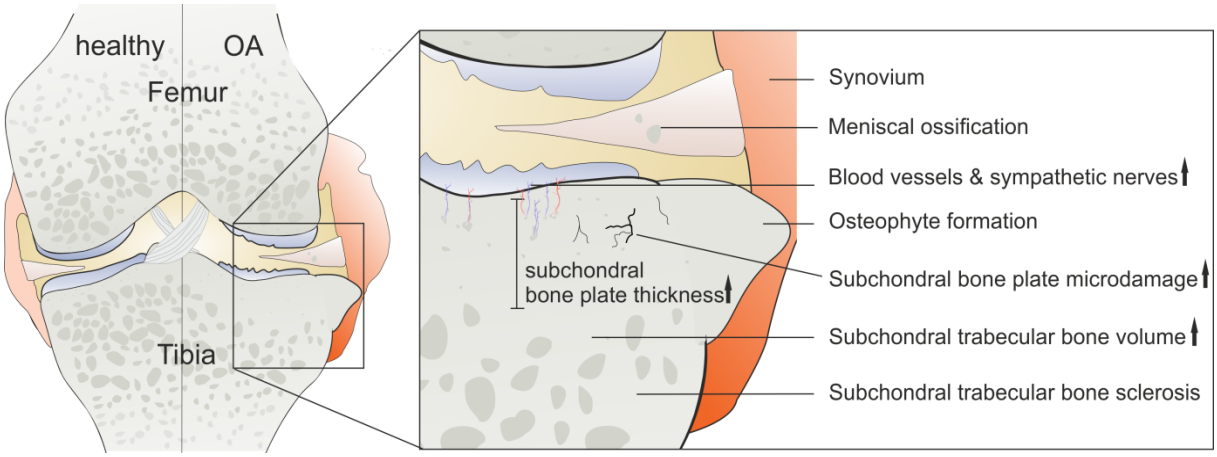

Figure 8 Model of osteoarthritic changes in subchondral bone.
The thickness and volume of the subchondral bone plate increases and becomes sclerotic. Accumulation of microdamage in the subchondral bone, the formation of osteophyte and the ossification of the meniscus arise in OA. The invasion of blood vessels and sympathetic nerves is enhanced in the osteoarthritic subchondral bone that can invade the overlying cartilage. Illustration was made using CorelDraw software.

metabolism were observed in OA (Prasadam et al. 2013; Hannan et al. 1993). In the early stage of OA, subchondral bone loss and osteoclast activity are elevated, while in the late OA stage, osteoblast activity is increased, leading to higher bone density and volume (Fazzalari and Parkinson 1997; Yuan et al. 2014).

The dysregulation of osteoblast and osteoclast activity in OA leads to an imbalance between bone formation and resorption, causing an increased and abnormal bone tissue mineralization and remodelling (McErlain et al. 2012). Osteoclasts can be detected histologically by staining of tartrate-resistant acid phosphatase (TRAP), an osteoclast enzyme (Hayman 2008). TRAP catalyzes dephosphorylation of bone matrix phosphoproteins, which are important for bone

formation (Blumer et al. 2012). TRAP enzyme activity is increased in early OA stage in the subchondral bone of OA patients (Prieto-Potin et al. 2015) or in a murine OA model (Fang et al. 2018), while it decreased at late stage OA. The link between the abnormal structure of the subchondral bone to the progression of cartilage degeneration is controversial. However, prospective studies reported a correlation between subchondral bone changes and cartilage degeneration (Liu et al. 2018; Nakasa et al. 2014). Bone stiffness, elevated bone mineral density, and increased bone volume in OA can increase cartilage damage (Greenwood et al. 2018). Cartilage loss leads to bones rubbing directly together causing pain. The increased fissures and blood vessels between cartilage and subchondral bone allow great crosstalk between chondrocytes, osteoblasts and osteoclasts. Furthermore, factors such as MMPs released by hypertrophic chondrocytes are exposed in the subchondral bone (Yuan et al. 2014), also leading to cartilage damage.

Another pathological change in OA is the formation of osteophytes which are bony lumps that grow at the margins of osteoarthritic joints (Buckland-Wright 2004). Osteophytes that *develop* along bone edges in degenerative joints, can limit joint movement and can be a source of pain in OA patients (Pottenger, Phillips, and Draganich 1990). Additionally, microdamage, microcracks (Herman et al. 2010), subchondral bone cysts and sclerosis, which is the thickening and the hardening of the bone, also occur in OA (Li et al. 2013).

1.3.4 Murine OA model to analyze pathological changes in the knee joint

To explore various aspects of OA, many experimental animal models were established. Most existing animal OA studies use mice due to their musculoskeletal system that develops quickly, thus allowing for testing a large number of subjects in a short time (Bapat et al. 2018). The destabilization of the medial meniscus (DMM) is the most common method for surgical OA induction in mice (Lorenz and Grässel 2014). The severity and location of lesions following DMM are consistent with lesions observed in aged spontaneous mouse models of OA, which makes DMM a preferred model of OA (Glasson, Blanchet, and Morris 2007).

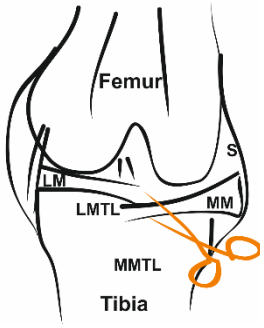

Figure 9 Schematic Illustration of the DMM model.
OA induction of the right knee joint of the mouse induced by transection of the medial meniscotibial ligament (MMTL). LMTL = lateral meniscotibial ligament; MM = medial meniscus; LM = lateral meniscus; S = synovium. Image adapted and modified by (Glasson, Blanchet, and Morris 2007).

DMM surgery leads to cartilage degeneration that corresponds with the subchondral bone defects similar to OA in humans (Tanamas et al. 2010). Currently, the DMM model is considered to be the gold standard for studying OA progression. The transection of the medial meniscotibial ligament causes biomechanical instability and abnormal joint loading resulting in cartilage degeneration (Glasson, Blanchet, and Morris 2007); (Figure 9). The meniscal injury is known to be a risk factor for the development of human OA that makes the model clinically relevant (Ding et al. 2007). The method provides high reproducibility, with the OA progression detected within 3–6 weeks (Bapat et al. 2018).

1.3.5 Osteoarthritis risk factors

OA is considered to be an interaction of local and systemic factors. Local factors such as prior trauma or anatomic abnormalities can lead to abnormal joint loading which alters the biomechanical forces across the joint (Chaganti and Lane 2011). Systemic factors such as age, sex (Magnusson, Turkiewicz, and Englund 2019), genetics (Spector et al. 1996) and hormones or neurotransmitters (Bay-Jensen et al. 2013) can also influence the development of OA (O'Neill, McCabe, and McBeth 2018). The neurotransmitters of the nervous system gained significance regarding OA pathogenesis during the past decades (Grässel, Straub, and Jenei-Lanzl 2017). Many studies indicate that the SNS might be a systemic parameter that is linked to OA development.

1.4 Sympathetic nervous system

The autonomic nervous system (ANS) controls physiologic actions unconsciously and maintains internal homeostasis and stress responses (Duke 2011). The ANS is divided into the sympathetic nervous system (SNS), the parasympathetic nervous system (PNS) and the enteric nervous system (Elefteriou, 2018). The SNS and the PNS exhibit opposite actions: while the SNS acts in “fight-flight” situations, the PNS acts in “rest and digest” situations. Both mediate their effects via neurotransmitters released by the nerve fibers at the postganglionic synapse, that bind to specific receptors expressed by target cells and activate intracellular signaling pathways (Karemaker 2017). The SNS exhibits its effects through the catecholamines such as norepinephrine (NE), dopamine (DA) and epinephrine (E). The neurotransmitter NE might be important in OA pathogenesis since it was detected in the synovial fluid of OA or knee-trauma patients (Figure 10), while DA and E were not detectable (Miller et al. 2000; Jenei-Lanzl et al. 2014). If the SNS is active, NE is released from the

sympathetic nerve endings innervating target organs. NE is synthesized from the amino acid tyrosine by tyrosine hydroxylase (TH), which is the rate-limiting enzyme of catecholamine biosynthesis (Nagatsu, Levitt, and Udenfriend 1964) that controls catecholamine levels within the body.

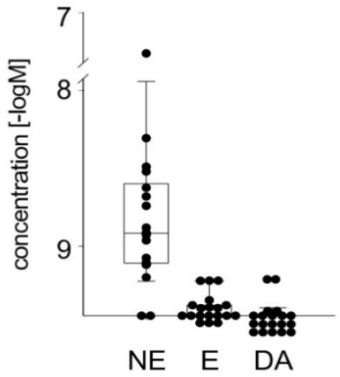

Figure 10 Sympathetic neurotransmitter in the synovial fluid.
NE was analyzed in the synovial fluid of of trauma- patients by HPLC. NE-norepinephrine, E-epinephrine, D- dopamine. (Jenei-Lanzl et al. 2014)

Therefore, the enzyme TH is a marker for sympathetic nerves innervating different tissues in the body. NE, a major neurotransmitter of the SNS can activate α- and β-adrenergic receptors depending on its concentration. All α and β adrenergic receptor (AR) subtypes (α1A, α1B, α1D, α2A, α2B, α2C, β1, β2, β3) belong to the G protein-coupled receptor family. Different intracellular signaling pathways become activated, depending on the activation of the specific alpha subunits of ARs (Gs, Gi or Gq) (Venkatakrishnan et al. 2013). At low concentrations ($\leq 10^{-7}$ M), NE mainly acts via α-ARs followed by protein kinase A (PKA) and cAMP inhibition (Gαi signaling). In contrast, NE at high concentrations ($\geq 10^{-7}$ M) preferentially acts via β-ARs leading to PKA and cAMP elevation (Gαi signaling). The α2-adrenergic receptors are linked to inhibition of adenylylcyclase, while α1-adrenergic receptors activate phospholipase C. An alternative signal transduction is mediated by β-arrestin binding to the β2-AR causing receptor desensitization, and internalization, which in turn leads to the alternate extracellular signal-regulated kinase-1/2 (ERK1/2) pathway (Yang et al. 2010). Furthermore, the protein β-arrestin regulates AR-mediated signaling while binding to phosphorylated ARs which in turn activate the alternative ERK1/2 pathway (Blesen et al. 1995; Bogoyevitch et al. 1996; Alblas et al. 1993).

1.5 Sympathetic nervous system and OA

1.5.1 Sympathetic nerve fibers and neurotransmitters in the joint

In the human musculoskeletal system, sympathetic nerves innervate the synovium (Eitner et al. 2013), the subchondral bone, the periosteum (Hukkanen et al. 1992) and their activity is implicated in the development of OA pathogenesis (Lorenz et al. 2016). The innervation by sympathetic nerves in OA knee joint tissues as well as the existence of TH-positive cells that release NE have been observed. The levels of released NE that are sufficient for the activation of ARs, have been detected in the synovial fluid of trauma patients (Jenei-Lanzl et al. 2014); (Figure 10) and of OA patients (Miller et al. 2000). The innervation of sympathetic nerves has been reported in adult joint tissues such as subchondral bone and synovium altered, but not much is known if and to what extent these nerves contribute to OA pathology. In OA, sympathetic nerves cross the tidemark and invade the calcified cartilage, suggesting their involvement in OA pathogenesis (Suri et al. 2007). Furthermore, it remains unclear if and how NE influences the self-regeneration capacity of articular cartilage or regenerative joint-resident cells and therefore the pathogenesis of OA. Many cell types in the joint can respond to noradrenergic stimulation. Most of the adrenergic α- and β-receptor subtypes along with TH are expressed in human and murine chondrocytes (Lorenz et al. 2016; Takarada et al. 2009; Lai and Mitchell 2008). Furthermore, synoviocytes, osteoblasts and osteoclasts express most of the adrenergic receptors (Huang et al. 2009; Mlakar et al. 2015). The effect of NE on OA joint cells has been studied *in vitro* but its role therein has not been delineated. A dependency on the dose of NE for activation of the different adrenergic receptors has been however described (Courties, Sellam, and Berenbaum 2017; Molinoff 1984).

1.5.2 The effect of NE on articular chondrocytes and joint-resident MSC

The effects of NE on chondrocytes vary and depend on the activated AR and further differ in normal and pathophysiological conditions of chondrocytes. NE exhibits catabolic effects on healthy chondrocytes by inhibiting cartilage matrix synthesis via the induction of cartilage degrading enzymes (Lai and Mitchell 2008; Mitchell et al. 2011) and increased apoptosis. On the other hand, NE can inhibit the release of pro-inflammatory IL-8 by OA chondrocytes (Lorenz et al. 2016).

The effect of NE on MSC chondrogenic differentiation has been demonstrated (Jenei-Lanzl et al. 2014). However, there are no studies regarding NE sensitivity and the chondrogenic potential of sASCs, which are reported to contribute to cartilage repair (Murphy et al. 2002). There are few studies describing the NE effect on bone marrow-derived MSC (BMSC) obtained

from trauma patients (Jenei-Lanzl et al. 2014). Treatment with NE or β2-AR agonist has been shown to inhibit type II collagen and sGAG synthesis and accelerate the hypertrophic pathway by induction of MMP-13 and type X collagen expression (Jenei-Lanzl et al. 2014). These effects were reversed by a specific β2-AR antagonist. Furthermore, most of the existing studies regarding cartilage regeneration by MSC have been performed under normoxia, although the cartilage microenvironment contains only about 2% O2 representing the 'physioxic condition' (Lafont 2010; Pattappa et al. 2019). All together, these few data indicate that signaling through β2-AR influences chondrogenic differentiation.

1.5.3 SNS effects on OA

The first and only study from 1996 described a direct relationship between the SNS and OA in a human patient. Sympathectomy was performed in the left hand of the patient with vasospastic syndrome with ischemia. More than 20 years later, the patient developed OA in the right hand with extensive OA characteristic bone changes such cartilage degeneration indicated by joint space narrowing and osteophyte formation. In contrast to the right hand, the left sympathectomized hand developed no OA suggesting that sympathectomy might have protected against OA (Lilly 1966). Since then, no study has systematically evaluated the effects of sympathectomy in OA. Only a few studies described that OA patients receiving α-AR or β-AR blocker medication because of hypertension, had significantly less knee pain and radiographic OA changes (Valdes et al. 2017; Driban et al. 2016). Furthermore, the use β-AR blockers prevented bone loss fracture risk in post-menopausal women (Reid 2008). Regardless, it is controversial whether β-blockers reduce knee pain as reported in a recent study (Zhou et al. 2020).

An association of the SNS with OA pathogenesis was described in a murine model of experimental temporomandibular joint OA (Jiao, Niu, Li, et al. 2015). These studies reported that the injection of the α2-AR agonist aggravates OA features via the activation of the ERK1/2 signal pathway. Additionally, several animal studies without OA pathogenesis confirm that the SNS is involved in bone metabolism and that increased sympathetic activity promotes bone loss through the β2-AR signaling by osteoclast activation and bone resorption (Elefteriou et al. 2005; Ducy et al. 2000). There is evidence that the SNS contributes to bone homeostasis (Elefteriou, Campbell, and Ma 2014; Kajimura et al. 2011; Yirmiya et al. 2006), suggesting potential involvement in OA.

Altogether, these data strongly imply that the SNS and in particular its major neurotransmitter NE might influence the regeneration capacity of joint-resident MSC via the β2-AR signalling and therefore, pathological changes in joint tissues during OA. The association of cartilage degeneration, synovitis and osteoarthritic bone changes with the SNS was never established

before in OA. To date, no study determined the impact of the SNS for example by suppressing its activity by sympathectomy on knee-OA pathogenesis in a murine model. Moreover, no study analysed the role of the β2-AR in an OA model using transgenic β2-AR deficient mice. We therefore aim to investigate the role of the SNS in OA manifestation and pathogenesis for better understanding the mechanisms of OA pathogenesis and to establish novel future therapeutic options.

1.6 Aim of this study

Several recent reports demonstrated that sympathetic nerve fibers are present in healthy and osteoarthritic knee joint tissues and that the SNS mediates numerous effects on the skeletal system. Studies regarding SNS involvement in OA manifestation and progression are sparse. Furthermore, not much is known about NE, which is found in OA synovial fluid, on the proliferation and regenerative potential of joint-resident MSC and on the pathophysiologic alteration in cartilage, synovium and subchondral bone in OA. The aim of this study was to investigate the impact of the SNS on the regenerative potential of sASCs in OA and on the development of OA in a murine model. This study is divided into two parts. First, the effect of NE on chondrogenesis of MSC will be investigated *in vitro* using pellet cultures. Second, the role of the SNS will be studied *in vivo* in mice that will be sympathectomized chemically followed by surgically induced OA. To narrow down the role of specific AR receptors, OA will be induced in β2-AR deficient mice.

The chondrogenic differentiation of sASCs was first established, as these cells are known to play an important role in cartilage regeneration. NE-dependent changes in chondrogenic capacity were determined by the expression of ECM or hypertrophic markers. Furthermore, NE-dependent signaling pathways were characterized. It was of interest to examine which AR is mediating the effects post NE activation as previous reports suggest the involvement of the β2-AR, that can activate the ERK1/2 signal pathway.

In the second part, the direct relationship between SNS and OA initiation and progression was examined *in vivo.* In a surgically induced OA model, peripheral sympathetic nerve fibers were depleted chemically to reduce the SNS signal transmission. The aim was to investigate if reduced NE release by the deprivation of sympathetic nerve fibers affected the OA progression. The resulting OA alterations in joint-tissues such as articular cartilage, synovium and subchondral bone were analyzed biochemically and by microscopy techniques. Additionally, this study describes for the first time the resulting phenotype of sympathectomized mice and the impact of the SNS on OA severity in a murine model. Furthermore, this study gives new insights about the role of β2-AR in OA progression utilizing β2-AR deficient mice and about the role of SNS in OA pathogenesis in different knee joint tissues that can potentially offer novel therapeutic approaches for OA treatment.

2 Material and methods

2.1 Antibodies

The primary and secondary antibodies used in this study are summarized in Table 1 and Table 2.

Table 1 Primary antibodies used in this study.

Antigen	Company	Cat. No.	Dilution or µl/test	Analysis	Source
ERK	Cell Signalling	9102	1:2500	WB	Mouse
pERK	Cell Signalling	4370	1:2500	WB	Rabbit
PKA	Abcam	ab32514	1:5000	WB	Rabbit
pPKA	Abcam	ab32390	1:2500	WB	Rabbit
GAPDH	Thermo Fisher	MA5-15738	1:2500	WB	Mouse
α2a-AR	Abcam	ab85570	1:200	IHC	Rabbit
β2-AR	Abcam	ab213651	1:200	IHC	Rabbit
Type II collagen	Merck	II-4C11	1:250	IHC	Mouse
TH	Abcam	ab137869	1:200	IHC	Rabbit
MMP-13	Abcam	ab39012	1:500	IHC	Rabbit
CD 11b/FITC	Thermo Fischer	11-0118-41	(0.5 µg/test)	FACS	Mouse
CD 19/PE	Thermo Fischer	12-0199-41	(0.25 µg/test)	FACS	Mouse
CD 34/PE	Thermo Fischer	12-0349-41	(0.5 µg/test)	FACS	Mouse
CD 45/FITC	Thermo Fischer	11-0459-41	(0.25 µg/test)	FACS	Mouse
CD 73/FITC	Thermo Fischer	11-0739-41	(0.25 µg/test)	FACS	Mouse
CD 90/PE	Thermo Fischer	12-0909-41	(0.25 µg/test)	FACS	Mouse
CD 105/PE	Thermo Fischer	12-1057-41	(1 µg/test)	FACS	Mouse
HLA-DR/FITC	Thermo Fischer	11-9952-41	(0.06 µg/test)	FACS	Mouse
Mouse IgG1/FITC	Thermo Fischer	11-4714-41	(1 µg/test)	FACS	Mouse
Mouse IgG1/PE	Thermo Fischer	12-4714-41	(0.5 µg/test)	FACS	Mouse
Mouse IgG2a/FITC	Thermo Fischer	11-4724-41	(1 µg/test)	FACS	Mouse

Table 2 Secondary antibodies used in this study.

Antigen	Company	Cat. No.	Dilution or µl/test	Analysis	Source
Mouse IgG/ HRP	DAKO	P026002-2	1:1000	WB	Rabbit
Rabbit IgG /HRP	DAKO	P039901-2	1:1000	WB	Swine
Rabbit IgG /HRP	Zytomed Systems	ZUC0532	50 µl/section	IHC	Not specified
Mouse IgG/HRP	Zytomed Systems	ZUC050	50 µl/section	IHC	Not specified
Mouse IgG /HRP	Vectorlabs	MP-7802	50 µl/section	IHC	Horse
Rabbit IgG /HRP	Vectorlabs	MP-7401	50 µl/section	IHC	Horse

2.2 Primer sequences

The primer sequences used in this study are summarized in Table 3 and were ordered from Thermo Scientific.

Table 3 Primer sequences used for PCR in this study.

Gene Name	NCBI Reference	Forward (5′-3′)	Reverse (5′-3′)
GAPDH	NM_001289745.2	CTCCTGTTCGACAGTCAGCC	TTCCCGTTCTCAGCCTTGAC
ADRA1A	NM_000680.3	CCATGCTCCAGCCAAGAGTT	TCCTGTCCTAGACTTCCTCCC
ADRA1B	NM_000679.3	GTCCACCGTCATCTCCATCG	GAACAAGGAGCCAAGCGGTAG
ADRA1D	NM_000678.3	TGACTTTCCGCGATCTCCTG	TTACCTGCCACGGCCATAAG
ADRA2A	NM_000681.3	TGGTCATCGGAGTGTTCGTG	GCCCACTAGGAAGATGGCTC
ADRA2B	NM_000682.6	GACATTTCACCGGCAACACC	GGGACTGAGAACCAGGAAGC
ADRA2C	NM_000683.3	CGATGTGCTGTTTTGCACCT	GGATGTACCAGGTCTCGTCG
ADRB1	NM_000684.2	TAGCAGGTGAACTCGAAGCC	ATCTTCCACTCCGGTCCTCT
ADRB2	NM_000024.5	CAGAGCCTGCTGACCAAGAA	GCCTAACGTCTTGAGGGCTT
ADRB3	NM_000025.3	GCCAATTCTGCCTTCAACCC	GCCAGAGGTTTTCCACAGGT
COL2A1	NM_001844.4	TTCAGCTATGGAGATGACAATC	AGAGTCCTAGAGTGACTGAG
COL10A1	XM_011535433.3	CCCTCTTGTTAGTGCCAACC	AGATTCCAGTCCTTGGGTCA
RUNX2	XM_011514966.2	GGAGTGGACGAGGCAAGAGTTT	AGCTTCTGTCTGTGCCTTCTGG
SOX9	NM_000346.4	ACACACAGCTCACTCGACCTTG	AGGGAATTCTGGTTGCTCCTCT
TH	NM_000360.3	CAGGCAGAGGCCATCATGT	GTGGTCCAAGTCCAGGTCAG

(El Bagdadi et al. 2019)

2.3 *In vitro* experiments

The study was approved by the Ethics Committee of the University of Regensburg (vote number 13-101-0135) and of the Goethe University Frankfurt am Main (vote number 148-17B).

2.3.1 Patients

The adipose synovial tissue was obtained from 32 patients during knee joint replacement surgery. The characteristics of patients and their medication is summarized in Table 4. All patients gave their informed consent after they were informed about the purpose of the study. In this study patients with non-selective β-AR blocker medication, which is targeting not only β1- but also the β2-AR, were excluded from this study. The experiments were carried out under relevant guidelines and regulations.

Table 4 Characteristics and medication of patients under study.

Characteristics	
Total number	32
Female (number/ %)	12 / 37,5%
Male (number/ %)	20 / 62,5%
Age in years (mean ± std [range])	65.92 ± 9.84 [46-88]
C-reactive protein conc. (mean ± std)	1.48 ± 1.11 mg/l
Medication	**Number / (%)**
Non-steroidal antiinflammatory drugs	31 (97%)
Steroids (other than prednisolone)	n.a.
Opioid analgesics	2 (6.25%)
Biologicals	n.a.
Antihypertensive drugs	19 (59.3%)
Non-selective beta blockers (β1 and β2)	0 (0%)
Selektive beta blockers (β1)	8 (25%)
Other (AT1, ACE, CCB)	11 (34.4%)

Abbreviation: n.a.- not applicable, std. - standard deviation, AT1- angiotensin II type 1 (AT1) receptor blockers, ACE- Angiotensin converting enzyme (ACE) inhibitors, CCB- calcium channel blockers (El Bagdadi et al. 2019)

2.3.2 Isolation of sASCs from adipose syovium tissue

Human sASCs were isolated as described previously (Estes, Diekman, and Guilak 2008). Fresh 1 % (v/v) bovine serum albumin (BSA); (fraction V) was prepared in 1x phosphate-buffered saline (PBS). Collagenase I (Roche) with an enzyme activity of 50-100 U/ml was prepared in 10 ml 1% BSA in PBS. The Adipose synovial tissue was minced into small pieces with a sterile scalpel and placed in a falcon tube. Collagenase I was sterile filtered with a 0.22 µm pore size, low protein binding filter and was added to the tissue followed by incubation for 1 h at 37°C in a water bath till the fat was well separated and settled upwards in the solution. After incubation, the suspension was filtered through 100 µm filter and 10 ml cell culture medium was added to the suspension. Cell culture practice was performed as described previously (Schmitz, 2011). Cell suspension was centrifuged for 5 min at 478 x g and the cell pellet was washed twice in the culture medium. The supernatant was discarded and the cell pellet was resuspended in cell culture medium and incubated in a 125 cm^2 tissue culture flask at 37 °C, 2% O_2 and 5% CO_2. For cell expansion, $1x10^5$ cells/ml were seeded in a 75 cm^2 tissue culture flasks and cultured in Dulbecco's modified Eagle medium (DMEM/F12; Gibco Invitrogen) containing 1% penicillin/streptomycin (Gibco Invitrogen) and 10% MSC qualified

FBS (Gibco Invitrogen) at 37 °C in a humidified atmosphere containing 2% O_2 and 5% CO_2 (Schmitz, 2011).

2.3.3 Determination of viable and dead cells

Cells were stained with trypan blue, which can be used to discriminate between viable and non-viable cells as described previously (Schmitz, 2011; Doyle et al. 1997). Depending on the cell density, cell suspension was diluted 1:5 or 1:10 with PBS. The trypan blue staining was mixed (1:2) with the cell suspension. Cells were counted under phase contrast microscopy using the Neubauer improved cell counting chamber (Schmitz, 2011; Doyle et al. 1997).

2.3.4 FACS Analysis

The investigation of MSC characteristic surface markers on isolated sASCs was performed by FACS analysis (Bonner,1972) according to the suggestions of *The Mesenchymal and Tissue Stem Cell Committee of the International Society for Cellular Therapy* (Dominici et al. 2006). Cells incubated in 75cm^2 flasks were first harvested using 5 ml accutase (PAN-Biotech). FACS protocol was followed as described in: *Direct Immunofluorscence Staining* of Becton and Dickinson bioscience (Holmes et al. 2002). Cells were centrifuged for 8 min at 478 x g. After centrifugation, cells were washed 2 times in 1 ml cold 1xPBS followed by centrifugation at 478 x g for 8 min to obtain the cell pellet. After cell counting, $0.25x10^6$ - $1x10^6$ cells were transferred into FACS tubes and centrifuged. Cell pellet was washed with 1 ml cold 1xPBS and centrifuged (478 x g/ 8 min) and was resuspended in 100 µl cold 1xPBS. Antibodies were added according to Table 1 and incubated for 30 min 4°C in the dark. After incubation cells were washed 2x with cold 1xPBS and then resuspended in 300 µl cold 1xPBS. FACS Analysis was performed with BD FACS calibur system (Holmes et al. 2002).

2.3.5 Cell proliferation assay

Isolated human synovial sASCs were seeded at a cell number of $2x10^5$ in 75 cm^2 tissue culture flasks (Schmitz, 2011). Untreated and NE (Sigma) treated cells were cultured in an incubator (Heracell™ VIOS, Thermo Scientific) at 37 °C in a humidified atmosphere containing 2% O_2 and 5% CO_2. Cells were treated for 7 days with NE at different concentrations (10^{-9}-10^{-6} M). Cell culture medium with or without NE was freshly added at day 0, 3, and 6. After seven days, total viable and dead cell number was determined as described in chapter 2.3.3.

2.3.6 Determination of cell viability LDH

The measurement of Lactate dehydrogenase (LDH) activity is a well-established assay to analyze cell viability (Decker and Lohmann-Matthes 1988; Nachlas et al. 1960). Possible toxic effects of treatments with NE or AR-antagonists were determined by the measurement of

released lactate dehydrogenase according to the manufacturer's instructions (LDH Cytotoxicity Detection Kit; TaKara MK401). LDH was measured in supernatants of monolayer cell cultures at day 7. In addition, LDH in supernatants was analyzed at day 1, 7, 14 and 21 of pellet culture in chondrogenesis assays. For the preparation of the LDH mix, the catalyst (diaphorase/NAD+) was dissolved in 1 ml dH_2O and then diluted 1:45 with the dye solution containing iodotetrazolium chloride (INT) and sodium lactate. For the positive control, 10µl cell suspension was lysed with 1ml Triton X-100 about 5-10 min before incubation with LDH mix. Cell culture medium without cells was used as a negative control and as a blank. Supernatants, positive, and negative controls were added in triplicates (50 µl/well) in a 96-well flat bottom plate. 50 µl of the prepared LDH mix was added into each well and was incubated in the dark for 30 min at room temperature. The optical density of the samples was measured at 490 nm using a microplate reader (Infinite 200 PRO, Tecan).

2.3.7 *In vitro* Chondrogenesis

In vitro chondrogenesis was performed as described earlier (Hennig et al. 2007; Jenei-Lanzl et al. 2014; Johnstone et al. 1998). $2x10^5$ cells/well were seeded in a 96-well plate with conical bottom (Nunc/Fisher Scientific) and pellets obtained by centrifugation (637 x g / 5min). Serum-free high glucose DMEM containing 1% P/S, 100 nM dexamethasone, 200 µM ascorbate-2-phosphate, 10 ng/ml TGF-β3, 10 ng/ml BMP-6 and ITS+3 premix (containing human insulin, transferrin, and sodium selenite) (Sigma) was added into each well and the pellets cultured for 21 days at 37 °C in a humidified atmosphere containing and 2% O_2 and 5% CO_2. Additional supplements were added to the medium as required. Pellets were treated with NE (10^{-9}-10^{-6} M, Sigma) for 21 days. Additionally, pellets were treated with specific α1-AR antagonist doxazosin (10^{-7} M, Tocris), specific α2-AR antagonist yohimbine (10^{-6} M, Tocris), and specific β2-AR antagonist propranolol (10^{-6} M, Tocris Bioscience), alone or in combination with NE (10^{-6} M) for 21 days. The cell culture medium with freshly diluted supplements was changed every two days.

2.3.8 NE quantification with HPLC

The stability of NE was measured in cooperation with the laboratory of Neuroendocrinoimmunology (Department of Internal Medicine I, University Hospital, Regensberg, Germany). The stability of NE in cell culture conditions was investigated by adding a concentration of 10^{-6} M NE to the culture medium in the presence of the antioxidant glutathione (GSH 0.1% or 1%) and cultured at 37 °C in a humidified atmosphere containing 2% O_2 and 5% CO_2. The NE amount was analysed in the cell culture medium at time zero and after 4, 8, 12 and 24 h of culture with high-pressure liquid chromatography (HPLC) of media samples as previously described (Kees et al. 2003; Aguilar and Hearn 1996).

2.3.9 Macroscopic investigations of chondrogenic pellets

A standard binocular with Polaroid PDMC-3 camera was used to take macroscopic images of pellets after 7, 14, and 21 days of chondrogenesis.

2.3.10 Analysis of pellet volume

Macroscopic images were used to analyse the surface areas of spherical pellets (5 pellets/treatment) using ImageJ software. The pellet sphere volume was calculated using the formula for the volume of a sphere and the determined average radius.

2.3.11 Homogenization and enzymatic digestion of pellets

To analyse the concentration of dsDNA, sGAG, and type II collagen at day 21 of chondrogenesis, pellets were homogenized as described previously (Jenei-Lanzl, 2010). Four replicate pellets from each treatment were homogenized in 200 µl of 0.05 M acetic acid plus 0.5 M NaCl (pH 2.9–3.0) and mechanically homogenized using a Polytron PT-1200 homogenizer (Kinematica). The pellets were digested with 25 µl of pepsin (10 mg/ml, Sigma) overnight on the rotator (Loopster digital rotator, IKA) at 4°C. On the next day, 25 µl of pepsin was again added to the pellets and digestion was continued for 24 h on the rotator at 4 °C. After that, 50 µl 10xTBS was added and the pH value was adjusted to 8.0 with 1 N NaOH. The pellets were then digested with 50 µl elastase (1 mg/ml, Sigma) on the rotator for 24 h at 4 °C (Jenei-Lanzl, 2010). The solution was centrifuged at 10000 x g for 5 min and the supernatant was frozen down at -80 °C for the analysis of double-stranded DNA (dsDNA), sGAG and type II collagen. 10 mg/ml of chondroitinsulfate (Sigma) was also digested in the above manner and the solution was used for serial standards in the DMMB-assay for the quantification of sGAG.

2.3.12 dsDNA quantification

After homogenization and digestion of the samples, the dsDNA concentration was determined using the Quant-iT PicoGreen assay kit (Invitrogen) according to the manufacturer's instructions. Samples were diluted 1:30 with the assay buffer (10 mM Tris-HCl, 1 mM EDTA, pH 7.5). Serial standard solutions were prepared (1; 0.5; 0.25; 0.125; 0.0625; 0.0315 µg/ml) using the assay buffer. PicoGreen reagent was diluted 1:200 with the assay buffer followed by loading the samples and standards in triplicates (100 µl/well) in a flat bottom 96-well plate. The fluorescence values were measured using a fluorescence microplate reader (Infinite 200 PRO, Tecan; excitation: 480 nm, emission: 520 nm).

2.3.13 Biochemical analysis of sGAGs

Concentration of sGAG was obtained as described previously (Farndale, Buttle, and Barrett 1986; Chandrasekhar, Esterman, and Hoffman 1987) using a colorimetric reaction with DMMB. The ability of the DMMB assay to detect sGAG is based on the characteristic colour shift of the cationic DMMB dye from blue to violet when it binds polyanionic substrates such as sGAG (Zheng and Levenston 2015). One litre of the DMMB reagent was prepared by dissolving 18mg DMMB (Sigma) in 5 ml absolute Ethanol with 2 mg formic acid and 2 g sodium formate (pH~3). Digested chondroitin sulfate solution was used to prepare the standard solution followed by serial dilutions in dH_2O to prepare the standards (40; 20; 10; 5; 2.5; 1.25; 0.625 µg/ml). In a flat bottom 96-well plate, 50 µl digested sample (diluted 1:15 in dH_2O) and standards were loaded in triplicates. 200µl of DMMB reagent solution was added to each sample/well. Optical density was measured at 595 nm using a microplate reader and the sGAG content was obtained normalized to the dsDNA content.

2.3.14 Biochemical analysis of type II collagen

ELISA (Rehm, 2006; Kemeny 1994) was used to analyze the type II content in the pellets of chondrogenesis assay after 21 days. Type II collagen was quantified using ELISA (Chondrex, Redmond, WA) according to the manufacturer's instructions. The capture antibody was pre-coated overnight at room temperature. Standards solutions (200; 100; 50; 25; 12.5; 6.25; 3.13 ng/ml) were prepared and samples were diluted 1:5 in assay buffer. 100 µl of standards and samples were loaded in triplicate in a flat bottom 96-well plate. After 5x washing of the plate, 100 µl of the biotinylated antibody was added and the plate incubated for 1 h at room temperature. After 5x washing of the plate, 100 µl of streptavidin peroxidase solution was added into each well and further incubated for 1 h at room temperature. After 5x washing, 100 µl of substrate solution (o-Phenylenediamine) was added and incubation continued for 30 min at room temperature. The reaction was stopped with 50 µl of 2 M sulfuric acid and the optical density was measured at 490 nm in a plate reader.

2.3.15 Fixation and sectioning of pellets

Pellets from the chondrogenesis assay were fixed after 7, 14, and 21 days in 4% paraformaldehyde overnight at room temperature. Pellets were infiltrated with PBS and then with increasing sucrose concentrations (10, 20 and 30%), for 1 day at each concentration (Bancroft, 2019). The pellets were finally embedded in Tissue-Tek (Sakura) and sectioned at a thickness of 8 µm using a cryotom (Thermo Scientific Cryostar NX70).

2.3.16 Immunohistochemistry of sASC pellets

Cryosections were rehydrated for 5 min in 1 x PBS. For adrenergic receptor stainings, epitope retrieval was performed using 10 mM sodium citrate (0.05% tween 20, pH 6) for 20 min at 95°C (Bancroft, 2019). For type II collagen stainings, sections were digested with 1mg/ml pepsin (Sigma) in 1x McIlvaine buffer (McIlvaine,1921) with a pH 3.6 for 12-15 min at 37°C. Endogenous alkaline phosphatase and peroxidase were blocked with Bloxall blocking solution (Vectorlabs) for 10 min at room temperature. The sections were then incubated with primary rabbit antibodies directed against α2a AR, β2-AR, and type II collagen at 4°C overnight. Secondary HRP-antibody (Vectorlabs) incubation was performed for 45 min at room temperature and specific staining was detected using peroxidase substrate solutions (Vectorlabs).

2.3.17 Staining of sulphated proteoglycans

To detect sulphated glycosaminoglycans in the cartilage, sections were stained with 1,9-dimethyl-methylene blue (DMMB, Sigma-Aldrich, Munich, Germany) for 3-4 min and then mounted in Kaiser´s glycerol gelatine (Jenei-Lanzl, 2010). The amount of sGAG synthesized is proportional to the colour change of DMMB from blue to purple.

2.3.18 Microscopy analysis

Nikon Eclipse Ti microscope was used for microscopy analysis using Nis Elements program (version: 3.07).

2.3.19 Protein extraction for western blot analysis

Proteins were extracted using PhosphoSafe™ Extraction Reagent (Merck Millipore) according to the manufacturer's instructions. Proteins were extracted from cells which were cultured in monolayer and from chondrogenic pellets. Lysis of $2x10^5$ cells was performed with 200 µl extraction reagent. For the protein extraction from chondrogenic pellets, 5 replicate pellets were mechanically homogenized (on ice) in 200µl extraction reagent using Polytron PT-1200 (Kinematica) homogenizer. Cell lysate was centrifuged for 20 min at 4°C, 11000 x g and supernatant was transferred into new tube. 50 µl of 4x SDS sample buffer (NuPAGE, Thermo-Fischer), containing 10 % β-mercaptoethanol was added to each cell lysate and homogenized with a 29 g syringe *(*BD SafetyGlide) and the samples were stored at -80 °C.

2.3.20 Western blot analysis

After treatments with NE in monolayer culture or in the chondrogenesis assay, the phosphorylation of PKA and ERK1/2 were explored as two major AR-dependent signalling pathways. Proteins were separated based on molecular weight in a 10 % sodium sodecyl

sulfate (SDS) polyacrylamide gel (Laemmli,1970). The SDS gels were prepared as described in Table 5. In a gel chamber, 4.5 ml separating gel was filled and layered with isopropanol. After the separating gel polymerized, isopropanol was removed and stacking gel was added and a comb placed immediately into the gel.

Table 5 SDS Gel contents.

10% Separating Gel		**4%Stacking Gel**	
2.4 ml	H_2O	1.3 ml	H_2O
1.25 ml	40 % Acrylamide	0.2 ml	40 % Acrylamide
1.25 ml	1.5 M Tris pH 8,8	0.5 ml	1.5 M Tris pH 6,8
50 µl	10 % APS	20 µl	10 % APS
5 µl	TEMED	2 µl	TEMED

Protein samples were heated at 70 °C for 10 min. 25 µl of protein samples were loaded along with an unstained protein molecular weight marker (Thermo Fisher Scientific) on 10 % SDS gel. Gels were run for 75 min at 150 V with 1X running buffer (25 mM Tris, 192 mM glycine and 0,1 %(v/v) SDS) and Western blotting (Towbin, 1979) was performed. Proteins on the gel were electrotransfered to a polyvinylidene difluoride membrane (GE Healthcare) for 1 h at 200 mA with 1x transfer buffer (25 mM Tris, 192 mM glycine, 0,1% SDS, 20% methanol). Membranes were blocked with 5% BSA in 1x TBS for 1 h at room temperature followed by incubation with 5 ml primary antibodies (ERK, pERK, PKA, pPKA, GAPDH) diluted in 1% BSA in 1x tris-buffered saline buffer (TBS;150 mM NaCl, 10 mM Tris pH 8.0) for 16 h at 4 °C. After 4x washing with 1x TBS buffer, membranes were incubated with an HRP-conjugated secondary antibody (1% BSA in 1x TBS) for 1h at room temperature. After 4 x washing with 1x TBS-T (0.1 % Tween 20, target proteins were detected using the enhanced chemiluminescence (ECL) reagent. GAPDH was used as an endogenous loading control. Bands were detected and images were acquired using Molecular Imager® ChemiDoc™ XRS+ with Image Lab™ Software (Version 5.2.1 build 11, Bio-Rad Laboratories). Densitometric values of the detected bands were quantified using the Image J Software.

2.3.21 RNA extraction

RNA isolation was performed using the NucleoSpin RNA kit (Machrey Nagel) according to the manufacturer's instructions. Genomic DNA was removed by DNase I treatment according to the manufacturer’s instructions. RNA was measured using NanoDrop™ ONE spectrophotometer (Thermo Fisher).

2.3.22 cDNA synthesis

cDNA synthesis was performed using qScript cDNA Supermix (Quanta Biosciences). One microgram of total RNA was used for cDNA synthesis using qScript cDNA Supermix containing qScript reverse transcriptase, buffer, dNTPs, MgCl2, primers, and RNase inhibitor protein. The reactions were incubated for 5 min at 25 °C, 30 min at 42 °C, 5 min at 85 °C and held at 4 °C using PCR Thermocycler (Analytik, Jena).

2.3.23 PCR

All primers used in this study are shown in Table 3. Adrenergic receptor expression was analysed by reverse transcription polymerase chain reaction (RT-PCR) (Sambrook, 2001) using TaqPCR Master Mix Kit (QIAGEN, Hilden, Germany). For RT-PCR, 10 ng cDNA was added to the TaqPCR Master Mix. Primers were added to the reaction mix (final concentration of each primer 0.2 µM) and PCR was performed using qTOWER^3 real time PCR Thermocycler (Analytik Jena) under the thermal cycling profile at 94 °C/3 min followed by 95 °C/30 s, 66°C/30 s, and 72 °C/1 min for 36 cycles. PCR products were loaded onto a 1.8% agarose gel which was stained with GelRed Nucleic Acid Gel Stain (Biotium, Fremont, CA, USA). The gel was run for 1.5 h at 110 V. Bands were detected with Molecular Imager® ChemiDoc™ XRS and with the Image Lab™ software (Version 5.2.1 build 11, © Bio-Rad Laboratories).

Gene expression of chondrogenic markers (*SOX9, COL2A1*) and hypertrophic markers (*RUNX2* and *COL10A1*) were obtained by real-time quantitative PCR (Sambrook, 2001). 10 ng cDNA was used for each reaction and qRT-PCR was performed using Quanta PerfeCta SYBR Green FastMix (Quanta Biosciences). The final primer concentration was 1 µM. The reactions were incubated with the thermal cycling profile: 95 °C/3 min followed by 95 °C/15 s, 60 °C/30 s, and 72 °C/30 s for 40 cycles, using qTOWER^3 real time PCR Thermocycler. Expression data were obtained according to the standard ($2^{-\Delta\Delta Ct}$) method with GAPDH as a housekeeping gene (Livak and Schmittgen, 2001) using qPCRsoft 3.4 software (Analytik Jena).

2.4 *In vivo* experiments

2.4.1 Animals

Male C57BL/6J mice at an age of ten weeks were purchased from Janvier Laboratories (Le Genest St. Isle, France) and housed at 5 animals per cage. Mice were kept under standard animal housing conditions with a 12-hour light/dark cycle and unrestricted access to standard food and water. Animals were allowed to adapt for 2 weeks before use in any experiment. Adrb2$^{-/-}$ mice were kindly offered by the laboratory of Prof. Susanne Grässel (Department of Orthopedic Surgery, Experimental Orthopedics, Regensburg) and housed in the same way. All experiments were approved by the institutional and governmental regulations for experimental animal usage (Ethical Review Committee, Government of Unterfranken, GZ 55.2-2532-2-368) and were conducted according to the set guidelines.

2.4.2 Peripheral sympathectomy

At an age of 12 weeks, mice were sympathectomized peripherally by intraperitoneal injections of 80 mg of 6-hydroxydopamine (6-OHDA, in 0.1 % ascorbic acid, Sigma-Aldrich, Munich, Germany;) per kilogram body weight at three consecutive days beginning three days before DMM surgery as described previously (Harle et al. 2005). The neurotoxin 6-OHDA destroys sympathetic nerves selectively. Only the peripheral sympathetic nerve fibers are eliminated by 6-OHDA without affecting any central nervous function as 6-OHDA is not able to pass the blood-brain barrier in mature animals (Kostrzewa and Jacobowitz 1974). In order to maintain sympathectomy, the injection was repeated every two weeks until termination of experiments (2, 4, 8 or 12 weeks post-DMM surgery).

2.4.3 OA induction

Mice were divided into 4 groups: WT DMM, Syx DMM, WT sham, and Syx sham. Eight mice were used for the histological analysis at 2, 4, 8 and 12 weeks post surgery and 5 mice were used for each group at 8 weeks after surgery for the micro-CT analysis. The surgical DMM model was utilized to induce OA on the right knee by the transection of the meniscotibial ligament. Sham surgery was performed by opening the joint capsule without transecting the medial meniscotibial ligament (Glasson, Blanchet, and Morris 2007). The starting time point of DMM surgery was one day after the third injection of 6-OHDA in Syx mice (day 0 of the DMM timeline). All animals were 12 weeks old when operated. Analgesia and anesthesia protocols were followed according to Muschter et al. 2020. Before surgery, mice were under anesthesia with an intraperitoneal injection of ketamin-hydrochloride (90-120 mg/g body weight; Medistar Arzneimittelvertrieb GmbH) and xylazin (6-8 mg/g/body weight; Serumwerk), which led to a stable anesthesia after approximately 20 min. During the anesthesia period,

Bepanthen creme (Bayer) was applied on the eyes to prevent them from drying out. After surgery, the cage with the animals was placed in front of a heat lamp to prevent them from cooling down. For post-surgery treatment, mice were given subcutaneous analgesia (buprenorphine in 0.9 % NaCl solution, 0.1 mg/g body weight; Buprenovet, Bayer Vital GmbH, Leverkusen, Germany). Mice were sacrificed by asphyxiation with CO_2 after 2, 4, 8 and 12 weeks. 1-2 ml blood were immediately collected via cardiac puncture for serum analyses. Blood samples were allowed to stand for 30 min at 4 °C before centrifugation for 10 min at 1000 x g. The serum was removed and stored at -80 °C. Body weight and harvested spleen weight were determined. The harvested spleen was immediately stored at -80 °C. Legs were harvested for histological and for micro-CT analysis and fixed as described in detail in the chapters 2.4.5 and 2.4.11.

The age at surgery time and the number of Adrb2$^{-/-}$ mice were the same as for WT and Syx mice. The sham and DMM surgery and medication of Adrb2$^{-/-}$ mice were performed in the same way as in WT and Syx mice. Eight weeks after DMM or sham surgery, the animals were sacrificed. After determination of body and spleen weight, legs were harvested for histological and for micro-CT examinations.

2.4.4 Analysis of sympathectomy efficiency

The efficiency of sympathectomy was analyzed by the measurement of NE in spleen samples, which were taken from DMM-operated, and sham- operated mice (2, 4, 8 or 12 weeks post-surgery) via HPLC as described before (Härle et al. 2008). This was performed in cooperation with the Institute of Pharmacy, University of Regensburg. To exclude possible effects of sham surgery, spleen samples of healthy, non-operated mice, with or without sympathectomy, were analyzed. The absence of sympathetic nerves in the synovium of Syx mice was confirmed by immunohistochemical staining for TH.

2.4.5 Fixation for histology of knee joints

Harvested mice legs were fixed in 4% paraformaldehyde overnight and then washed in 1x phosphate-buffered saline (1xPBS) for 24 h. The knee joints were decalcified in 10 % tris-ethylenediaminetetraacetic acid (EDTA) for 10-14 days (Bancroft, 2019). Decalcified limbs were embedded in paraffin in frontal orientation. Serial sections of 8 µm thickness were cut using a microtome (Leica RM2235).

2.4.6 Immunohistochemical analysis of mice joint tissues

Sections of mice limbs were digested with pepsin (516360, Merck) (0,025 % in 0,2 N hydrochloric acid), hyaluronidase (H3506, Sigma-Aldrich) (500 U/ml) and proteinase K (19133, Qiagen; (10 µg/ml) for type II collagen and MMP-13 staining. To prevent non-specific binding of antibodies, blocking was performed using Zytomed Blocking Solution (ZUC007-100, Zytomed). The sections were then incubated with the primary anti-type II collagen antibody or anti-MMP13 antibody. Sections stained for type II collagen were incubated with the secondary anti-mouse antibody (Zytomed) and those for MMP-13 were incubated with the secondary anti-rabbit antibody (Zytomed). Detection was performed using 0.05 % 3,3'-diaminobenzidine (DAB; Fluka), (Bancroft, 2019).

2.4.7 Immunohistological staining for TH and ARs in joint tissues

The expression of TH and α2A-AR and β2-AR were analyzed in joint tissues of WT and Syx mice by immunohistochemistry. Non-specific bindings of antibodies were blocked with 2.5 % normal horse serum blocking solution (Vectorlabs). Sections were incubated with primary antibody for TH, α2A-AR and β2-AR followed by incubation with secondary HRP-Anti-Rabbit antibody (Vectorlabs). Detection was performed using chromogenic substrate 3-amino-9-ethylcarbazole (AEC) for TH and for α2A-AR and β2-AR with 0.05 % DAB followed by counterstaining with hematoxylin (Merck), (Bancroft, 2019).

2.4.8 OARSI scoring

Cartilage lesions are most apparent in the central weight-bearing region of the medial tibial plateau post DMM surgery. Therefore, the OA severity was analysed in this region and evaluated using a standardized histopathological assessment of cartilage degeneration of the Osteoarthritis Research Society International (OARSI) as described before (Pritzker et al. 2006). According to OARSI scoring, OA severity is divided into five grades (Grade 0: cartilage surface intact, cartilage and cells intact; Grade 1: intact surface, cell death; Grade2: surface discontinuity, fibrillation through superficial zone; Grade 3: vertical fissures; Grade4: erosion, Grade 5: denudation).

Six DMMB-stained sections in 80 µm intervals from each mouse (8 in total) per time point were taken and scored by three blinded observers and their scores were averaged. The number of mice for each time point in the resulting figures varied between 5-8 due to artifacts in the sections.

2.4.9 Synovitis scoring

The synovitis score was determined by analyzing two features of synovitis: the enlargement of lining layer and cellular density of the sublining layer of the synovium. To obtain the synovitis

score, DMMB-stained sections were taken from six mice at each time point. The enlargement of the synovial lining layer was graded semi-quantitatively from 0 to 3 (0 points: the lining cells form one layer; 1 point: the lining cells form 2–3 layers; 2 points: the lining cells form 4–5 layers; 3 points: the lining cells form more than 5 layers) (Krenn et al. 2006). The density of the resident cells in the synovium was analysed in defined regions of interest as described before (Krenn et al. 2006). Cells were counted in the defined region and cellular density was graded from 0-3 (0 points: shows normal cellularity ≤ 20 cells; 1 point the cellularity is slightly increased ≤ 50 cells; 2 points: shows cellularity ≤ 100 cells; 3 points the cellularity is greatly increased ≤ 150). Scoring of the sections was performed by three blinded observers and their scored were averaged. The sum of the scores for synovial lining layer and synovium cell density were interpreted as follows: 0: no-; 1: mild-; 2: moderate-; and 3: severe synovitis. In addition, the thickness of the synovium was measured using the NIS-Elements (Nikon) imaging software.

2.4.10 CTX-II quantification by ELISA

Cartilage degeneration was further analyzed by the measurement of serum levels of CTX-II, an OA-specific degradation fragment of type II collagen (Garnero and Delmas 2003), by using ELISA as described previously (Rehm, 2006; Kemeny 1994). The serum CTX-II concentration was determined in WT and Syx mice with the Linked C-telopeptide of Type II Collagen ELISA (Biomatik) according to the manufacturer´s protocol. The specific CTX-II antibody was pre-coated onto a microplate over night at RT. Standards and serum samples (diluted 1:50 with the sample diluent) were pipetted into the wells. After 4x washes to remove any unbound substances, a specific biotin-conjugated antibody for CTX-II was added to the wells. After further 4x washes, the avidin conjugated HRP was added to each well. After final washes, substrat solution (3,3',5,5'-Tetramethylbenzidine) was added and the color development was stopped with the stop solution containing sulphuric acid. The optical density of the wells was measured using a microplate reader (Infinite 200 PRO, Tecan) at 450 nm.

2.4.11 Micro-CT analyses

The knee joints harvested 8 weeks after surgery were fixed for 16 h in 4 % paraformaldehyde and stored in 70 % ethanol at 4 °C. Subchondral bone plate (SCBP) thickness, bone surface (BS) and bone mineral density (BMD) of meniscal ossicles, osteophyte formation, and the calcified cartilage thickness (CC) were all analysed using the 3D-reconstructed models in cooperation with the Clinic for Trauma Surgery, Orthopedic Surgery and Plastic Surgery, Universitätsmedizin Göttingen. The knee joints were scanned using a Scanco µCT 50 (Scanco Medical, Brüttisellen, Switzerland) device and images were acquired at 90 kVp, 88 µA, 3.4 µm voxel size. The length of the medial condyle was measured as an indicator for osteophyte

formation. The Scanco's OpenVMS software was used for the measurement of all the parameters. Subchondral bone parameters were further analyzed in cooperation with the microCT facility of the RCBE (Regensburg Center of Biomedical Engineering) at the University of Applied Sciences Regensburg. For this purpose, the knee joints were scanned in air using Phoenix v tome XS computer tomograph (GE Sensing & Inspection, Boston, MA, USA) and an x-ray voltage of 35 kV and x-ray current of 270 µA at 20-fold magnification and 10 µm voxel size. To visualize the micro CT-data, the VGStudio MAX 2.4.0 software (Volume Graphics, Heidelberg, Germany) was used. The medial subchondral bone paramaters: Bone volume to total volume ratio (BV/TV), bone surface to bone volume ratio (BS/BV), trabecular thickness (TbTh), trabecular number (TbN), as well as trabecular space (TbSp) were analyzed in the medial subchondral bone using the myVGL 3.0 software (Volume Graphics, Heidelberg, Germany). The volume of interest (VOI) was adjusted in the medial subchondral bone compartment of the tibia as previously described (Das Neves Borges, Vincent, and Marenzana 2017).

2.4.12 Tartrate-resistant acid phosphatase (TRAP) staining

In order to determine osteoclast activity, TRAP activity was detected histologically as described in a previous protocol (Blumer et al., 2012) with minor modifications. The sections were incubated for 45 min at 37 °C in a freshly prepared TRAP staining solution containing 0.1 M sodium acetate, 50 mM sodium L-tartrate, 1.6 mM Fast Red Violet LB salt, 0.3 mM Naphthol AS-MX phosphate and 0.5 % (v/v) 2-ethoxyethanol. After washing in dH_2O, sections were mounted in Kaiser´s glycerol gelatine.

2.4.13 Statistical analysis

Statistical analysis was performed using SigmaPlot software (SigmaPlot V.13, Systat Software, Erkrath, Germany). Comparisons between groups were performed using one-way-ANOVA or ANOVA on ranks or Wilcoxon/Mann–Whitney-Test followed by Bonferroni or Student-Newman-Keuls Method. For comparisons between 2 groups or timepoints t-test was performed. Linear regression curves were generated and Spearman´s correlation coefficient was used to assess strength of relationship. P-values less than 0.05 were considered significant.

2.5 Programs

2.5.1 CorelDraw

For the generation of figures in this study the graphic software CorelDraw (version X8; https://www.coreldraw.com/) was used.

2.5.2 Endnote

The reference management software Endnote (version X8; https://www.endnote.de) was used for the management of references in this study.

2.5.3 Pubmed

For the search of articles and publications PubMed database of the National Center for Biotechnology Information (NCBI; https://www.ncbi.nlm.nih.gov/pubmed) was used in this study.

2.5.4 Image J

For the quantification of densitometric values of the western blot bands Image J software (version: 1.8.0; https://imagej.nih.gov/ij/) was used.

3 Results

This study aimed to analyze the effects of sympathetic activity on OA progression. For this purpose, both *in vitro* and *in vivo* experiments were performed. The *in vitro* part focused on the effect of NE on chondrogenic differentiation of sASCs, and the *in vivo* part addressed the influence of peripheral sympathectomy on OA progression using a murine experimental OA model.

3.1 NE effects on the chondrogenesis of OA sASCs

3.1.1 sASCs express MSC characteristic markers

The chondrogenic differentiation of sASCs was examined *in vitro* using sASCs isolated from the adipose synovial tissues of osteoarthritic patients undergoing knee replacement surgery. The stem cell characteristic surface markers were examined first using fluorescence-activated cell sorting (FACS) (Figure 11A). The surface markers CD73, CD90, and CD105 were expressed by >90% of sASCs while HLA-DR, CD11b, CD19, CD34, and CD45 were not expressed by them (Figure 11B). This ensures that the isolated cells from synovial tissues possess the minimal MSC characteristics proposed by the Mesenchymal and Tissue Stem Cell Committee of the International Society for Cellular Therapy (Dominici et al. 2006).

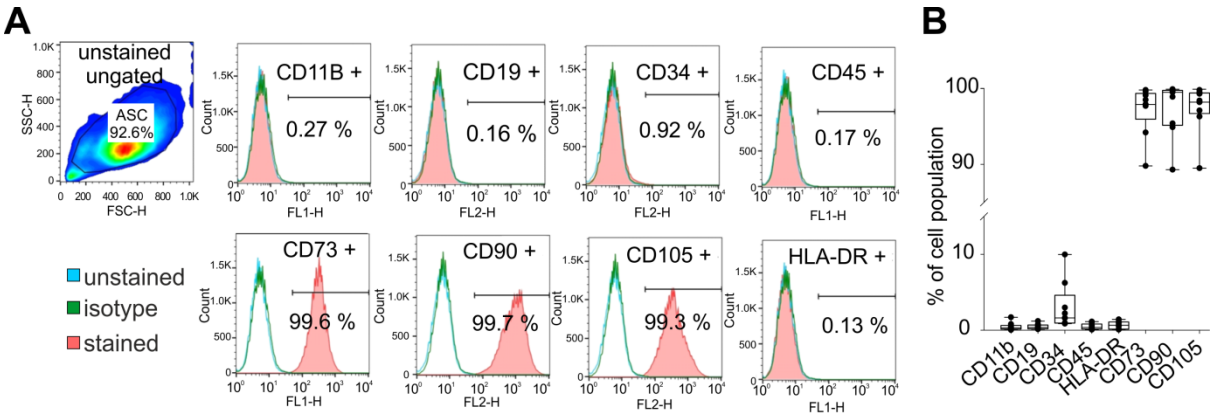

Figure 11 Analysis of MSC-specific surface markers of sASCs.
(A) Human sASCs derived from OA patients were positive for CD73, CD90, and CD105 and were negative for CD11b, CD19, CD34, CD45 and HLA-DR using FACS analysis (blue line - unstained negative control, green line -isotype control, red line - the target surface marker). (B) Quantification of MSC-specific marker expression on sASCs. Data are presented as box plots, where the boxes represent the 25th to 75th percentiles, the lines within the boxes represent the median, and the lines outside the boxes represent the 10th and 90th percentiles. Each black circle represents the mean of 3 replicates of an individual patient (n=8). Abbreviations: SSC-H – side scatter height, FSC-H – forward scatter height, FL1 – fluorescence. (El Bagdadi et al. 2019)

3.1.2 sASCs differentiate to chondrogenic phenotype

To investigate the potential of sASCs to differentiate into chondrocytes, *in vitro* chondrogenesis assay was performed. Within one day, cells underwent cellular condensation and pellet formation (Figure 12). The pellets had a nodular morphology characteristic of increased sGAG synthesis, which was confirmed histologically by the metachromatic DMMB staining. Additionally, an increase of type II collagen protein synthesis was observed histologically from day 1 until day 21 (Figure 12A). The chondrogenic potential of sASCs was also confirmed by analyzing the gene expression of the two major chondrogenic markers *SOX-9* and *COL2A1* (Figure 12B). The gene expression of *SOX-9* and *COL2A1* increased significantly from day 1 to day 21 post initiation of chondrogenesis.

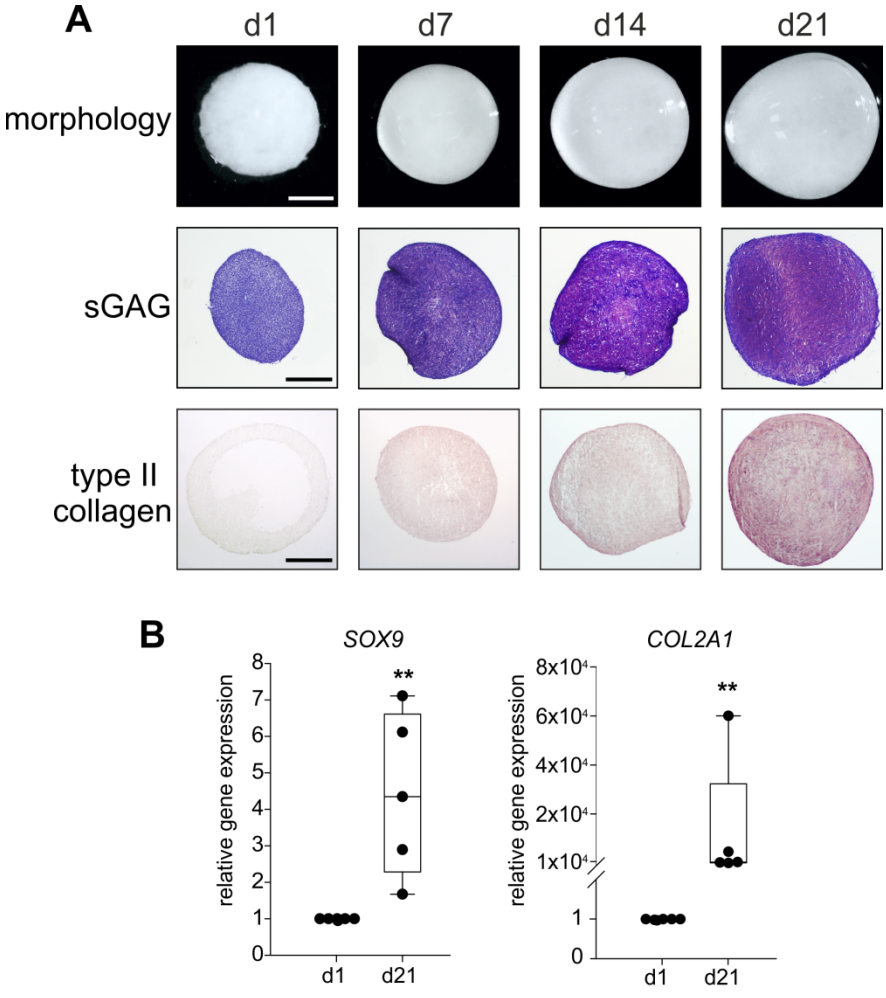

Figure 12 Analysis of chondrogenic differentiation capacity of sASCs.
(A) Morphology, sGAG and type II collagen analysis of untreated sASC pellets at d1, d7, d14 and d21 of differentiation (bars: 500 µm). (B) Relative gene expression of *SOX9* and *COL2A1* in untreated sASCs pellets 21 days after intitiation of chondrogenesis (*SOX9* gene expression on d21 compared to d1: p= 0.009; *COL2A1* gene expression on d21 compared to d1: p=0.008. Data are presented as box plots, where the boxes represent the 25th to 75th percentiles, the lines within the boxes represent the median, and the lines outside the boxes represent the 10th and 90th percentiles. Each black circle represents an individual patient (n=5-6). (El Bagdadi et al. 2019)

3.1.3 sASCs express several α- and β-AR subtypes

Since the presence of ARs on the cell is a prerequisite for its response to NE, gene expression of AR was investigated, (Figure 13A). Synovial ASCs in monolayer culture expressed α1B, α2A-, α2B-, α2C-and β2-AR. While α2C- and β2-AR were highly expressed, the receptor subtypes α1B-AR, α2A-AR, and α2B-AR were expressed only moderately. The AR subtypes α1A-, α1D-, β1-AR, and β3-AR were not detected. TH, the key enzyme of NE synthesis was not expressed either, suggesting that the autocrine effects of cells by producing NE or other neurotransmitters can be excluded. After chondrogenic differentiation, the AR subtypes: α1A-, α1B-, α2A-, α2B-, α2C-, β1- and β2-AR were expressed, whereas AR subtype α1D, β3-AR and TH were not detectable (Figure 13B). The most prominent receptor subtypes α2A-AR and β2-AR, with opposing downstream signalling pathways, were also stained immunohistochemically to confirm their expression at the protein level (figure 14). Both α2A-AR and β2-AR were detected at each time point during chondrogenesis, suggesting that cells undergoing chondrogenesis can respond to NE. No age-, gender-, or medication-dependent effects regarding AR expression were observed either in monolayer or in pellet cultures.

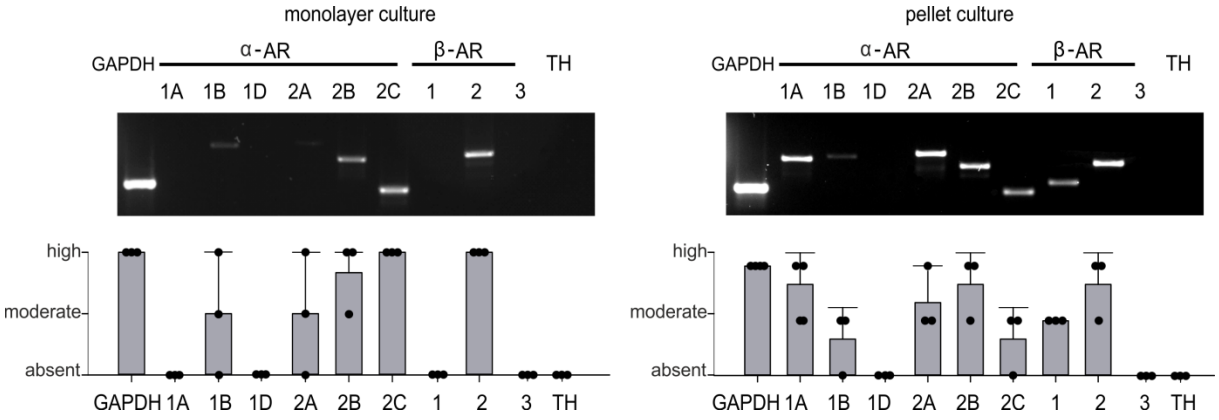

Figure 13 Adrenergic receptor (AR) and tyrosin hydroxylase (TH) expression of sASCs.
(A) RT-PCR of AR and TH gene expression in untreated sASCs and average score of AR and TH gene expression in monolayer culture. (B) RT-PCR of AR and TH gene expression in untreated sASCs and average score of AR and TH gene expression in pellet culture at day 21 day of chondrogenesis. Data are presented as means ± standard deviation in vertical bars. Each black circle represents an individual patient (n=3-4). (El Bagdadi et al. 2019)

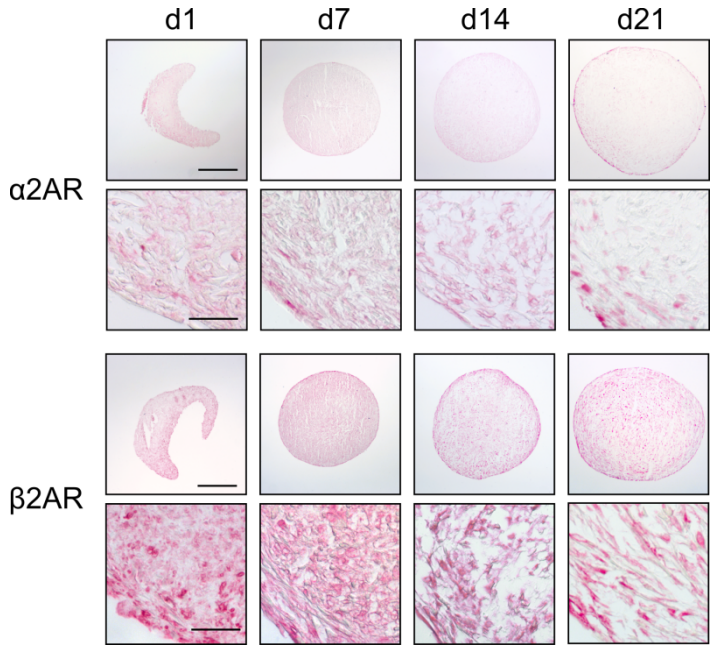

Figure 14 Immunohistochemical detection of α2A-AR and β2-AR during sASCs chondrogenesis. α2A-AR and β2-AR are expressed in sASCs on day 1, 7, 14, and 21 of chondrogenic differentiation (bars: 500 µm in upper panels and 50 µm in lower panels). (El Bagdadi et al. 2019).

3.1.4 Stability of NE in cell culture medium

In order to analyse possible instabilities of NE in the cell culture medium, HPLC was performed using a solution of glutathione (GSH), which is an antioxidant with long half-life (Yamamoto and Ishihara 1994). Norepinephrine in the cell culture medium was reduced to 40-50% of the initial concentration in the presence of glutathione (0,1 % or 1%) after 24 h (Figure 5). These findings revealed that NE is not stable under cell culture conditions and indicate that the initially applied NE concentrations rapidly decrease after media change and that a reduced NE concentration is acting during chondrogenesis.

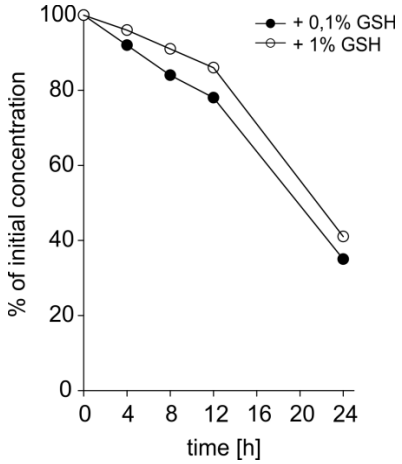

Figure 15 Stability of NE in cell culture medium.
NE stability was measured for 24 h in the presence of the antioxidant glutathione (GSH 0.1% or 1%). (El Bagdadi et al. 2019)

3.1.5 NE activates the ERK1/2 signalling pathway

After assessing the expression ARs in sASCs, it was examined whether these cells respond to NE by activating the two major AR-dependent pathways namely PKA and ERK1/2 signaling pathways. To this end, western blot analysis of sASCs treated with 10^{-6} M and 10^{-8} M NE in monolayer culture was performed (Figure 16A). NE treatment with 10^{-6} M and 10^{-8} M for 15 min resulted in ERK1/2 phosphorylation, compared to untreated (0 min) cells. In contrast to elevated phosphorylation of ERK1/2 by NE, there was no influence on phosphorylation of PKA by NE when compared to untreated cells (Figure 16A). Results obtained by western blot showed that the ERK1/2 signalling and not PKA is induced by NE treatment. Additionally, chondrogenic pellets treated with NE (10^{-9}–10^{-6} M) for 21 days were analysed by western blot at the end-point (Figure 16B). ERK1/2 phosphorylation increased dose-dependently by NE treatment and significantly by 10^{-6} M NE, suggesting that NE signalling is mediated by β2-AR (Figure 16C). No differences between ratio of total and phosphorylated PKA were detected between untreated and NE treated pellets as in monolayer cultures. However, the levels of total and phosphorylated PKA were reduced in untreated pellets, while GAPDH level was similar in all groups (Figure 16B). These findings demonstrate that NE activates the ERK1/2 signalling pathway but not the PKA pathway.

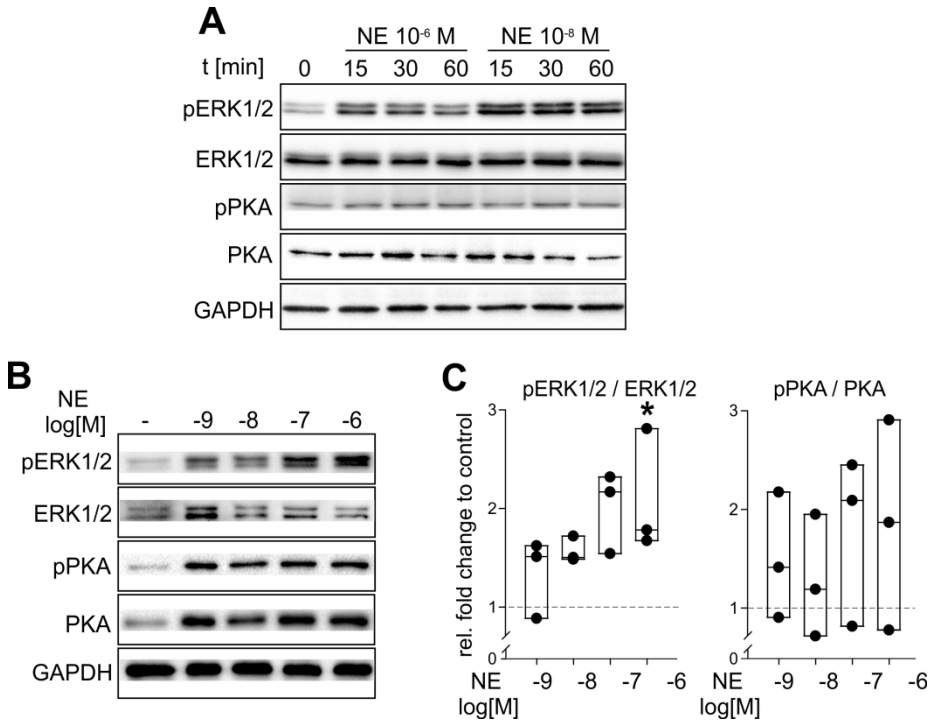

Figure 16 NE-mediated activation of the PKA and ERK1/2 signaling pathways.
(A) Western blot analysis of total and phosphorylated ERK1/2 and PKA of monolayer sASC culture in the absence or presence of NE (10^{-8} M and 10^{-6} M, representative blot of one OA patient). GAPDH was used as an endogenous loading control (B) Western Blot analysis of total and phosphorylated ERK1/2 and PKA of chondrogenic sASC pellets at day 21 of chondrogenesis in the absence or presence of NE (10^{-9}- 10^{-6} M, representative blot of one OA patient). GAPDH served as an endogenous loading control. (C) Relative fold change of total and phosphorylated ERK1/2 and PKA of sASC pellets at day 21 of chondrogenesis in presence of NE (10^{-9}- 10^{-6} M) compared to untreated group (NE10^{-6} compared to control p= 0.034. Data are presented as box plots, where the boxes represent the 25th to 75th percentiles, the lines within the boxes represent the median, and the lines outside the boxes represent the 10th and 90th percentiles. Each black circle represents a individual patient (n=3). Significant p-values against untreated control are presented as * p<0.05. (El Bagdadi et al. 2019)

3.1.6 NE did not influence sASC proliferation

After confirming gene and protein expression of NE binding ARs in sASCs (Figure 13) possible cytotoxic effects of NE treatment on proliferation and cell viability were examined. It was previously reported that the number of stem cells in the cartilage increased in OA compared to healthy cartilage and that NE is present in the osteoarthritic synovial fluid (Jenei-Lanzl et al. 2014). The effect of NE on proliferation and viability of sASCs was therefore investigated in both monolayer and pellet culture (Figure 17). In monolayer culture, sASCs were treated with different concentrations of NE (10^{-9}–10^{-6} M) for seven days (Figure 17A). There were however no differences in total or dead cell count between untreated and NE treated monolayer cultures, indicating that NE had no impact on cell proliferation (Figure 17A). Similarly, NE did not affect cell viability as determined by the LDH assay (Figure 17B). As expected, markedly increased LDH activity was observed in the dead cell control (Figure 17B). Additionally, the

LDH-activity was measured after treatment with NE in different concentrations (10^{-9}–10^{-6} M) at day 1, 7, 14, and 21 of the chondrogenesis assay pellet cultures (Figure 17C). Similar to LDH activity findings in monolayer culture, the treatment with NE during chondrogenesis was not cytotoxic. No difference in LDH activity was detected between untreated and NE treated pellets at any time point post initiation of chondrogenesis (Figure 17C). In addition, dsDNA amount was measured to determine the relative cell amount in the pellets at day 21 of chondrogenesis. The dsDNA quantification revealed no differences between untreated and NE treated pellets, demonstrating that NE had no proliferative or apoptotic effect on cells during chondrogenesis (Figure 17D).

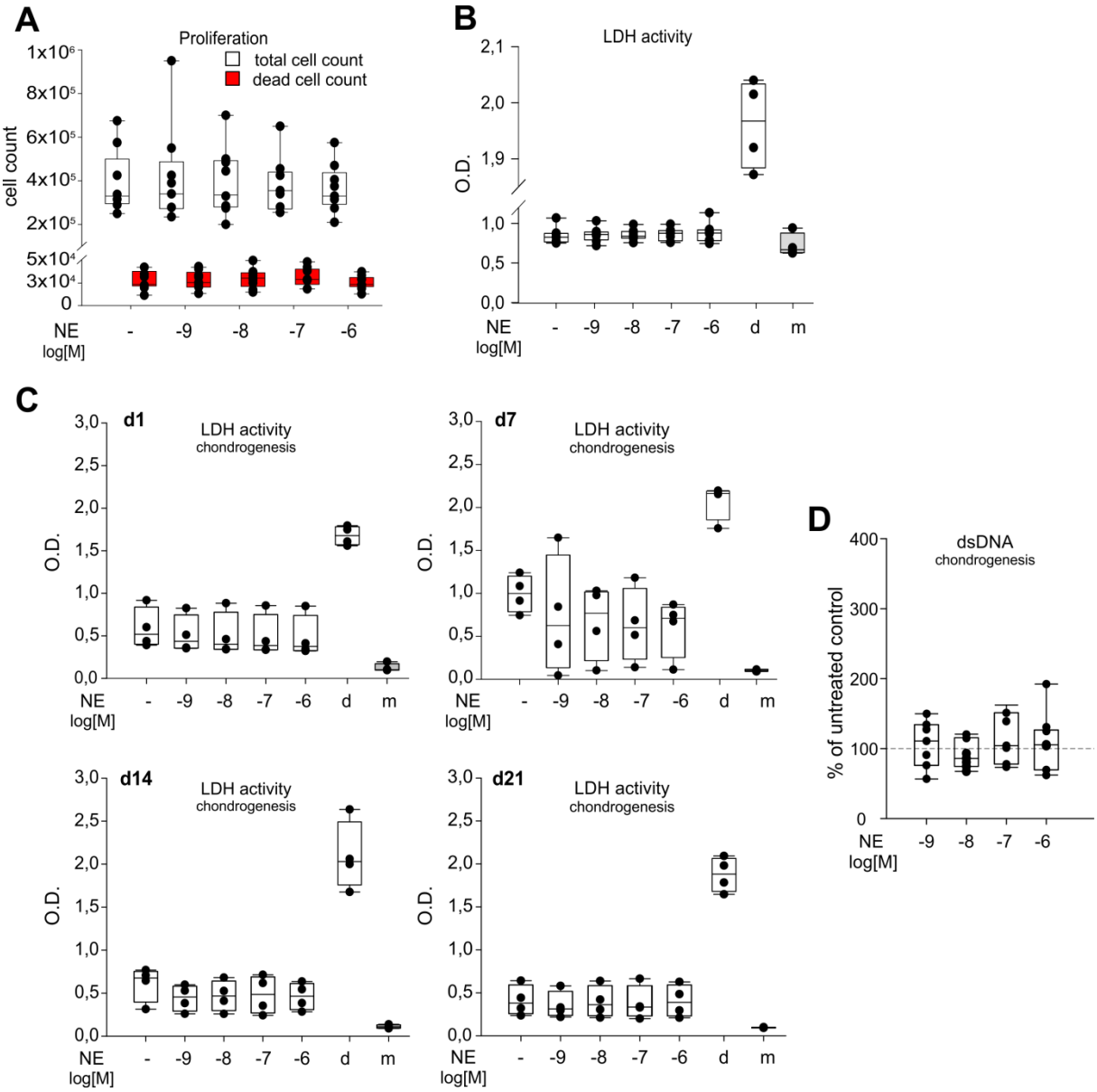

Figure 17 Concentration dependent effects of NE on sASCs cell viability and proliferation in monolayer and chondrogenic pellet cultures.
(A) Proliferation capacity of sASCs in the presence of NE at different concentrations. (B) LDH activity in sASCs monolayer culture in the presence of NE at different concentrations after seven days of culture. Abbreviations: d – dead control (positive control), m – medium (negative control) (C) LDH activity in sASCs chondrogenic pellet culture in the presence of different concentrations of NE at day 1, 7, 14 and 21 of chondrogenic differentiation. Abbreviations: d – dead control (positive control), m – medium (negative control). (D) Biochemical quantification of dsDNA content in untreated and NE-treated (10^{-9}-10^{-6}M) three-dimensional chondrogenic pellet culture at day 21 of differentiation. Values are shown as a percentage of the untreated control (= 100%, dashed line). Data are presented as box plots, where the boxes represent the 25th to 75th percentiles, the lines within the boxes represent the median, and the lines outside the boxes represent the 10th and 90th percentiles (untreated control = 100%, broken line). Each black circle represents the mean of 3 replicates of cells from an individual patient (n=8). (El Bagdadi et al. 2019)

3.1.7 NE decreases the chondrogenic capacity of sASCs dose-dependently

Macroscopic observation of untreated pellets revealed a nodular morphology and an increase of the pellet size during chondrogenesis from day 7 until day 21. The pellets increased in size after NE treatment until day 14, which was however reduced with increasing NE concentration at day 14 and 21 of chondrogenesis, compared to untreated pellets. The pellet volume was quantified after 21 days. A significantly reduced pellet volume was detected after treatment with NE at higher concentrations of 10^{-7} M and 10^{-6} M NE, compared to untreated pellets, suggesting a reduced matrix formation (Figure 18).

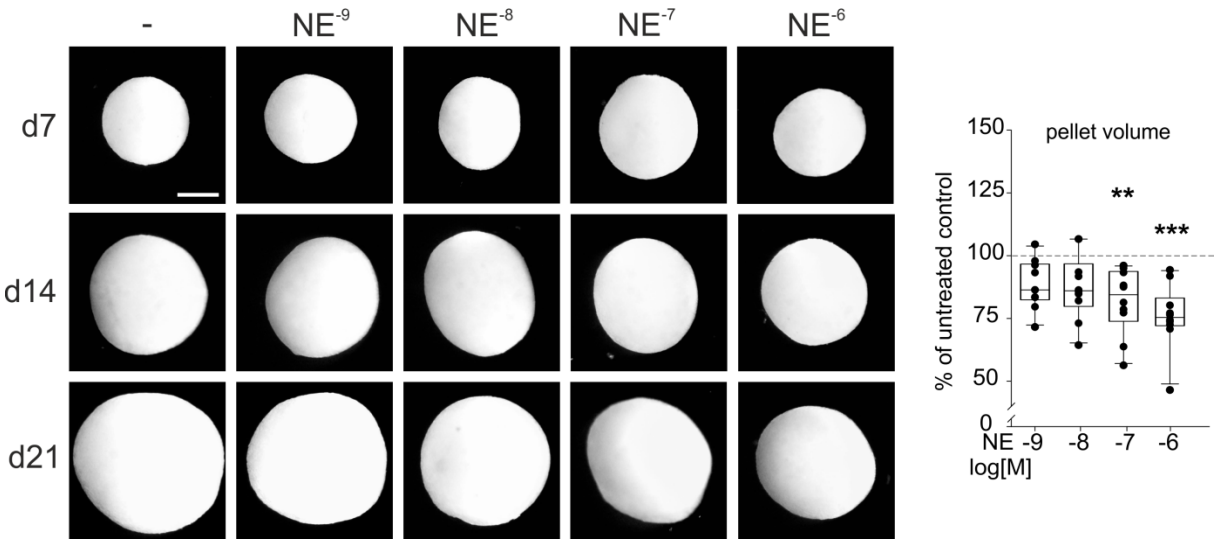

Figure 18 Dose dependent effects of NE on sASCs pellet morphology, volume during chondrogenic differentiation.
Analysis of morphology of untreated or NE-treated (10^{-9}-10^{-6} M) chondrogenic sASCs pellets at day 7, 14 and 21 of differentiation (bar: 500 µm). Quantification of the chondrogenic sASCs pellet volume in the absence or presence of NE (10^{-9}-10^{-6} M) at day 21 (NE10^{-7} compared to control: p= 0.006 and NE 10-6 M compared to control: p <0.001). Values are shown as a percent of the untreated control (control =100%, dashed line). Data are presented as box plots, where the boxes represent the 25th to 75th percentiles, the lines within the boxes represent the median, and the lines outside the boxes represent the 10th and 90th percentiles. Each black circle represents the mean of an individual patient (n=10). Significant p-values against untreated control are presented as ** p<0.01, *** p<0.001.(El Bagdadi et al. 2019)

After assessing the effects of NE on pellet morphology and volume, the synthesis of cartilage-specific matrix molecules influenced by NE was analysed. The levels of sGAGs and type II collagen, the predominant molecules of cartilage, were assessed histologically or immunohistochemically (Figure 19).

In general, untreated and NE treated pellets produced sGAG from day 7 until day 21, which is indicated by the increase of the blue-to-purple colour change of the metachromatic DMMB dye by histochemical analysis. However, the colour change of sGAG to purple appeared to be reduced after NE treatment. Additionally, the sGAG concentration was determined biochemically at day 21 of chondrogenesis (Figure 19).

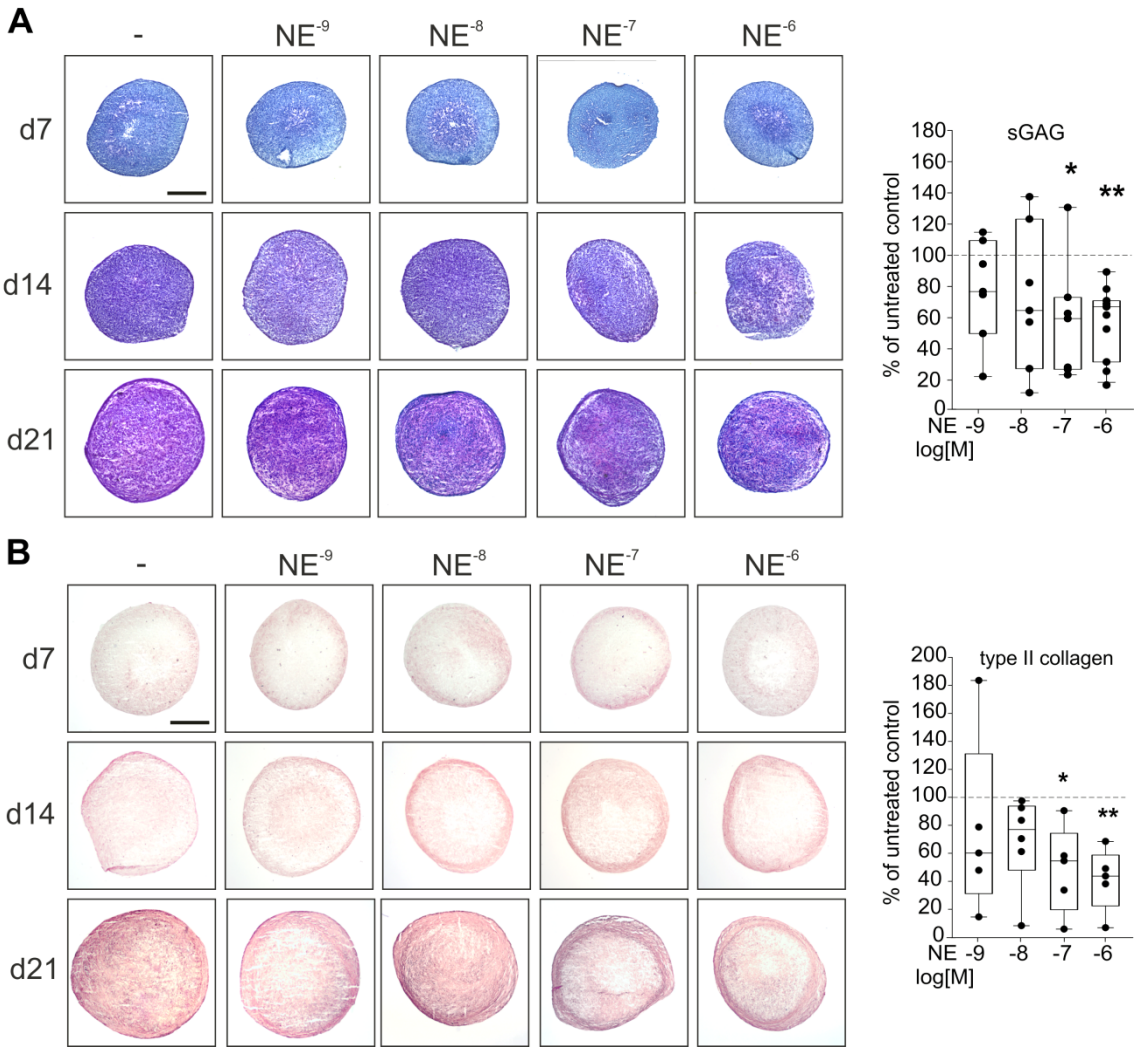

Figure 19 Dose-dependent effects of NE on sGAG and type II collagen synthesis.
(A) Histological analysis of sGAG in untreated or NE-treated (10^{-9}-10^{-6} M) chondrogenic sASCs pellets at day 7, 14, and 21 of differentiation (bar: 500 µm).Quantification of sGAG content of chondrogenic sASCs pellets in untreated or NE-treated (10^{-9}-10^{-6} M) chondrogenic sASCs pellets at day 21 of differentiation. (NE 10^{-7} M compared to control p= 0.036 and NE 10^{-6} M compared to control p = 0.006). (B) Immunohistochemical analysis of type II collagen in untreated or NE-treated (10^{-9}-10^{-6} M) chondrogenic sASCspellets at day 7, 14, and 21 of differentiation (bar: 500 µm). Quantification of type II collagen content of chondrogenic sASCs pellets in the absence or presence of NE (10^{-9}-10^{-6} M) at day 21 (NE 10^{-7} M compared to control: p= 0.0014 and NE 10^{-6} M compared to control: p = 0.008). Values are shown in percent of untreated control (control =100%, dashed line). Data are presented as box plots, where the boxes represent the 25th to 75th percentiles, the lines within the boxes represent the median, and the lines outside the boxes represent the 10th and 90th percentiles). Each black circle represents the mean of an individual patient (n=7-10). Significant p-values against untreated control are presented as * p<0.05, ** p<0.01. (El Bagdadi et al. 2019)

The analysis revealed a significant decrease of sGAG after treatment with 10^{-7} M NE and 10^{-6} M NE (Figure 19A). An increased type II collagen synthesis from day 7 to day 21 was observed in untreated and NE-treated pellets (Figure 19). However, the staining intensity of type II collagen was not homogeneous and reduced in NE-treated pellets at day 21 (Figure 19B) compared to untreated pellets. Similar to the effect of NE on reduced pellet volume and sGAG synthesis, both NE concentrations 10^{-7} M and 10^{-6} M decreased type II collagen concentration significantly, as determined.

In order to investigate if NE treatment affects the gene expression of cartilage degrading enzyme *MMP-13* or hypertrophic marker genes (*COLX* and *RUNX2)*, qRT-PCR was performed (Figure 20). After 21 days, the gene expression of all analysed genes was similar in untreated and NE treated pellets, indicating that NE did not increase the expression of the cartilage degrading enzyme *MMP-13* nor led to an increased formation of hypertrophic cartilage.

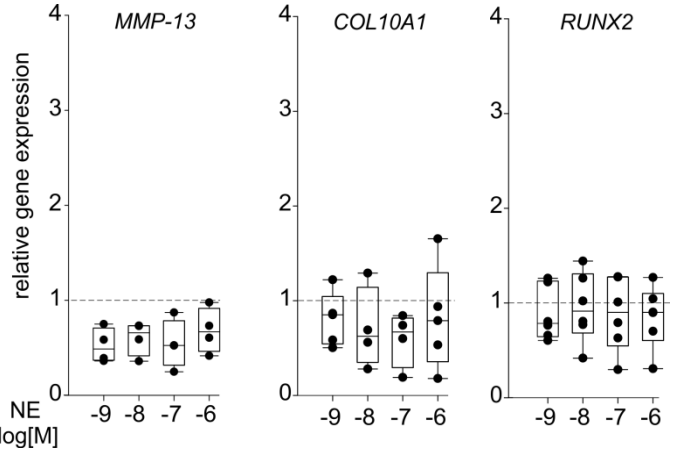

Figure 20 Effect of NE on the expression of *MMP-13* and hypertrophic marker genes *COLX* and *RUNX2* during sASC chondrogenesis.
(A) Expression of *MMP-13, COL10A1*, and *RUNX2* in untreated and NE-treated (10^{-9}-10^{-6} M) chondrogenic sASC pellets at day 21. Values are fold expression of control, where the control = 1 (represented by the dashed line). Data are presented as box plots, where the boxes represent the 25th to 75th percentiles, the lines within the boxes represent the median, and the lines outside the boxes represent the 10th and 90th percentiles. Each black circle represents the mean of 3 replicates of an individual patient (n=4-6).(El Bagdadi et al. 2019)

3.1.8 Reversal of NE-mediated effects by specific AR antagonists

After revealing that NE caused reduction in the chondrogenic capacity and activation of ERK1/2 signalling, the AR subtypes mediating these effects of NE were investigated. For this purpose, pellets were treated with NE in a concentration of 10^{-6} M alone or in combination with either of the following compounds: the α1A-AR antagonist doxazosin, α2A-AR antagonist yohimbine, or the β2-AR antagonist propranolol. The 10^{-6} M NE was used because this concentration affected the chondrogenic differentiation significantly in this study. Cytotoxic effects of the antagonists were excluded by the LDH assay (Figure 21A). Additionally, these treatments did not influence cell apoptosis or proliferation during chondrogenesis compared to untreated pellets as indicated by dsDNA quantification (Figure 21B).

The treatment of pellets with any of the above specific antagonists alone had no significant effects on pellet volume, sGAG and type II collagen protein content, compared to untreated pellets (Figure 22). The pellets appeared smaller after NE treatment alone but not if combined with any of the AR antagonists - yohimbine, propranolol, or doxazosin (Figure 23A). Histological and immunohistological staining revealed that compared to untreated pellets, sGAG and type II collagen were reduced by all the treatments. However, these effects were not homogenous as shown by intense staining only in the outer part of the pellets (Figure 23A). Interestingly, the effect of NE was reversed significantly by only the α2-AR antagonist yohimbine (Figure 23). To determine if the treatments influenced matrix formation, sGAG and type II collagen concentrations were determined (Figure 23B). None of the antagonists was able to modulate the observed NE-mediated effects on sGAG protein content. However, the reduction of type II collagen was reversed significantly by the α2-AR antagonist yohimbine, which was similar to its effects on pellet volume. Also, the β2-AR antagonist propranolol showed a trend in partly reversing the NE mediated effect, however, this was not significant. The α2-AR antagonist doxazosin did not affect the reduction of type II collagen by NE. Overall,these data suggest involvement of α2-AR in NE action, based on the rescue of NE mediated reduction of matrix formation by yohimbine.

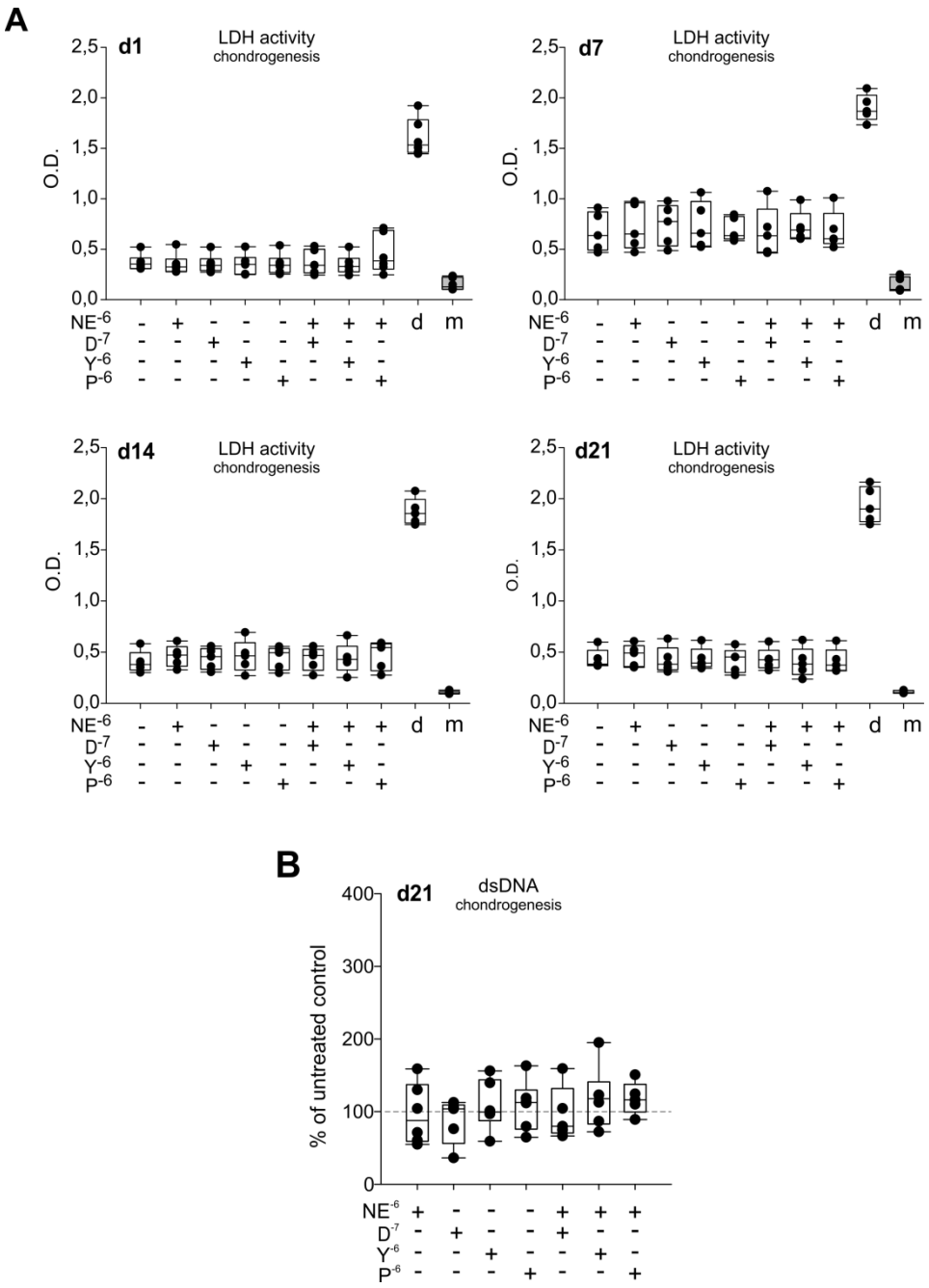

Figure 21 Effect of specific AR antagonists on sASC viability and cell number.
(A) LDH release in three-dimensional chondrogenic sASC pellets treated with NE (10^{-6} M) or with NE plus specific AR antagonists at day 1, 7, 14 and 21 of chondrogenic differentiation. (B) Biochemical quantification of dsDNA content in three-dimensional chondrogenic sASC pellets treated with NE (10^{-6} M) or with NE plus specific AR antagonists at day 21 of differentiation. Values are presented as a percent of the control (untreated control = 100%, dashed line). Each black circle represents an individual patient. Values are shown in percent of untreated control (= 100%, dashed line). Data are presented as box plots, where the boxes represent the 25th to 75th percentiles, the lines within the boxes represent the median, and the lines outside the boxes represent the 10th and 90th percentiles (untreated control = 100%, broken line). Each black circle represents the mean of 3 replicates of an individual patient (n=8). Abbreviations: D – doxazosin, Y – yohimbine, P – propranolol, d – dead control (positive control), m – medium (negative control). (El Bagdadi et al. 2019)

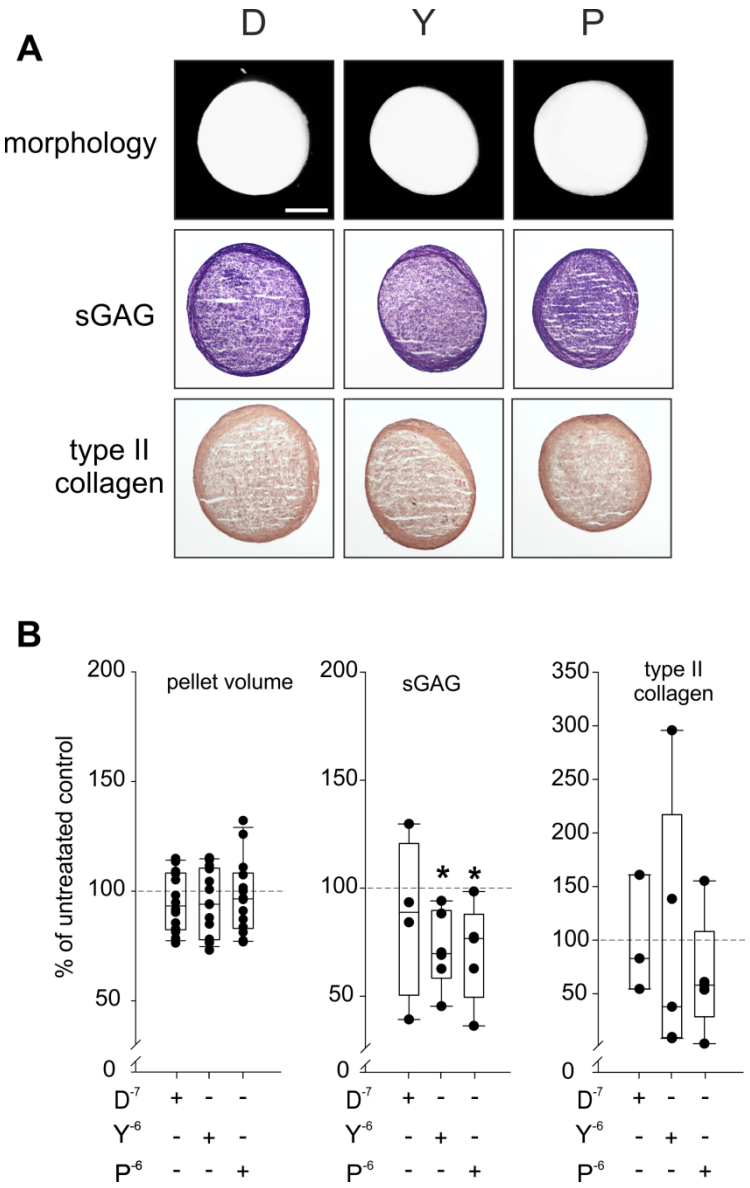

Figure 22 Effect of specific AR antagonists on sASC chondrogenesis.
(A) Analysis of pellet morphology, sGAG and type II collagen in chondrogenic sASCs pellets treated with specific AR antagonists at day 21 of differentiation (bars: 500 µm). (B) Quantification of pellet volume and biochemical quantification of sGAG and type II collagen content of chondrogenic sASCs pellets treated with specific AR antagonists at day 21. Values are presented as a percent of the control (control =100%, dashed line); (P compared to control p= 0.024; D compared to control p= 0.043). Data are presented as box plots, where the boxes represent the 25th to 75th percentiles, the lines within the boxes represent the median, and the lines outside the boxes represent the 10th and 90th percentiles. Each black circle represents the mean of 3 replicates of an individual patient (n=3-14). Abbreviations: D – doxazosin, Y – yohimbine, P – propranolol. (El Bagdadi et al. 2019)

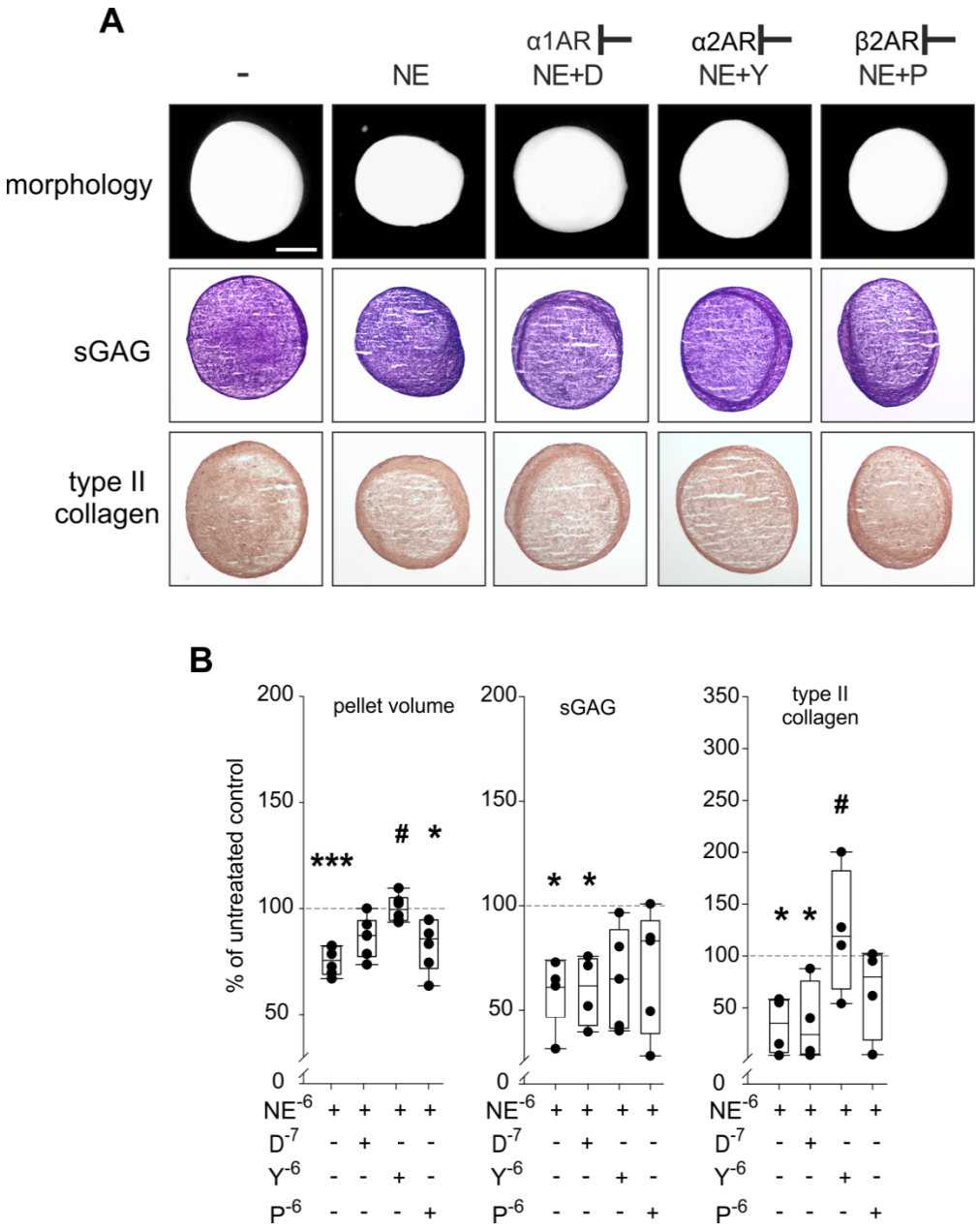

Figure 23 Effect of specific AR antagonists on NE effects during sASC chondrogenesis.
(A) Analysis of pellet morphology, sGAG and type II collagen in chondrogenic sASC pellets treated with NE (10-6 M) or with NE plus specific AR antagonists at day 21 of chondrogenic differentiation (bars: 500 µm). (B) Quantification of pellet volume and biochemical quantification of sGAG and type II collagen content of chondrogenic sASC pellets treated with NE (10^{-6} M) or with NE plus specific AR antagonists at day 21. Values are presented as a percent of the control (control =100%, dashed line). Data are presented as box plots, where the boxes represent the 25th to 75th percentiles, the lines within the boxes represent the median, and the lines outside the boxes represent the 10th and 90th percentiles. Each black circle represents the mean of 3 replicates of an individual patient (n=6-10). Significant p-values against untreated control are presented as * $p<0.05$, ** $p<0.01$, *** $p<0.001$ and compared to NE (10^{-6} M) as # $p<0.05$. Abbreviations: D – doxazosin, Y – yohimbine, P – propranolol (El Bagdadi et al. 2019)

3.1.9 Reversal of NE activated signaling pathways by specific AR antagonists

After demonstrating that NE effects on chondrogenic capacity are mainly mediated by the α2-AR (Figure 23B) and that NE activated the ERK1/2 signalling pathway (Figure 16), the ERK 1/2 pathway was analysed in presence of specific AR antagonists. Analysis of the ERK1/2 pathway by western blot showed that α2-AR antagonist yohimbine markedly reversed the NE-induced phosphorylation of ERK1/2 (Figure 24), confirming the involvement of α2-AR in the NE-mediated effects. The β2-AR antagonist propranolol also caused a partial reduction of the ERK1/2 phosphorylation. These results indicate that NE activates the ERK1/2 signal pathway via α2-AR stimulation.

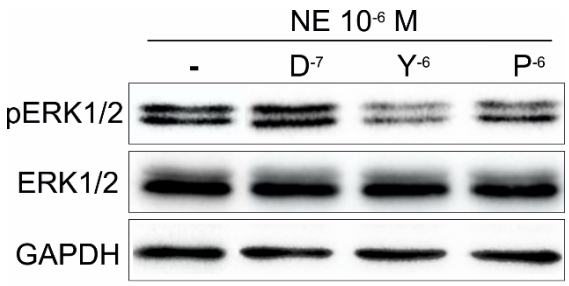

Figure 24 Western blot analysis of total and phosphorylated ERK1/2 of chondrogenic sASCs pellets.
Pellets were treated with NE (10^{-6} M) alone or in combination with specific AR antagonists. Representative blot of one OA patient. Abbreviations: D – doxazosin, Y – yohimbine, P – propranolol (El Bagdadi et al. 2019)

All the *in vitro* findings of the current study demonstrate for the first time that chondrogenic differentiation of sASCs is suppressed by NE activated α2-AR signalling as revealed by ERK 1/2 phosphorylation. Thus, the sympathetic neurotransmitter NE might contribute to reduced chondrogenic capacity of MSC and play also a role in OA progression and manifestation.

3.2 SNS involvement in development of OA in mice

The *in vivo* experiments aimed to identify sympathetic effects during OA development in the entire knee joint. For this purpose, sympathectomy, which creates a break in the sympathetic signalling pathway of all catecholamines was used to induce OA. In this murine experimental OA model, peripheral sympathetic nerve fibers were destroyed chemically using 6-OHDA in mice (Syx mice) and OA progression was analysed comparing them with WT mice. Apart from this chemical Syx OA model, the surgical DMM induced OA model was also analysed. A combination of the Syx model followed by DMM surgery was also analysed for OA progression.

3.2.1 Syx eliminated synovial TH-positive fibers and reduced splenic NE levels

The success of sympathectomy was first examined by immunohistochemical staining for TH in the synovium (Figure 25) and by measurement of spleen NE levels in WT and Syx mice (Figure 26). TH-positive nerve fibers were destroyed in the synovia after sympathectomy in DMM and sham operated Syx mice, in contrast to the normal TH-expression in DMM and sham operated WT mice (Figure 25).

The NE levels were measured not only in the spleen of DMM or sham-operated mice but also in those from healthy non-operated mice to analyse if the sham surgery itself affects NE DMM and sham operated in the spleen. Similar to the reduced TH expression in the synovia of Syx

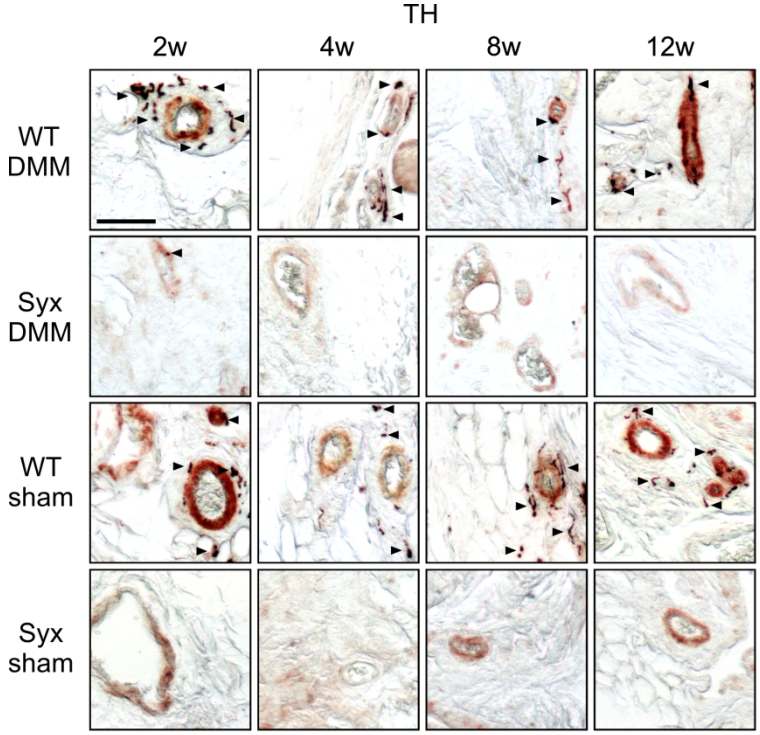

Figure 25 Effects of peripheral chemical sympathectomy on TH-positive nerve fibers in the synovia of mice undergoing DMM or sham surgery.
Detection of TH-positive sympathetic nerve fibers in the synovia (in dark brown, indicated by arrowheads in area of vessels (red circled structures) of WT and Syx mice after DMM or sham surgery (bar: 50 µm).

mice, spleen NE concentrations were lowered in Syx mice compared to the respective WT or healthy groups at all time points (Figure 26).

Notably, higher spleen NE concentrations were detected in WT mice after DMM surgery compared to healthy non-operated or sham-operated WT mice after 8 weeks, suggesting that the induction of OA by DMM elevated the sympathetic tone. Differences in body or spleen weight were not observed (Figure 26).

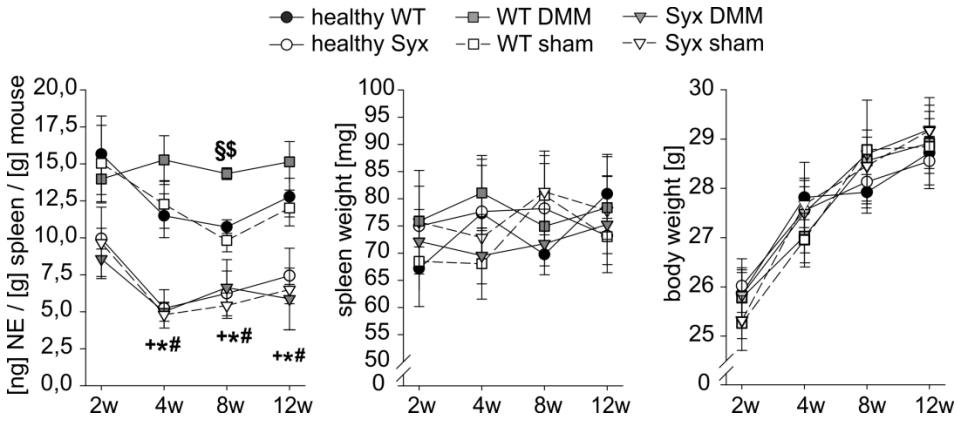

Figure 26 Effects of peripheral sympathectomy in healthy, sham- and DMM operated mice.
Effect of sympathectomy on NE concentrations in the spleen, as well as on body and spleen weight of healthy non-operated, as well as sham-operated and DMM-operated WT and Syx mice. Data are represented as means +/- standard deviation; (n=8-10 per group). Significant p-values ($p \leq 0.05$) of respective sympathectomized animals to healthy untreated mice are indicated by "*", to sham-operated mice by "+", and to DMM-operated mice by ''#''.Significant differences ($p \leq 0.05$) of WT DMM mice 8 weeks post-DMM to respective healthy mice are indicated by "§" and to WT sham by "$".

3.2.2 Syx attenuated cartilage degeneration

DMM leads to increased mechanical stress with cartilage lesions that are most apparent on the medial side. Therefore, cartilage degradation, which occurs predominantly on the medial side, was analyzed in this weight-bearing region (Figure 27). In order to characterize the cartilage damage after OA induction by DMM, sections of mice knee joints were stained with DMMB. This staining revealed visible cartilage damage and erosions in WT and Syx mice 8 and 12 weeks post DMM surgery. However, less pronounced cartilage lesions were detected in Syx mice compared to WT mice at both time points. None of the sham-operated mice showed any cartilage damage at the time points analysed. The quantification of cartilage degeneration by the OARSI scoring revealed an increasing score over time in WT DMM mice. In contrast, Syx mice had significantly less OARSI scores compared to WT mice 8 and 12 weeks after DMM, suggesting that less sympathetic activity is protective for the cartilage (Figure 27B). Furthermore, cartilage degeneration increased significantly in WT mice post DMM compared to WT sham mice after 8 and 12 weeks, while no significant differences were observed between DMM and sham-operated Syx mice (Figure 27B).

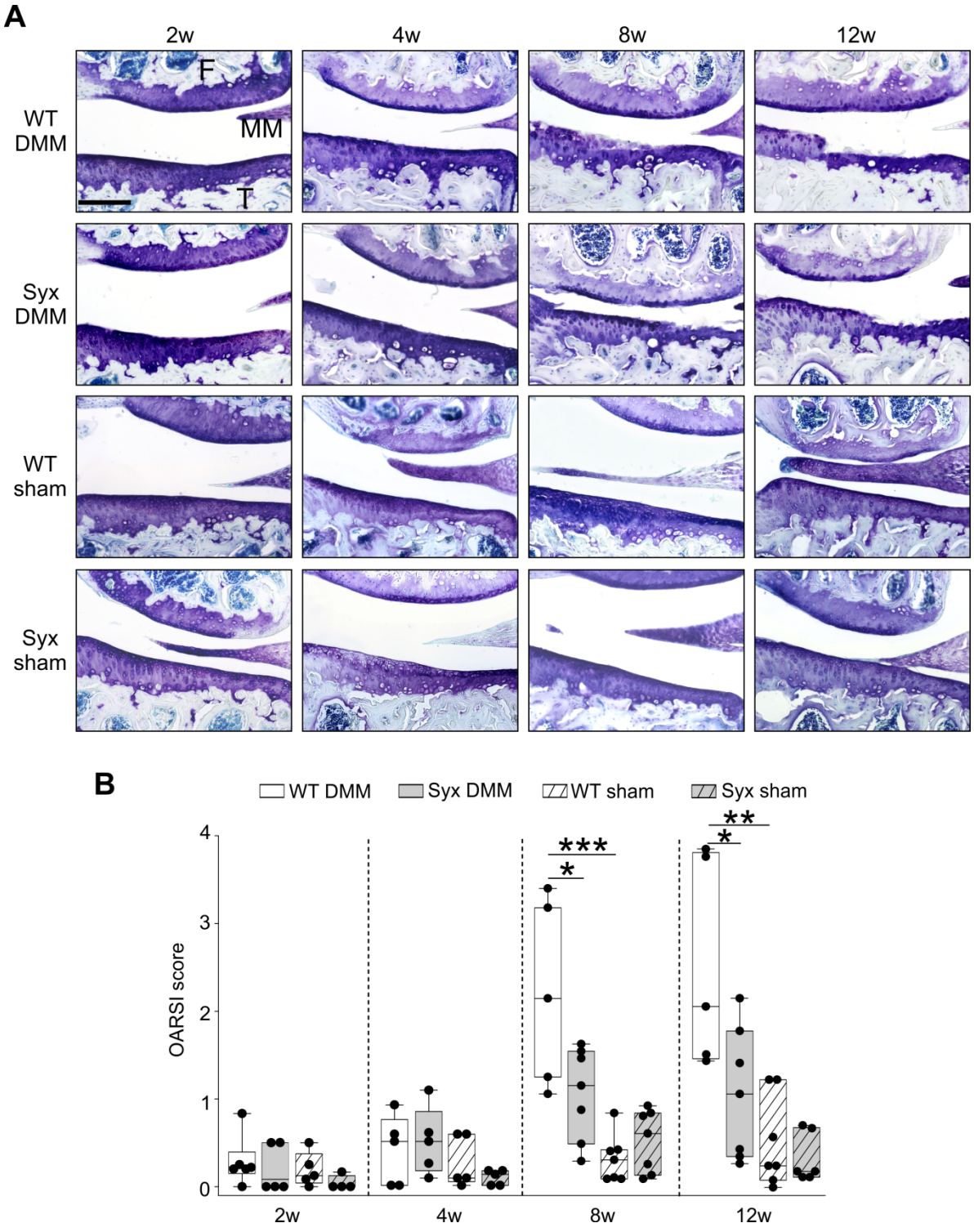

Figure 27 Increased cartilage degeneration in WT mice after DMM surgery.
(A) Histological analysis of the medial tibiofemoral articular cartilage contact area using DMMB staining in WT and Syx mice 2, 4, 8, and 12 weeks after DMM or sham surgery (F: femur, T: tibia, MM: medial meniscus, bar: 200 µm). (B) OARSI scores of the medial tibia plateau in WT and Syx mice 2, 4, 8, and 12 weeks after DMM or sham surgery (WT DMM compared to Syx DMM: 8 weeks p=0.026 and 12 weeks p=0.042; WT DMM compared to WT sham: 8 weeks p<0.001 and 12 weeks p<0.001). Data are presented as box plots, where the boxes represent the 25th to 75th percentiles, the lines within the boxes represent the median, and the lines outside the boxes the 10th and 90th percentiles. Each black circle represents an individual mouse (n=5-8 per group). Significant p-values between treatment groups are indicated by "*" when p ≤ 0.05, or as "**" when p ≤ 0.01, or as "***" when p < 0.001.

3.2.3 Syx abolished DMM-induced CTX-II release

After investigating OA grade in WT mice, the levels of type II collagen, a major protein of the articular cartilage, were assessed immunohistochemically. No differences in staining intensity were found between WT and Syx mice at any of the time points (Figure 28A). Additionally, no differences were detected between sham and DMM-operated mice. Interestingly, the levels of CTX-II, the small type II collagen degradation product, were different in serum samples from WT and Syx mice. A significantly increased CTX-II level was detected in WT mice compared to Syx mice 4 weeks after DMM (Figure 28B), indicating the degradation of type II collagen. In Syx mice, the CTX-II concentration did not increase at any measured time point. No significant differences between CTX-II levels of WT and Syx mice were observed after sham surgery at any time point (Figure 28B).

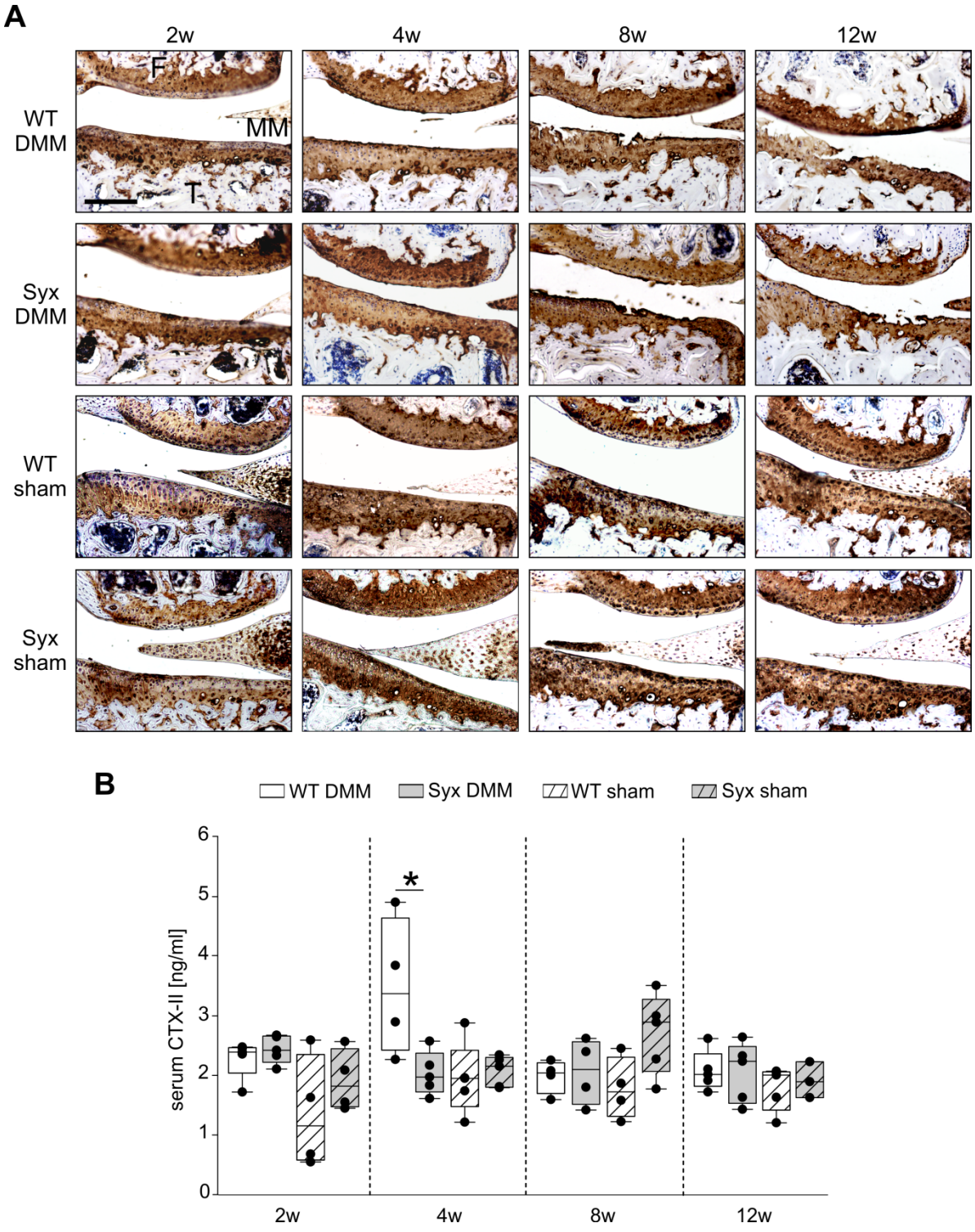

Figure 28 Detection of type II collagen in articular cartilage and of its degradation product in serum.

(A) Immunohistochemical detection of type II collagen in the tibiofemoral articular cartilage contact area of WT and Syx mice 2, 4, 8, and 12 weeks after DMM or sham surgery (F: femur, T: tibia, MM: medial meniscus, bar: 200 µm). (B) Serum CTX-II concentration in WT and Syx mice 2, 4, 8, and 12 weeks after DMM or sham surgery (WT DMM compared to Syx DMM 4 weeks p=0.046). Data are presented as box plots, where the boxes represent the 25th to 75th percentiles, the lines within the boxes represent the median, and the lines outside the boxes the 10th and 90th percentiles. Each black circle represents an individual mouse (n=3-5 per group). Significant p-values ($p \leq 0.05$) between WT and Syx are indicated by "*".

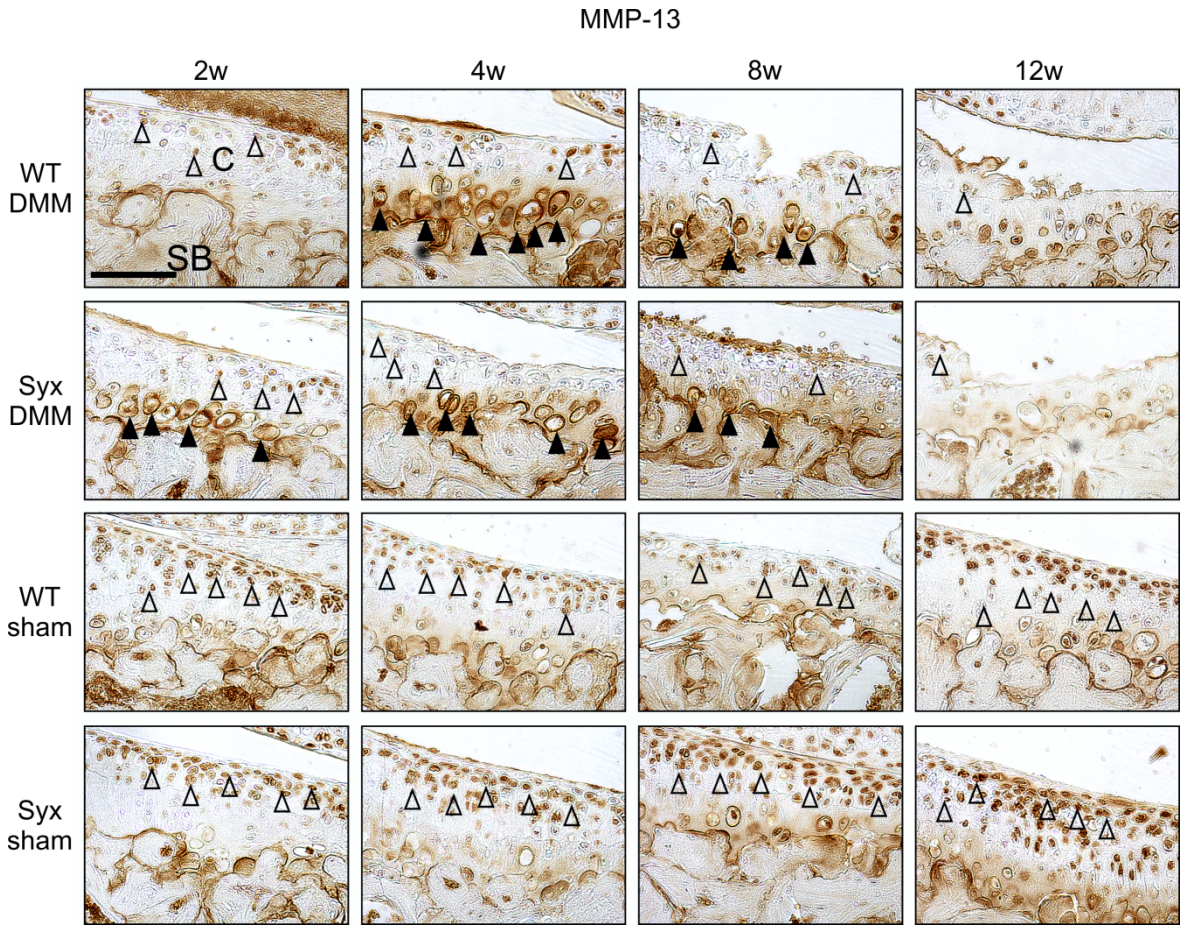

Figure 29 MMP-13 expression in articular cartilage of WT and Syx mice.
Immunohistochemical detection of MMP-13 in the upper zone (open arrowheads) and in the hypertrophic /calcified zone (black arrowheads) of articular cartilage in the tibia plateau of WT and Syx mice 2, 4, and 8 weeks after DMM or sham surgery (bar: 100 µm). SB – subchondral bone, C – cartilage.

Furthermore, to investigate whether the observed cartilage damage was accompanied by enhanced expression of cartilage degrading enzymes, the expression of the most prominent type II collagen-degrading enzyme MMP-13 was analysed immunohistochemically (Figure 29). Compared to sham-operated mice, a reduced number of MMP-13-expressing cells was detected in both WT and Syx mice in the contact area of the cartilage at all time points after DMM. However, MMP-13 was strongly expressed by hypertrophic chondrocytes in the deep zone of cartilage already 2 weeks after DMM in Syx mice, while it was 4 weeks after DMM in WT mice (Figure 29). Notably, MMP-13 was markedly expressed in the superficial zone of cartilage in all sham-operated mice and at all time points.

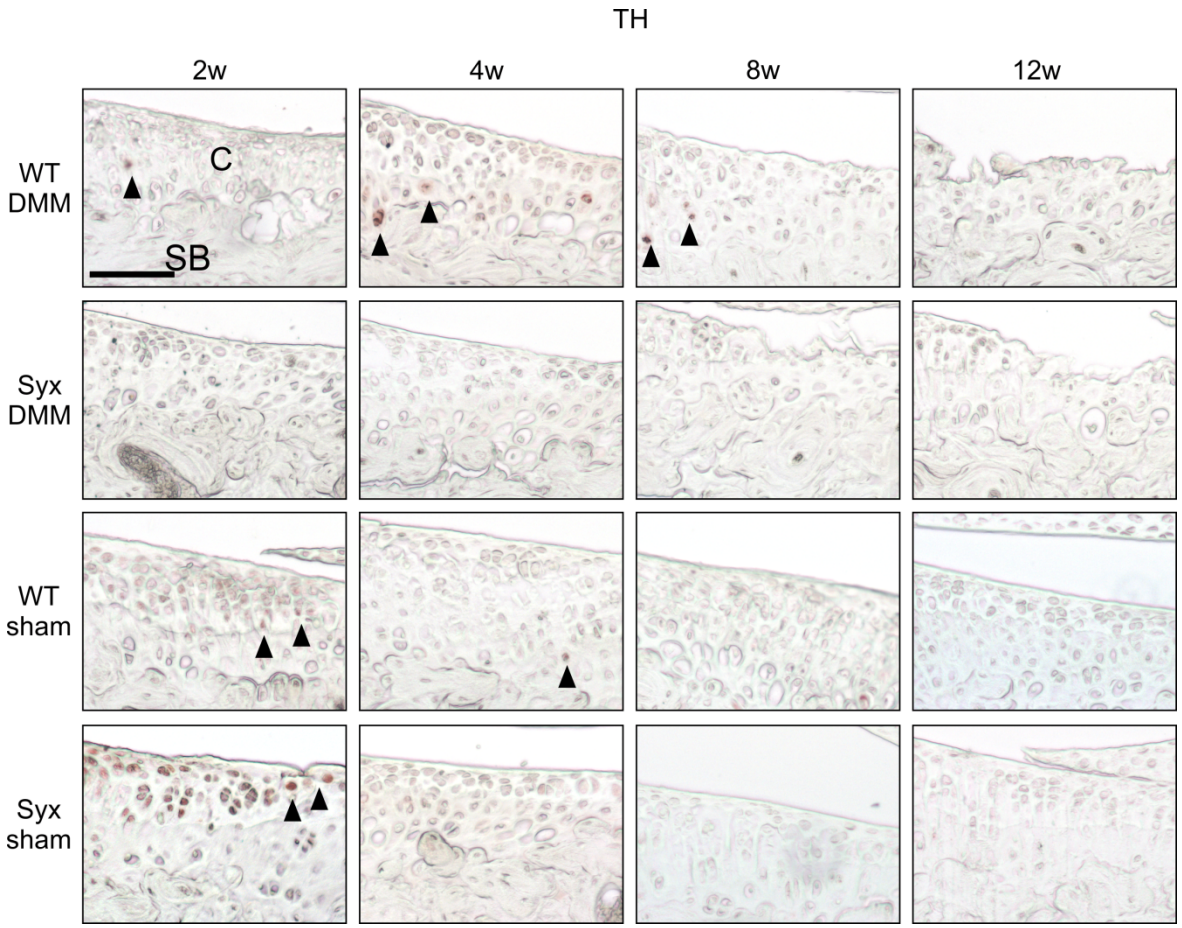

Figure 30 TH expression in articular cartilage of WT and Syx mice.
(A) Immunohistochemical detection of TH in the articular cartilage in the tibia plateau of WT and Syx mice 2, 4, and 8 weeks after DMM or sham surgery (bar: 100 µm). SB – subchondral bone, C – cartilage.

To examine if chondrocytes produce sympathetic neurotransmitters, TH expression was examined immunohistochemically (Figure 30). Only a few single TH-positive cells were detected in the superficial and calcified cartilage zone of WT mice after DMM or sham surgery.

After demonstrating that WT mice developed severe OA post DMM surgery indicated by increased cartilage damage compared to Syx mice, the expression of ARs was analysed in the cartilage immunohistochemically. The number of cells expressing the most prominent ARs, namely the α2A- and β2-AR, were counted and expressed in percentage of total cells. A few cells expressing the α2A-AR were detected in WT and Syx mice 2 weeks after DMM or sham surgery (Figure 31).

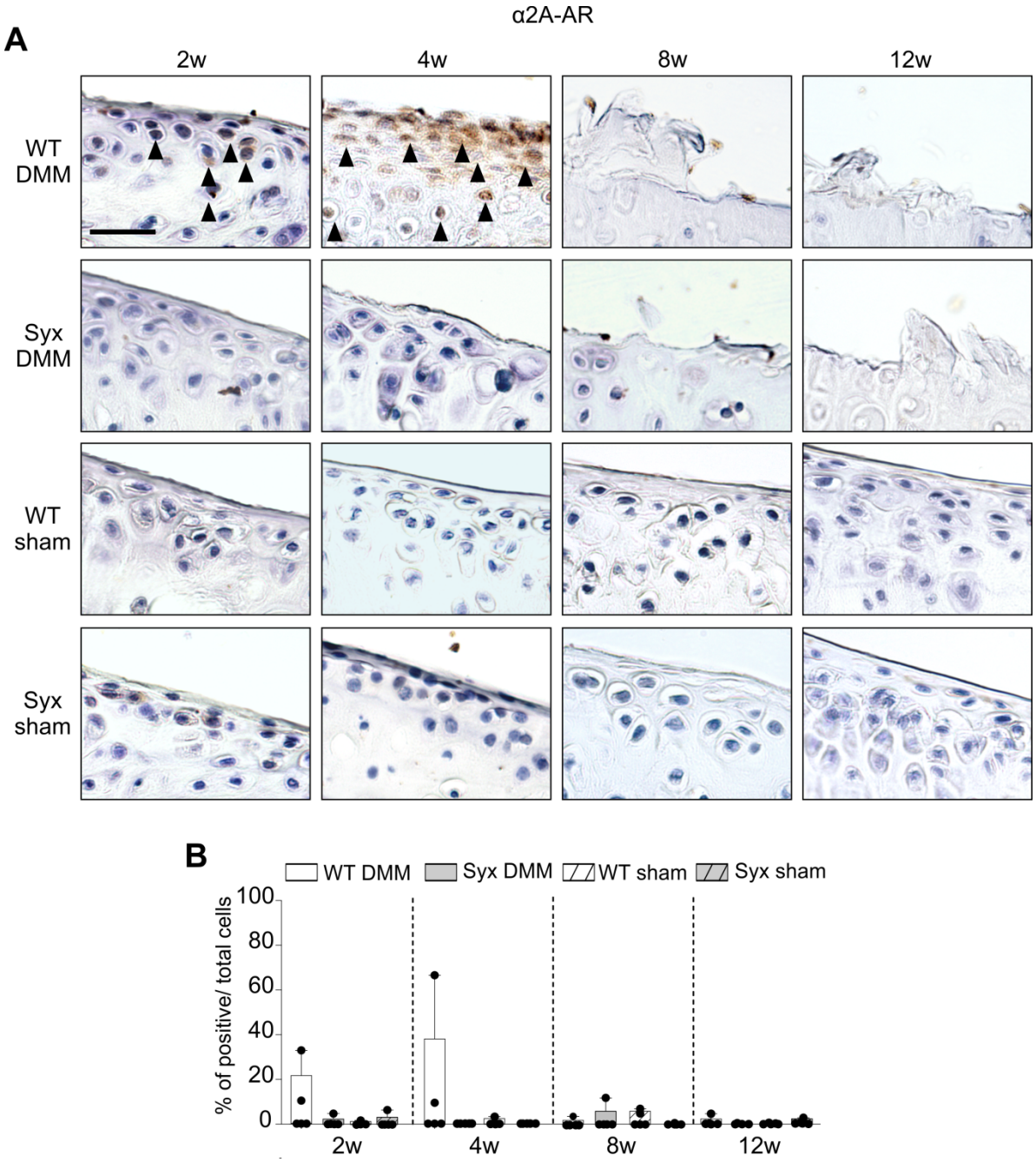

Figure 31 α2A-AR expression in articular cartilage of WT and Syx mice.
(A) Immunohistochemical detection of α2A-AR (in dark brown, black arrow heads).
(B) Quantification of α2A-AR-expressing cells in the articular cartilage in the tibia plateau of WT and Syx mice 2, 4, 8 and 12 weeks after DMM or sham surgery (bar: 50 µm). Nuclei were counterstained with hematoxylin (in dark blue). Data are presented as box plots, where the boxes represent the 25th to 75th percentiles; the lines within the boxes represent the median, and the lines outside the boxes the 10th and 90th percentiles. Each black circle represents an individual mouse (n= 5 per group).

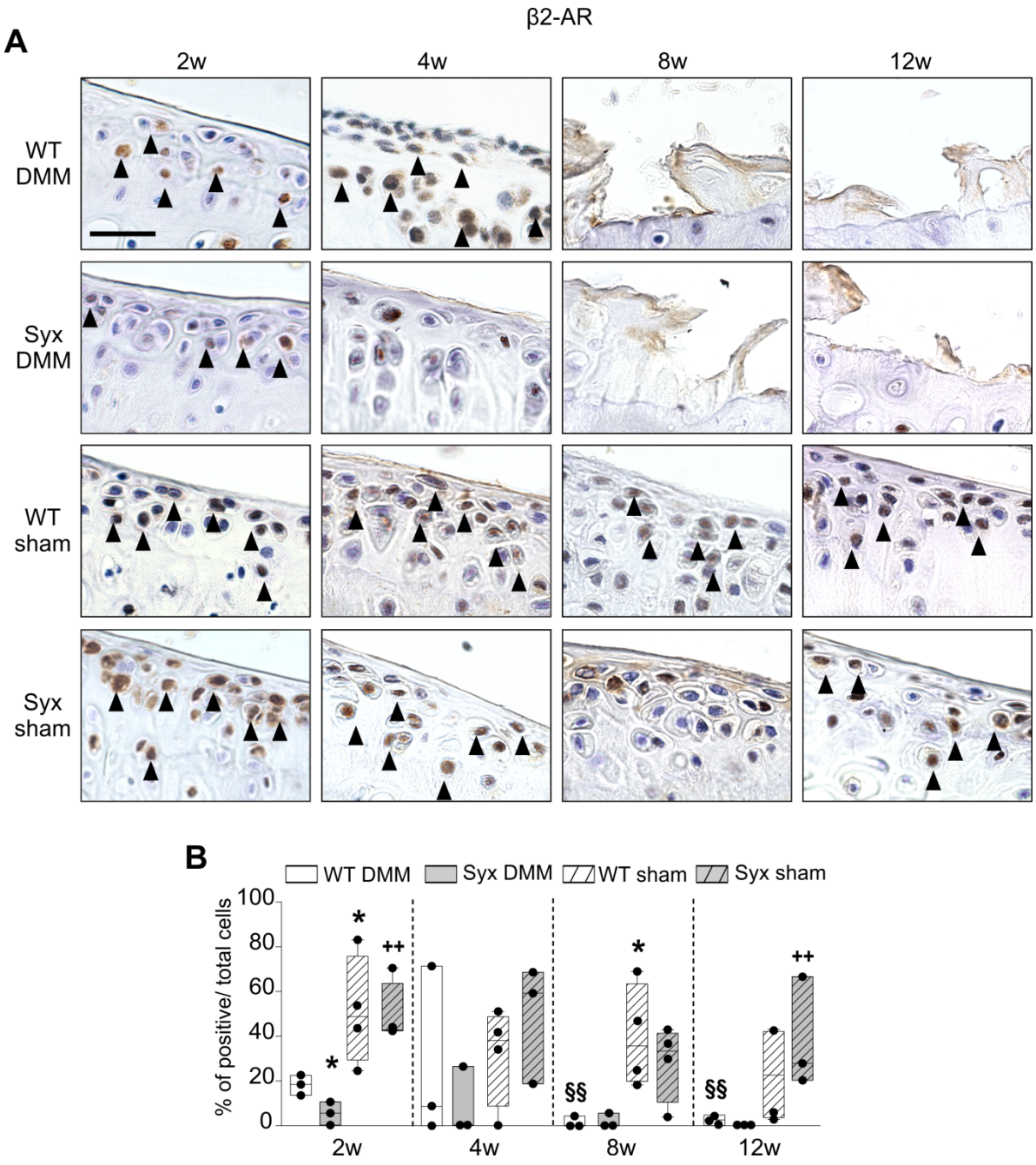

Figure 32 β2-AR expression in articular cartilage of WT and Syx mice.
(A) Immunohistochemical detection of β2-AR (in dark brown, black arrowheads) Bar: 50 µm.
(B) Quantification of β2-AR-expressing cells in the articular cartilage in the tibia plateau of WT and Syx mice 2, 4, 8 and 12 weeks after DMM or sham surgery (WT DMM 2 weeks compared to 8 and 12 weeks both p=0.002; WT DMM compared to WT sham: 2 weeks p=0.033, 8 weeks p=0.016; Syx DMM compared to WT DMM: 2 weeks p=0.033; Syx DMM to Syx sham: 2 weeks p=0.004, 12 weeks p=0.008; bar: 100 µm). Nuclei were counterstained with hematoxylin (in dark blue). Data are presented as box plots, where the boxes represent the 25th to 75th percentiles, the lines within the boxes represent the median, and the lines outside the boxes represent the 10th and 90th percentiles. Each black circle represents an individual mouse (n=3-4 per group). Significant p-values ($p \leq 0.05$) to WT DMM at the same time point are indicated by "*", significant p-values ($p \leq 0.01$) to WT DMM at 2 weeks in as "§§", and significant p-values ($p \leq 0.01$) to Syx DMM at the same time point as "++".

In WT DMM mice, this receptor tended to be expressed more by chondrocytes after 4 weeks, which was not significant when compared to Syx DMM or any sham-operated mice. In contrast to α2A-AR, β2-AR-expressing cells were more evident in both WT and Syx after sham or DMM surgery (Figure 32). Significantly less β2-AR-expressing cells were detected in Syx mice compared to WT mice 2 weeks after DMM. In sham mice, the percentage of β2-AR-positive cells tended to be higher at all time points compared to sham-operated mice. A significant reduction in the percentage of β2-AR-expressing cells was observed in WT mice at 2 and 8 weeks after DMM compared to sham animals (Figure 32B). Similarly, the percentage of β2-AR-expressing cells was reduced in Syx DMM mice compared to sham-operated mice at 2 and 12 weeks after DMM. Additionally, a significant reduction of β2-AR-expressing cells in WT mice after DMM after 8 and 12 weeks was observed, compared to WT DMM after 2 weeks. These results suggest that reduced AR levels potentially resulted from cartilage loss and cell death owing to OA in the mouse models employed.

3.2.4 Syx attenuated synovial inflammation

Synovitis, a potential predictive factor of OA, was analyzed by determining the synovitis score on the DMMB stained sections (Figure 33A). The thickening of the synovium, which is one indicator for synovitis, was slightly enlarged in both WT and Syx mice from week 2 until week 8 after DMM (Figure 33B). Significant differences of synovium thickness were detected between DMM and sham-operated WT and Syx mice after 4 and 8 weeks. No significant differences in synovium thickness were detected between WT DMM and Syx DMM mice Figure 33B). The synovitis score was increased in tendency in WT DMM mice from week 2 until week 12 (Figure 34A), which was not detected in Syx mice. However, significantly lower synovitis scores were detected in Syx mice compared to WT mice at 8 and 12 weeks post DMM surgery. (Figure 34A). The synovitis score of WT DMM correlated moderately with the OARSI score, the cartilage damage indicator (Figure 34B). There was however only a weak correlation between these two scores in Syx DMM mice and in WT, Syx sham-operated mice (Figure 34B).

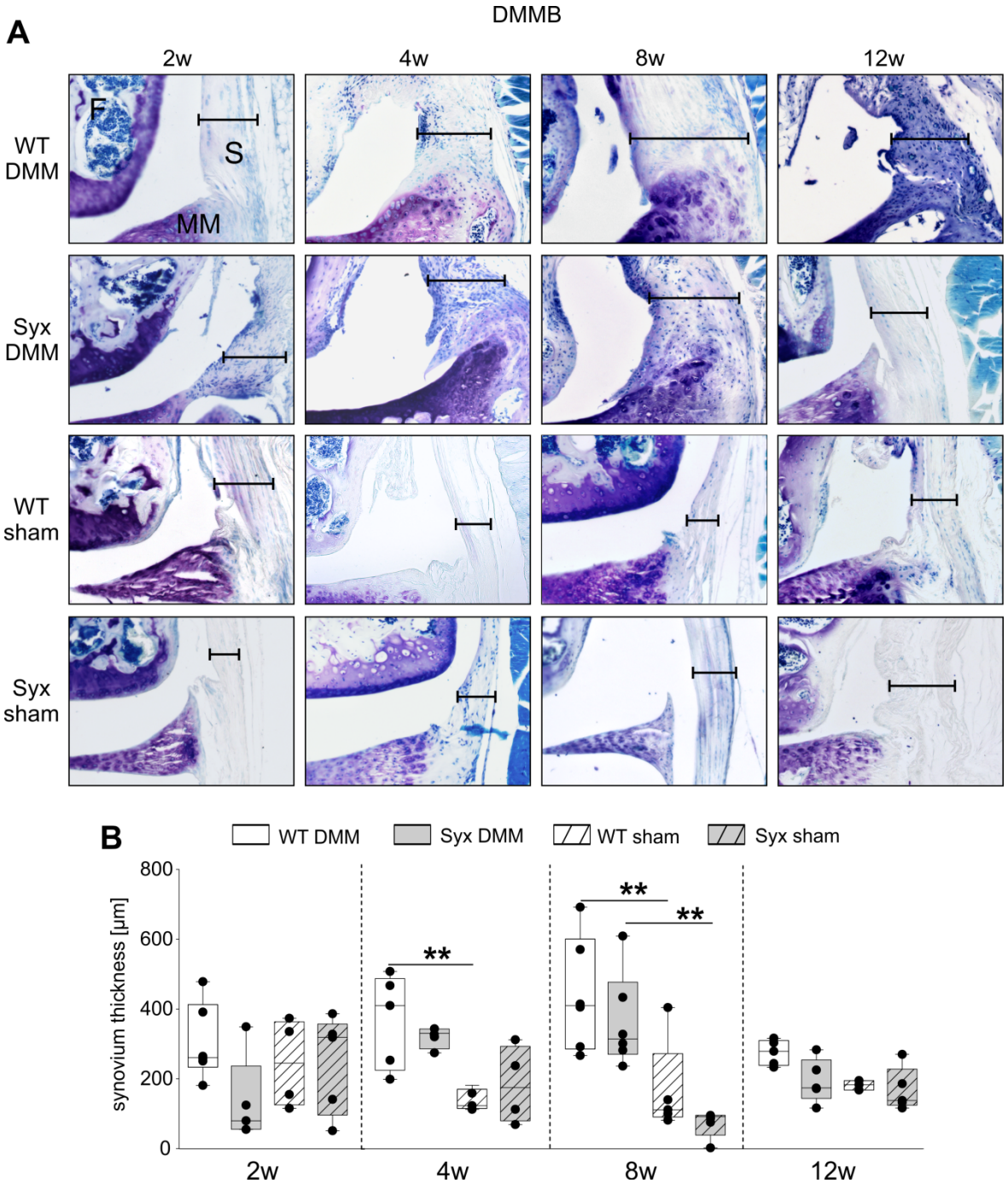

Figure 33 Synovitis development in WT and Syx mice after DMM.
(A) Histology of the synovium in WT and Syx mice 2, 4, 8, and 12 weeks after DMM or sham surgery (DMMB stainings, F: femur, S: synovium, MM: medial meniscus; lines with caps indicate the average thickness of synovium, bar: 200 µm). (B) Synovium thickness of WT and Syx mice 2, 4, 8, and 12 weeks after DMM or sham surgery (WT DMM compared to WT sham: 4 weeks p=0.009, 8 weeks p=0.017; Syx DMM compared to Syx sham: 8 weeks p=0.009). Data are presented as box plots, where the boxes represent the 25th to 75th percentiles, the lines within the boxes represent the median, and the lines outside the boxes the 10th and 90th percentiles. Significant p-values between treatment groups are indicated by "*" when $p \leq 0.05$, or as "**" when $p \leq 0.01$, or as "***" when $p < 0.001$.

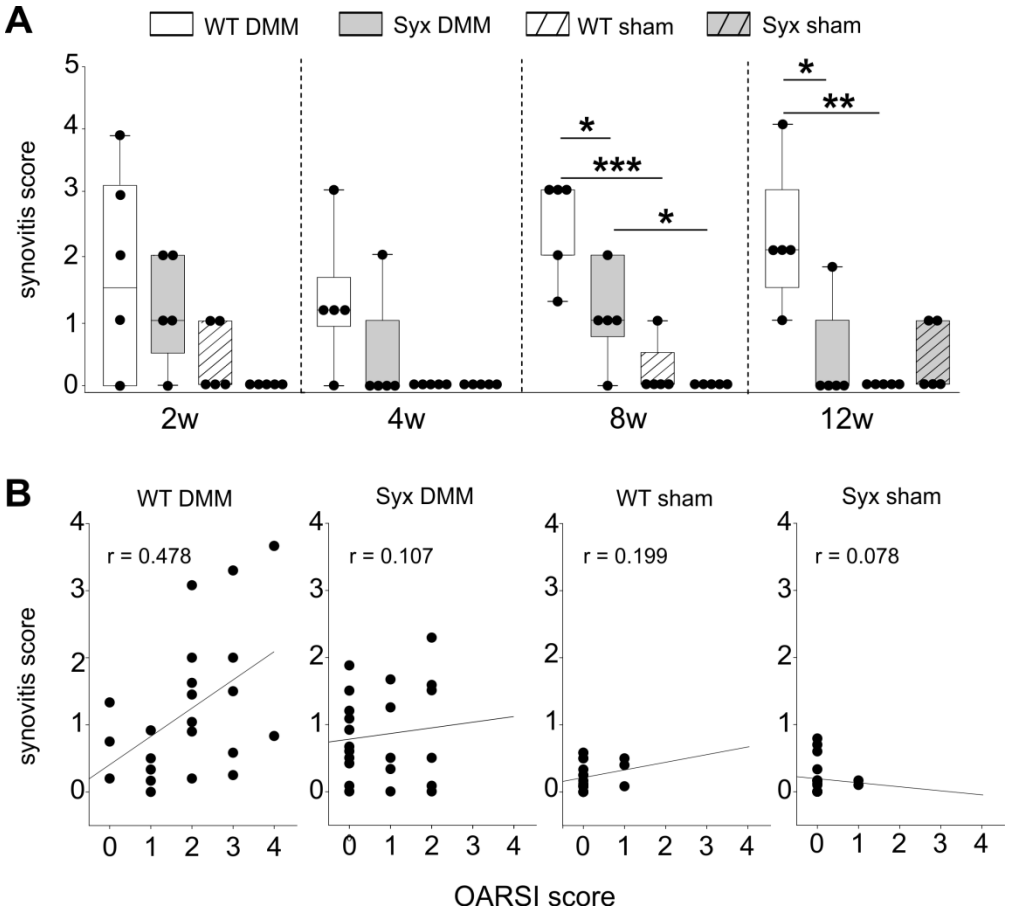

Figure 34 Correlations between articular cartilage damage (OARSI) and synovitis scores.
(A) Synovitis score of WT and Syx mice 2, 4, 8, and 12 weeks after DMM or sham surgery (WT DMM compared to WT sham: 8 weeks $p<0.001$, 12 weeks $p=0.002$; Syx DMM compared to WT DMM: 8 weeks $p=0.023$, 12 weeks $p=0.01$; Syx DMM compared to Syx sham: 8 weeks $p=0.031$). (B) Correlation between OARSI and synovitis score in WT and Syx mice 2, 4, 8, and 12 weeks after DMM or sham surgery ("r" indicates the correlation coefficient; WT DMM $r=0.478$, Syx DMM $r=0.107$, WT sham $r=0.199$, Syx sham $r=0.078$). Each black circle represents an individual mouse (n=5 per group).

3.2.5 Syx reduced MMP-13 and TH expression in synovial cells

Based on the correlation between cartilage damage and synovitis, the expression of the matrix-degrading enzyme MMP-13 was assessed in the synovium (Figure 35A). Notably, the synovia of WT DMM animals with increased synovitis showed a higher expression of MMP-13 compared to the healthy controls at the early OA stages of 2 and 4 weeks after DMM. These findings were consistent with the observed increasing synovitis score in WT mice post DMM surgery (Figure 34 A).

A weak expression of MMP-13 was observed in sham-operated mice (Figure 35A). Interestingly, MMP-13 expression was also lower in Syx DMM mice, which had less pronounced synovitis than WT DMM mice.

TH staining was performed to investigate if the inflammatory OA environment leads to the induction of TH expression in synovial cells as observed in rheumatoid arthritis patients (Capellino et al. 2010), (Figure 35B). More TH-positive cells were visible in WT mice after DMM, compared to sham-operated Syx or WT mice at any of the time points analysed. The expression of TH was weak in sham-operated mice (Figure 35B). Furthermore, the Syx DMM mice also had a low TH expression compared to WT DMM at most of the time points.

In order to investigate the response of synovial cells to catecholamines, the percentage of cells expressing the α2A-AR and β2-AR was assessed (Figure 36 A, B). The immunohistochemical analysis revealed a significant increase of α2A-AR-positive cells in WT mice 2 weeks after DMM compared to WT sham-operated mice (Figure 36A). Comparing DMM and sham-operated mice, more α2A-AR-positive cells were detected after DMM in both WT and Syx mice, which was however not significant. The number of β2-AR-expressing cells in the synovium was also not significantly different between DMM and sham-operated WT and Syx mice at any of the time points analysed (Figure 36 C, D).

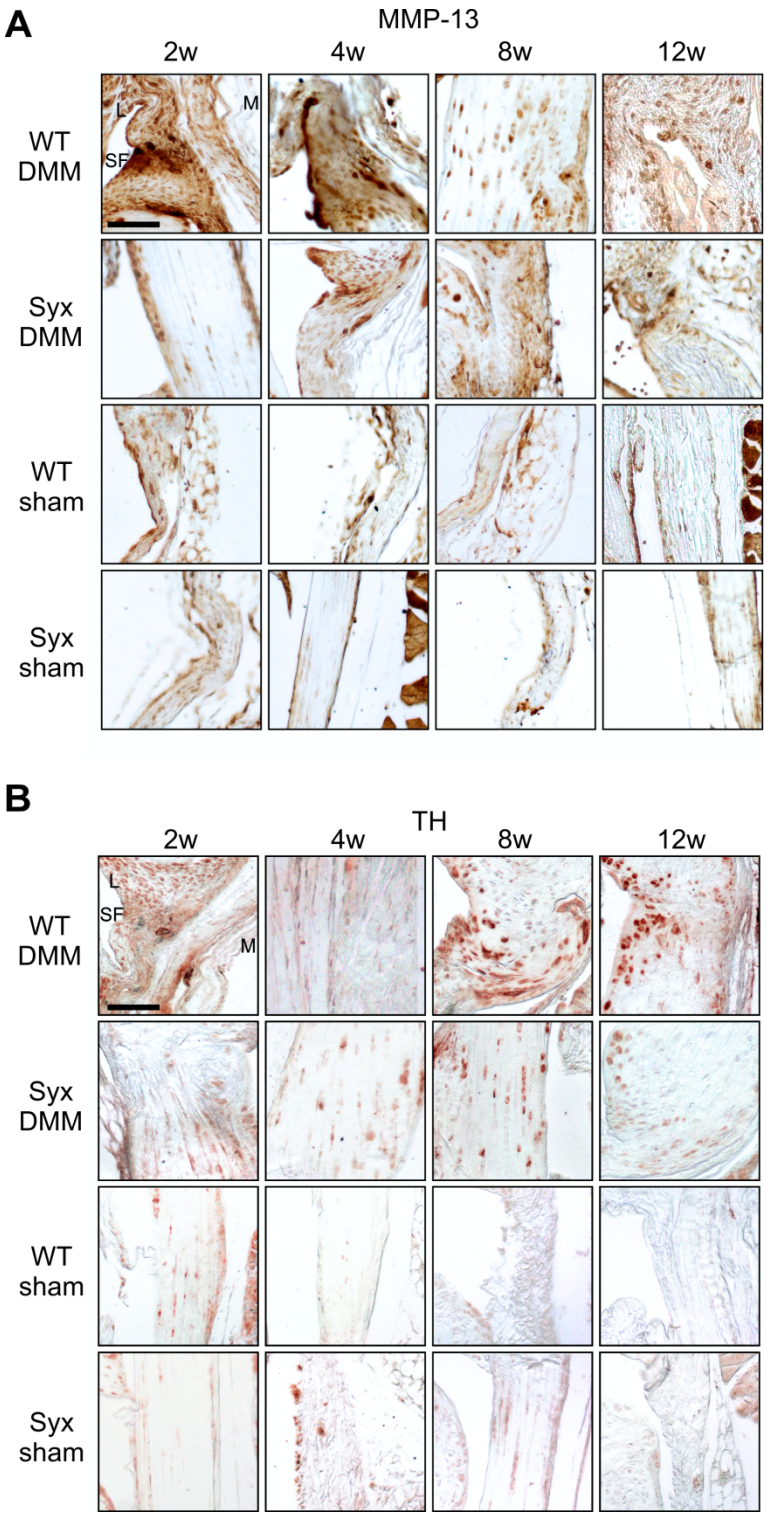

Figure 35 Immunohistochemical detection of MMP-13 in the synovium of WT and Syx mice.
(A) MMP-13 was detected in the in the medial synovium of WT and Syx mice 2, 4, and 8 weeks after DMM or sham surgery (bar: 100 µm). (B) Immunohistochemical detection of TH in the synovial tissue of WT and Syx mice 2, 4, and 8 weeks after DMM or sham surgery (bar 100 µm). SF – synovial fluid side, L – lining layer of the synovium; M – adjacent muscle.

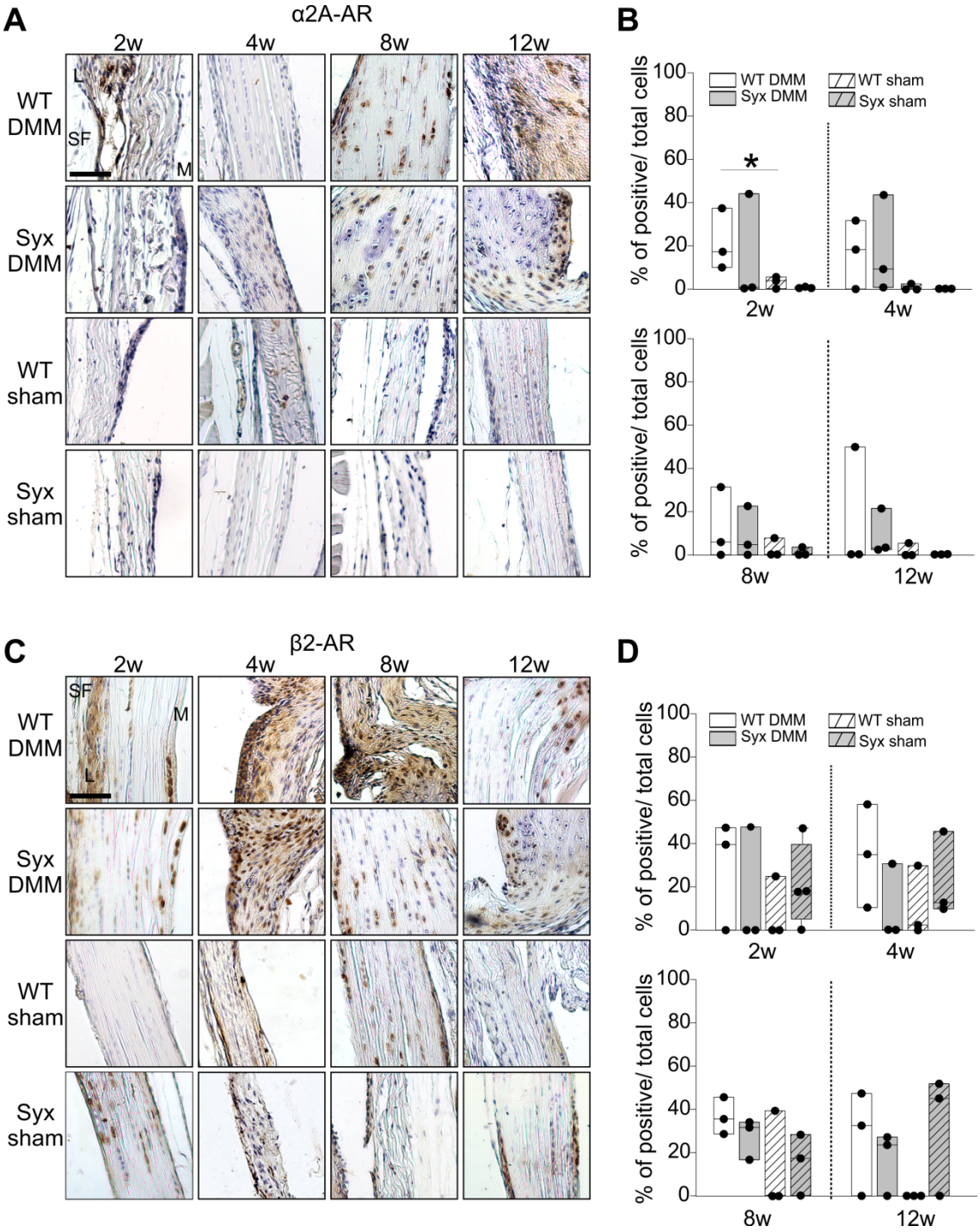

Figure 36 Adrenergic receptor expression in the synovium of WT and Syx mice.
(A) Immunohistochemical detection of α2A-AR and quantification of α2A-AR-expressing cells in the medial synovial tissue of WT and Syx mice 2, 4, 8 and 12 weeks after DMM or sham surgery (WT DMM compared to WT sham: 2 weeks p=0.02, bar: 100 µm). (B) Immunohistochemical detection of β2-AR and quantification of β2-AR-expressing cells in the medial synovial tissue of WT and Syx mice 2, 4, 8 and 12 weeks after DMM or sham surgery (bar: 100 µm). . Data are presented as box plots, where the boxes represent the 25th to 75th percentiles, the lines within the boxes represent the median, and the lines outside the boxes represent the 10th and 90th percentiles. Each black circle represents an individual mouse (n=3-4 per group). Significant p-values ($p \leq 0.05$) to WT DMM are indicated by "*". SF – synovial fluid side, L – lining layer of the synovium; M – adjacent muscle.

3.2.6 Syx aggravated OA specific subchondral bone changes

Increased subchondral bone in Syx mice post DMM

Since OA pathogenesis also involves tissues other than cartilage and synovium, subchondral bone changes were investigated. For this purpose, micro-CT analyses of subchondral bone changes in a defined region of interest were performed (Figure 37A). This analysis indicated that Syx mice had a significantly higher bone volume/ total tissue volume (BV/TV), compared to WT DMM or sham-operated Syx mice (Figure 37B). Consistent with these results, spaces between the trabecula (TbSp) were significantly smaller in Syx mice after DMM compared to WT DMM. The trabecular number (TbN) and trabecular thickness (TbTh) were significantly higher after DMM in both WT and Syx mice compared to the corresponding sham-operated mice. However, no significant differences in TbN or TbSP were detected between WT and Syx mice after DMM (Figure 37B).
To explore subchondral bone turnover due to osteoclast activity TRAP staining was performed (Figure 38) Osteoclast activity appeared to be increased in WT and Syx mice 2 weeks after DMM or sham surgery compared to the activity after 4, 8 and 12 weeks.

At 4 weeks, TRAP staining was mostly detected in WT DMM mice, but not in Syx DMM, Syx sham and WT sham mice. Furthermore, osteoclast activity slightly decreased in all DMM and sham-operated WT and Syx mice after 8 and 12 weeks compared to the earlier time points (Figure 38).

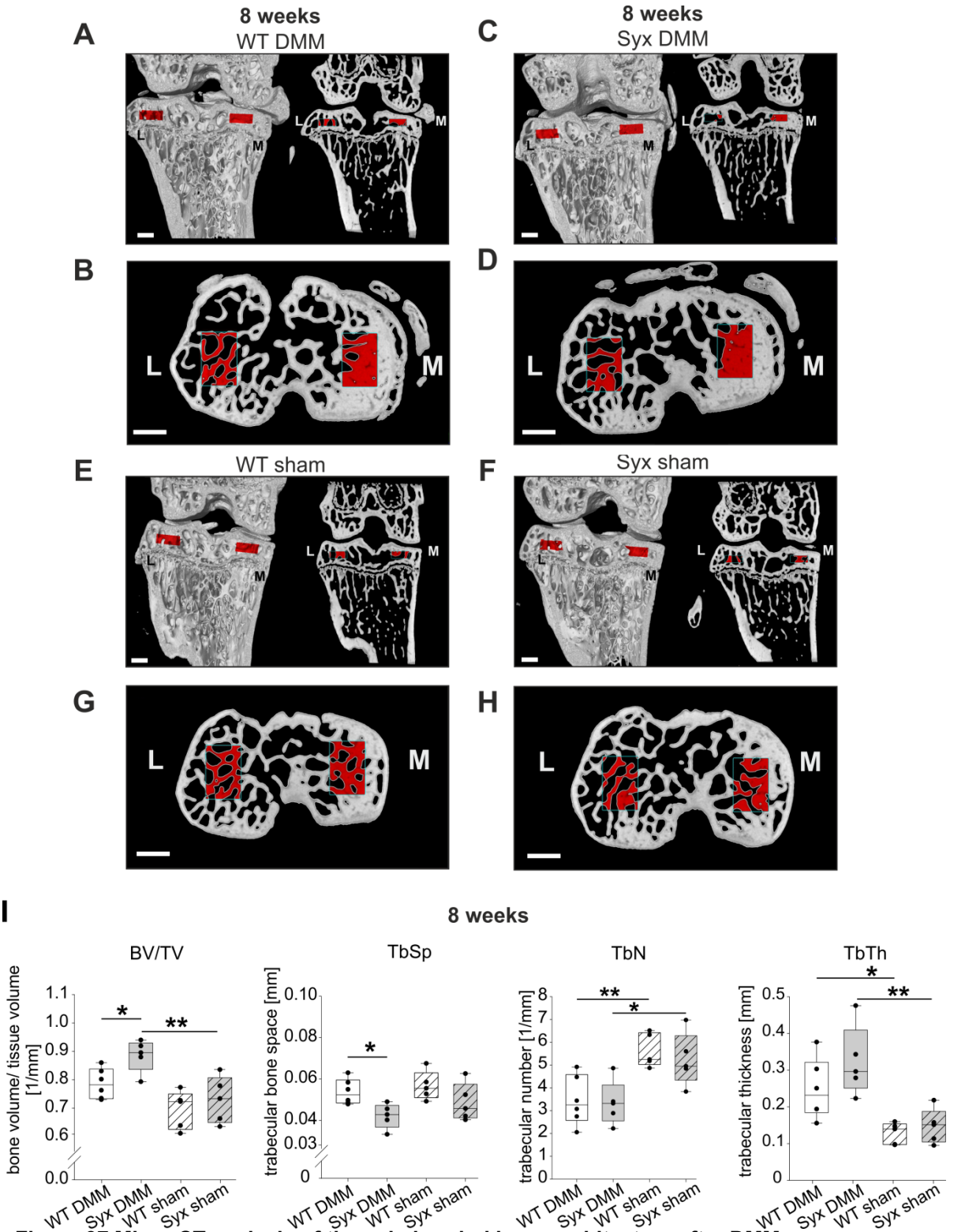

Figure 37 Micro-CT analysis of the subchondral bone architecture after DMM surgery.
(A) Representative micro-Ct images of the frontal knee joint and (B) top view of the tibia plateau showing the volume of interest (VOI, indicated by red rectangles) in the subchondral bone in WT mice and (C-D) Syx mice 8 weeks after DMMor (E-H) sham surgery. (I) Quantitative 3D analysis of BV/TV, TbSp, TbN, and TbTh within the VOI in WT and Syx mice 8 weeks after DMM or sham surgery (Syx DMM compared to WT DMM: BV/TV p=0.023, TbSp p=0.022; WT DMM compared to WT sham: TbN p=0.002, TbTh p=0.026; Syx DMM compared to Syx sham: BV/TV p=0.002, TbN p=0.026, TbTh p=0.002). BV/TV – bone volume to total tissue volume, TbSp – trabecular spacing, TbN – trabecular number, TbTh – trabecular thickness. Data are presented as box plots, as described in Figure 36. Each black circle represents an individual mouse (n=5 per group). Significant p-values p≤ 0.05 between treatment groups are indicated by "*", or p≤ 0.01 as "**". Bars: 0.45 mm.

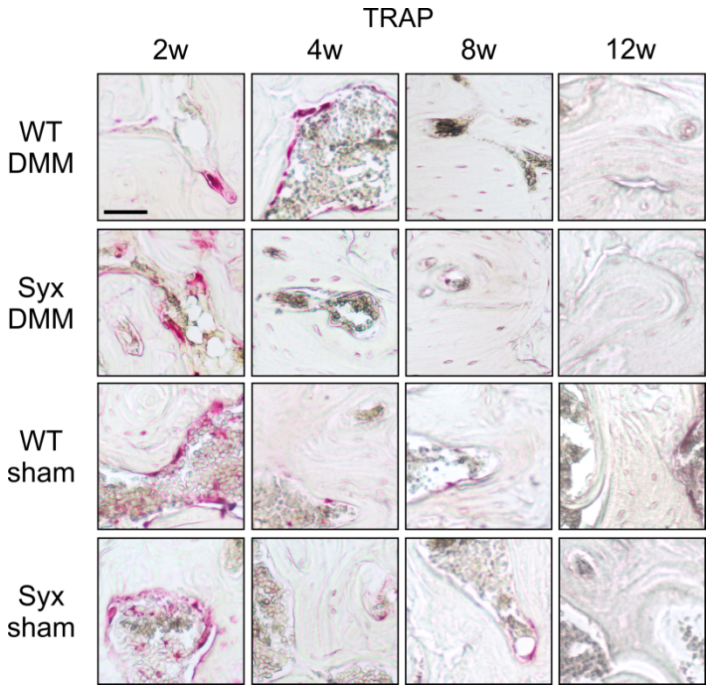

Figure 38 Osteoclast activity in the subchondral bone. Histological detection of TRAP (magenta) in the VOI 8 weeks after DMM or sham surgery. Bar: 50 µm.

Increased subchondral bone plate thickness in Syx mice post DMM

Additionally, micro-CT analysis revealed osteophyte formation in both WT and Syx animals after DMM but not after sham surgery (Figure 39A). Consistent with these results, the length of the medial condyle of the tibia was significantly increased after DMM in both WT and Syx mice compared to sham-operated mice (Figure 39B). Notably, no differences between WT DMM and Syx DMM mice were detected. Color-densitometric micro-CT images and their quantification showed significantly increased calcified cartilage (CC) thickness in both WT and Syx mice after DMM compared to sham-operated mice (Figure 39C). Furthermore, sympathectomy resulted in significantly increased CC compared to WT mice post DMM surgery (Figure 39C). Likewise, Syx DMM mice developed a significantly thicker subchondral bone plate (SCBP) compared to WT DMM mice (Figure 39D). OA induction itself resulted in a significantly thicker SCBP in DMM mice when compared to sham-operated mice (Figure 39D).

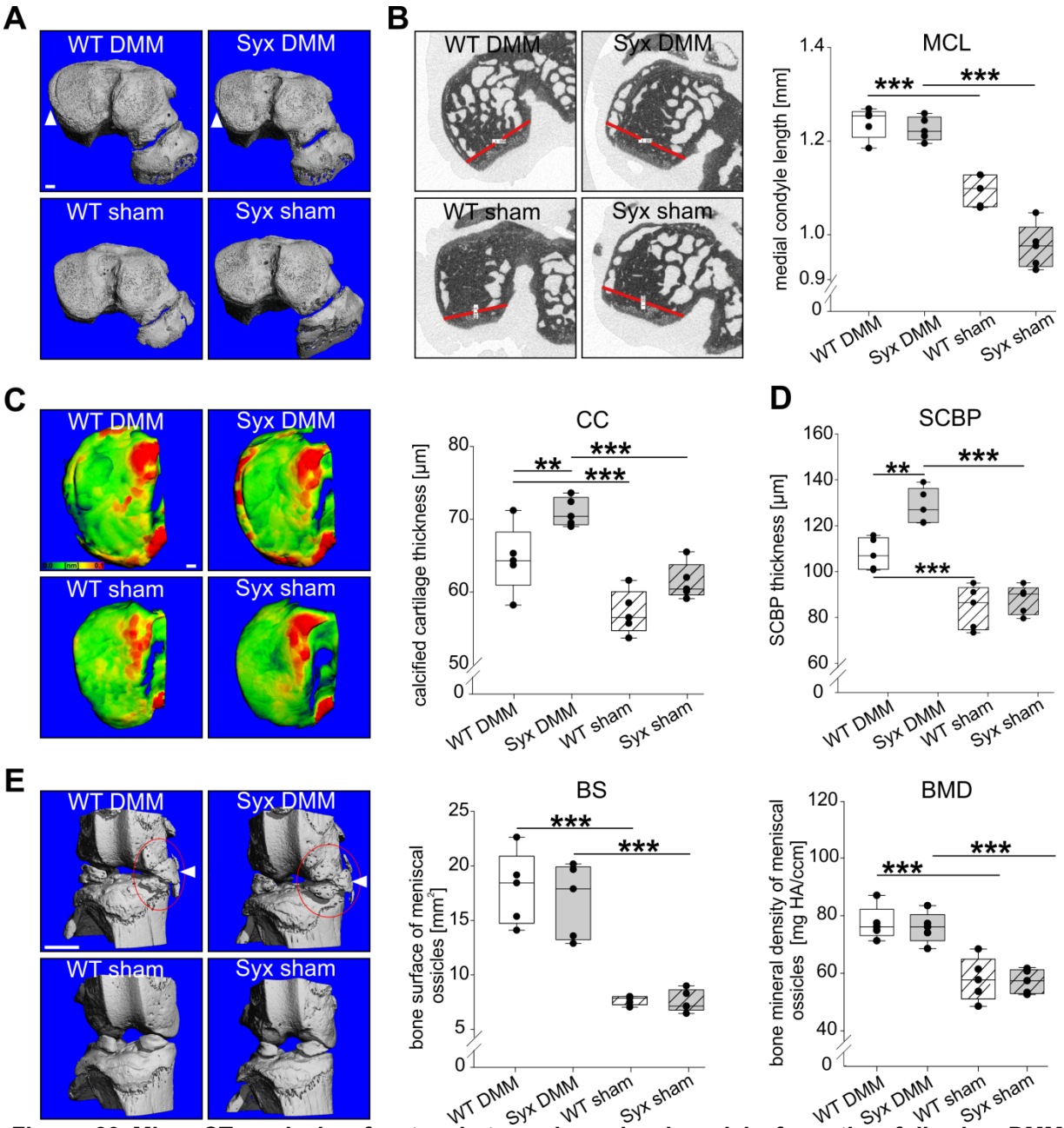

Figure 39 Micro-CT analysis of osteophyte and meniscal ossicle formation following DMM surgery.

(A) Representative micro-CT images showing osteophytes in WT and Syx mice 8 weeks after DMM or sham surgery (bar: 100 µm). (B) Representative pictures and quantification of the medial condyle lengths in WT and Syx mice 8 weeks after DMM or sham surgery (WT DMM compared to WT sham $p<0.001$, Syx DMM compared to Syx sham $p<0.001$). (C) Representative color-densitometric micro-CT images and quantification of the calcified cartilage (CC) thickness in WT and Syx mice 8 weeks after DMM or sham surgery (Syx DMM compared to WT DMM $p=0.006$, WT DMM compared to WT sham $p<0.001$, Syx DMM compared to Syx sham $p<0.001$). (D) Differences in the subchondral bone plate thickness in WT and Syx mice 8 weeks after DMM or sham surgery (Syx DMM compared to WT DMM $p=0.004$, WT DMM compared to WT sham $p<0.001$, Syx DMM compared to Syx sham $p<0.001$). (E) Representative pictures of meniscal ossicles as well as quantification of differences in the bone surface and bone mineral density of meniscal ossicles in WT and Syx mice 8 weeks after DMM or sham surgery (BS: WT DMM compared to WT sham $p<0.001$, Syx DMM compared to Syx sham $p<0.001$; BMD: WT DMM compared to WT sham $p<0.001$, Syx DMM compared to Syx sham $p<0.001$; bar: 100 µm). Data are presented as box plots, where the boxes represent the 25th to 75th percentiles, the lines within the boxes represent the median, and the lines outside the boxes represent the 10th and 90th percentiles. Each black circle represents an individual mouse (n=5 per group). Significant p-values $p \leq 0.05$ between groups are indicated by "*", or $p \leq 0.01$ as "**", or $p \leq 0.001$ as "***".

Possible ossification in the meniscus was analysed additionally (Figure 39E). Both WT and Syx animals after DMM surgery developed an increased bone surface of the meniscal ossicles (BS) compared to sham-operated mice (Figure 39E). Similarly, the bone mineral density (BMD) of meniscal ossicles was significantly higher in both WT and Syx DMM mice compared to the respective sham animals (Figure 39E). No differences in BS or BMD between WT and Syx mice were detected after DMM.

Increased expression of TH, TRAP and ARs in osteophyte region in WT and Syx mice post DMM

The expression of TH and the osteoclast activity was analysed in the osteophyte region by immunohistochemical staining for TH and TRAP (Figure 40A, B). To analyse whether cells in the osteophyte region could synthesize sympathetic neurotransmitters, staining was performed for TH. Only a few TH-expressing cells were detected in WT and Syx mice after DMM (Figure 40A). A reduction of TH expressing cell number occurred in Syx mice 8 weeks after DMM. Notably, in both WT and Syx mice, more TH expressing cells were detected 2 and 4 weeks after DMM compared to sham-operated mice (Figure 40A). TRAP staining was increased in WT and Syx mice 2 weeks after DMM compared to sham-operated mice. However, in Syx mice, less osteoclast activity was visible 4 weeks compared to WT mice after DMM (Figure 40 B?), which was consistent with the previous findings of TRAP staining in the subchondral bone (Figure 38). Additionally, the expression of α2A-AR (Figure 41) and β2-AR (Figure 42) after DMM or sham surgery was investigated in the region of osteophytes. Interestingly, a strong expression of α2A-AR was visible in WT mice 2 weeks after DMM, which was greatly increased when compared to WT sham (Figure 41B). Only a few α2A-AR-expressing cells were detected in Syx mice at 2 and 4 weeks after DMM. Whereas none to only a few α2A-AR-positive cells were present in sham-operated WT or Syx mice. Differences between DMM and sham-operated mice were significant in WT mice 2 and 4 weeks after surgery. Additionally, the percentage of α2A-AR-expressing cells decreased in WT mice 8 and 12 weeks after DMM, compared to mice 2 weeks after DMM.

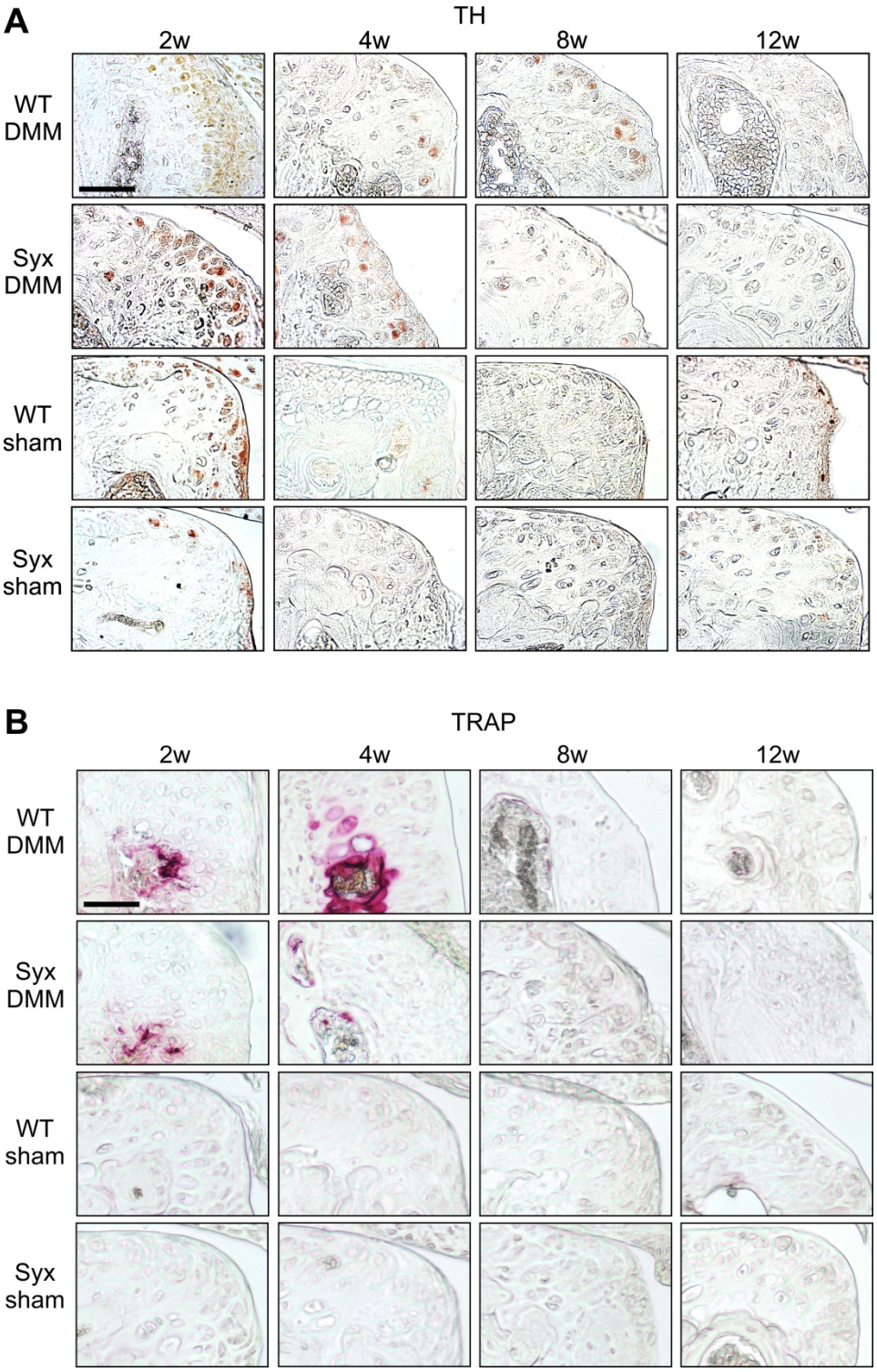

Figure 40 TH and TRAP expression in the region of osteophyte formation in WT and Syx mice.
Immunohistochemical detection of TH-expressing cells (brown) in the medial osteophyte region of WT and Syx mice 2, 4, 8 and 12 weeks after DMM or sham surgery (bar: 100µm). (B) Immunohistochemical detection of TRAP (magenta) in the medial osteophyte region of WT and Syx mice 2, 4, 8 and 12 weeks after DMM or sham surgery (bar: 100µm).

While in both WT and sham sham-operated mice only a few α2A-AR-expressing cells were detected, β2-AR-expressing cells were present in greater numbers (Figure 42). DMM surgery itself markedly increased the percentage of β2-AR expressing cells in WT mice at 2 and 4 weeks post-surgery compared to the sham operated animals. Similarly, in Syx DMM mice such a trend was found after 4 weeks, when more β2-AR-expressing cells were detected compared to sham-operated mice. Comparison of the percentage of β2-AR-expressing cells in WT and Syx mice revealed no significant differences at any of the time points. The percentage of β2-AR-expressing cells decreased in WT mice at 4 weeks, 8 weeks, and 12 weeks after DMM compared to earlier time points. Similarly, the percentage of β2-AR-positive cells in Syx mice 8 weeks and 12 weeks after DMM significantly declined compared to the expression after 4 weeks (Figure 42B).

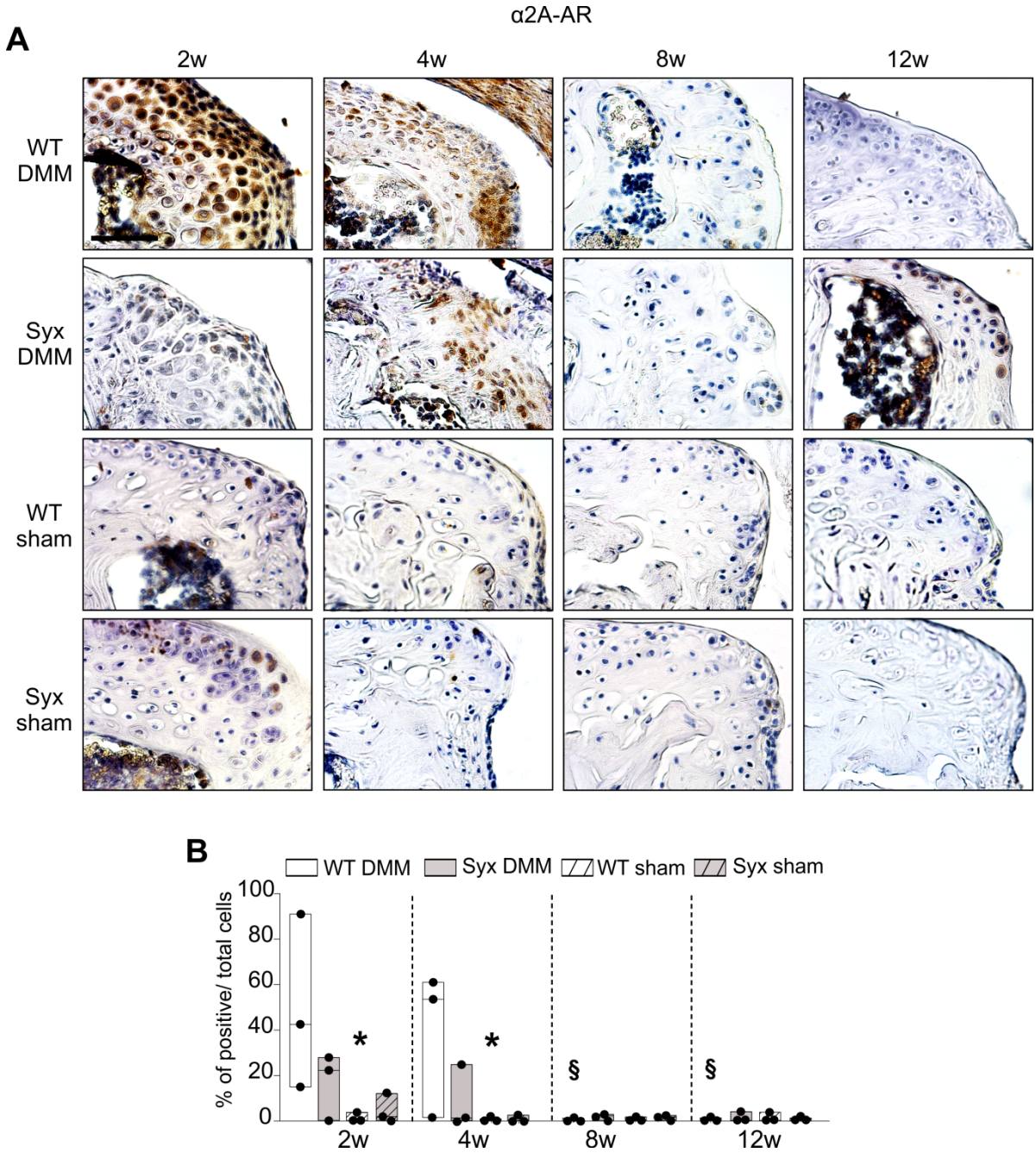

Figure 41 α2A adrenergic receptor expression in the osteophyte region of WT and Syx mice after DMM.

(A) Immunohistochemical detection of α2A-AR and quantification of α2A-AR-expressing cells in the medial osteophyte region of WT and Syx mice 2, 4, 8 and 12 weeks after DMM or sham surgery. Data are presented as box plots, where the boxes represent the 25th to 75th percentiles, the lines within the boxes represent the median, and the lines outside the boxes represent the 10th and 90th percentiles. Each black circle represents an individual mouse (n=3-4 per group). (WT DMM compared to WT sham: 2 weeks p=0.025, 4 weeks p=0.028; WT DMM 2 weeks-time point: to WT DMM 8 weeks p=0.021, to WT DMM 12 weeks p=0.021; bar: 100 µm).

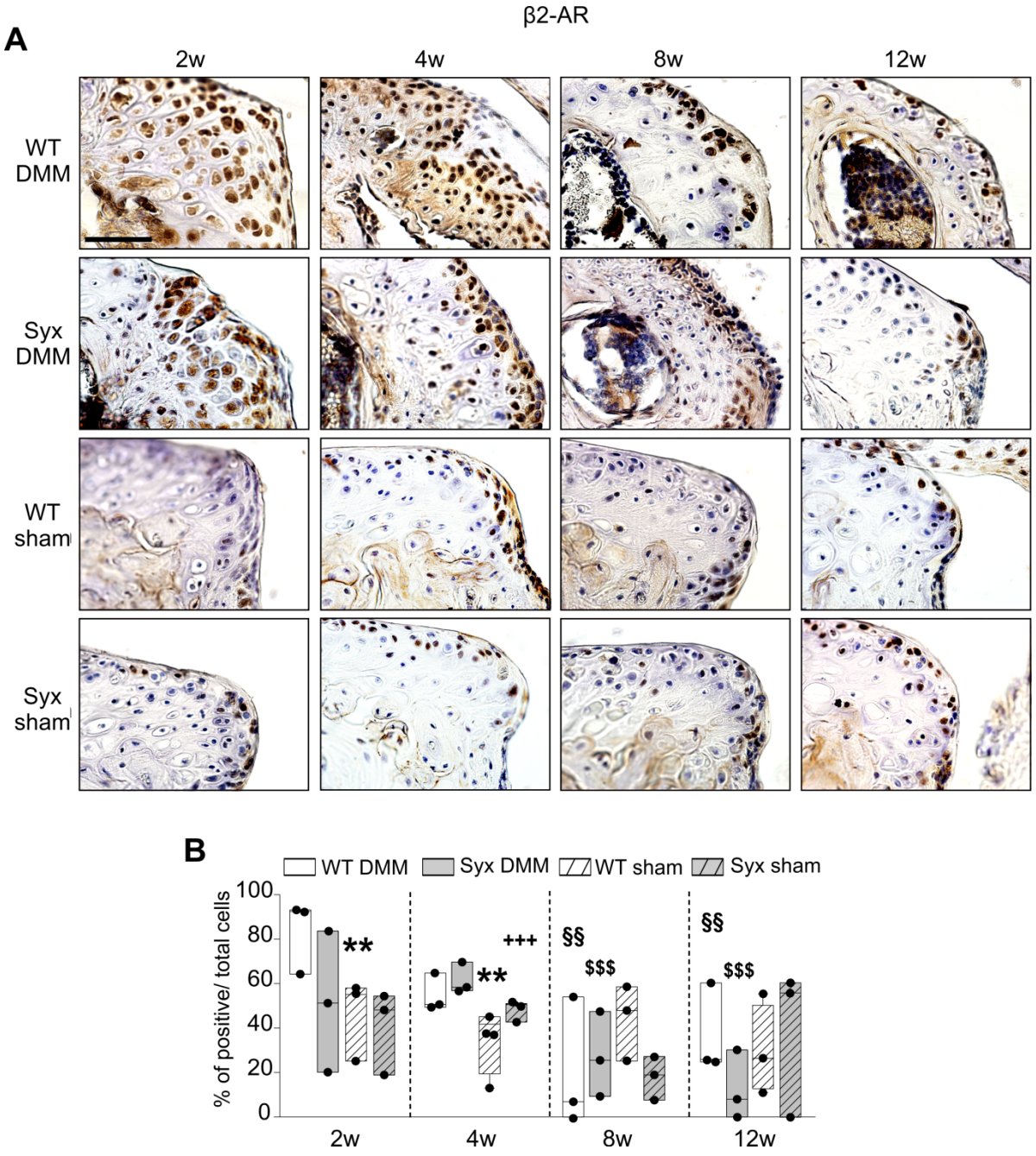

Figure 42 β2-AR adrenergic receptor expression in the osteophyte region of WT and Syx mice after DMM.

(A) Immunohistochemical detection of β2-AR and quantification of β2-AR-expressing cells in the osteophyte region of WT and Syx mice 2, 4, 8 and 12 weeks after DMM or sham surgery (WT DMM compared to WT sham: 2 weeks p=0.01, 4 weeks p=0.006; WT DMM 2 weeks-time point: to WT DMM 4 weeks p=0.01, to WT DMM 8 weeks p=0.004, to 12 weeks p=0.005; Syx DMM compared to Syx sham: 4 weeks p=0.008; Syx DMM 4 weeks-time point: to Syx DMM 8 weeks p<0.001, to 12 weeks p<0.001; bar: 100 µm). Data are presented as box plots, where the boxes represent the 25th to 75th percentiles, the lines within the boxes represent the median, and the lines outside the boxes represent the 10th and 90th percentiles. Each black circle represents an individual mouse (n=3-4 per group). Significant p-values ($p \leq 0.05$) to WT DMM at the same time point are indicated by "*", significant p-values to WT DMM at 2 weeks as "§§" when $p \leq 0.01$, significant p-values ($p < 0.001$) to Syx DMM at the same time point as "+++" and significant p-values ($p < 0.001$) to Syx DMM at 4 weeks as $$$.

3.2.7 Outlook: OA progression in β2-AR deficient mice

The present study demonstrated that sympathectomy suppressed the SNS signal transmission by reducing the number of synovial sympathetic nerves and the released splenic NE and that the SNS influences OA progression by increasing NE spleen levels, cartilage degradation, synovitis and also OA subchondral bone changes.

The next step was to narrow down if the β2-AR signaling is involved in these OA alterations and if these are similar to the alterations in Syx mice. To answer this question, DMM was induced in β2-AR deficient (Adrb2$^{-/-}$) mice to break off SNS signal transmission through the β2-AR.

The splenic NE concentration followed by the extent of cartilage degeneration, which were both increased in WT and Syx mice 8 weeks after DMM, were assesed in Adrb2$^{-/-}$ mice. In the last step, the subchondral bone changes of Adrb2$^{-/-}$ mice 8 weeks after surgery were analyzed and compared with WT and Syx mice.

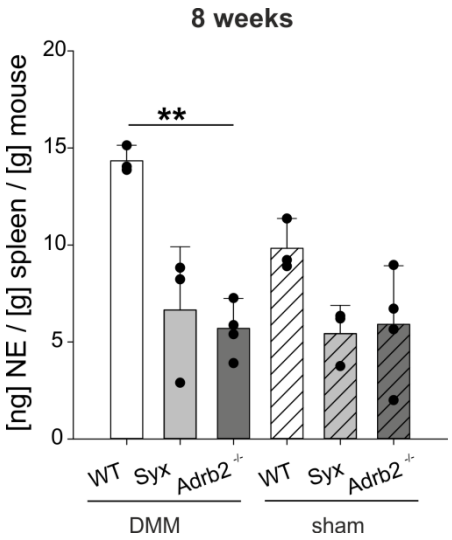

Figure 43 Splenic NE level of Adrb2-/- mice compared to WT and Syx mice.
Splenic NE level was significantly decreased in Adrb2-/- mice 8 weeks after DMM surgery compared to WT (Adrb2-/- DMM mice compared to WT DMM: p=0.031);. Data are presented as bars. The mean value of 3 technical replicates was calculated ±SE. Each black circle represents an individual mouse (n=3-4 per group). Significant p-values are indicated as ** when p ≤ 0.01.

At the initial step, NE level was measured in the spleen of Adrb2$^{-/-}$ mice and compared with NE levels of WT and Syx mice (presented in Figure 26). The analysis revealed that Adrb2$^{-/-}$ mice, similar to Syx DMM mice, had a significantly decreased NE level in the spleen after DMM compared to WT mice. No differences were detected between sham-operated Adrb2$^{-/-}$ mice and WT mice. However, the cartilage degeneration in Adrb2$^{-/-}$ mice was less pronounced after DMM (Figure 44A) compared to the excessive cartilage damage in WT mice (Figure 27). Consistent with this finding, the OARSI score was significantly decreased in Adrb2$^{-/-}$ mice compared to WT and also Syx mice 8 weeks after DMM (Figure 44B).

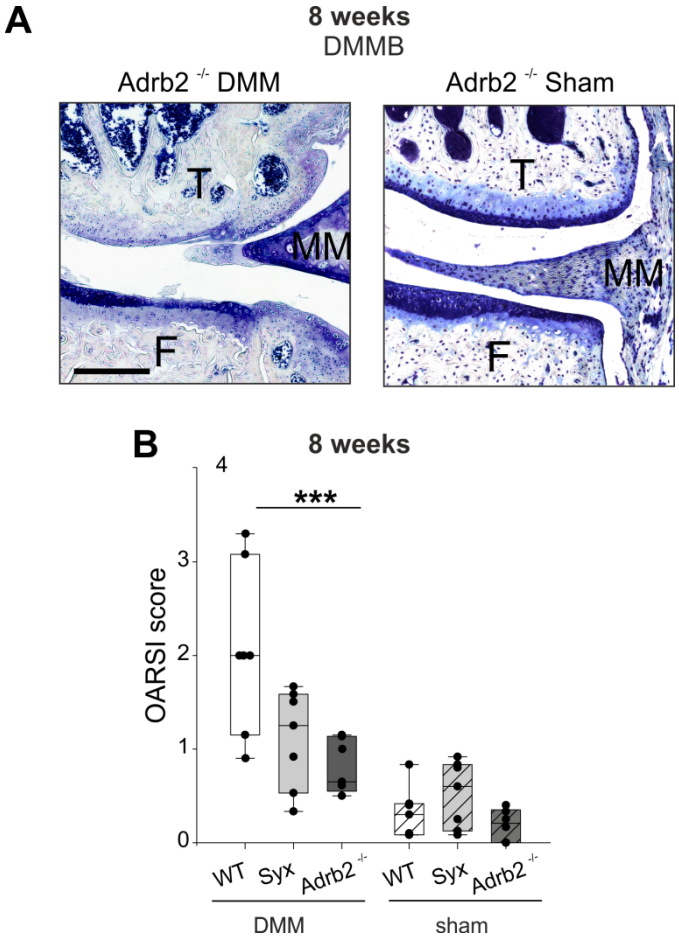

Figure 44 Cartilage degeneration in Adrb2$^{-/-}$ mice compared to WT and Syx mice.
(A) Histological analysis of the medial tibiofemoral articular cartilage contact area using DMMB staining in Adrb2$^{-/-}$ 8 weeks after DMM or sham surgery (F: femur, T: tibia, MM: medial meniscus, bar: 200 µm). (B) OARSI scores of the medial tibia plateau in Adrb2$^{-/-}$, Syx and WTmice 8 weeks after DMM and sham surgery. (Adrb2$^{-/-}$ DMM compared to Syx DMM: p= 0.05; Adrb2$^{-/-}$ DMM compared to WT DMM: p<0.001. Data are presented as box plots, where the boxes represent the 25th to 75th percentiles, the lines within the boxes represent the median, and the lines outside the boxes the 10th and 90th percentiles. Each black circle represents an individual mouse (n=3-5 per group). Each black circle represents an individual mouse (n=5 per group). Significant p-values p≤ 0.05 between groups. are indicated by "*", or p≤ 0.001 as "***".

These results suggest the involvement of β2-AR-signaling in cartilage degeneration. Additionally, the subchondral bone changes were analysed in Adrb2$^{-/-}$ mice by 3D micro-CT joint reconstruction. These images indicated a higher density of the subchondral bone on the medial side Adrb2$^{-/-}$ mice 8 weeks after DMM compared to a sham-operated Adrb2$^{-/-}$ mice (Figure 45A, B). In the top view of the tibia plateau, smaller trabecular spaces in DMM-operated mice on the medial side (Figure 45B) were visible, indicating a higher bone density compared to sham-operated mice (Figure 45D). The quantification revealed a significant increase of BV/TV, TbSp and TbTh in Adrb2$^{-/-}$ DMM compared to WT DMM mice (Figure 45E). Compared to Syx mice, Adrb2$^{-/-}$ mice developed significantly smaller TbSp after DMM, while other measured bone parameters were not altered. However, BV/TV in Adrb2$^{-/-}$ tended to be higher while TbTh and TbSp were smaller compared to Syx mice after DMM. Additionally, the subchondral bone volume in DMM-operated Adrb2$^{-/-}$ mice was increased compared to sham-operated Adrb2$^{-/-}$ mice, as indicated by the significant differences in BV/TV, TbSp, TbN and TbTh between these mice (Figure 45E).

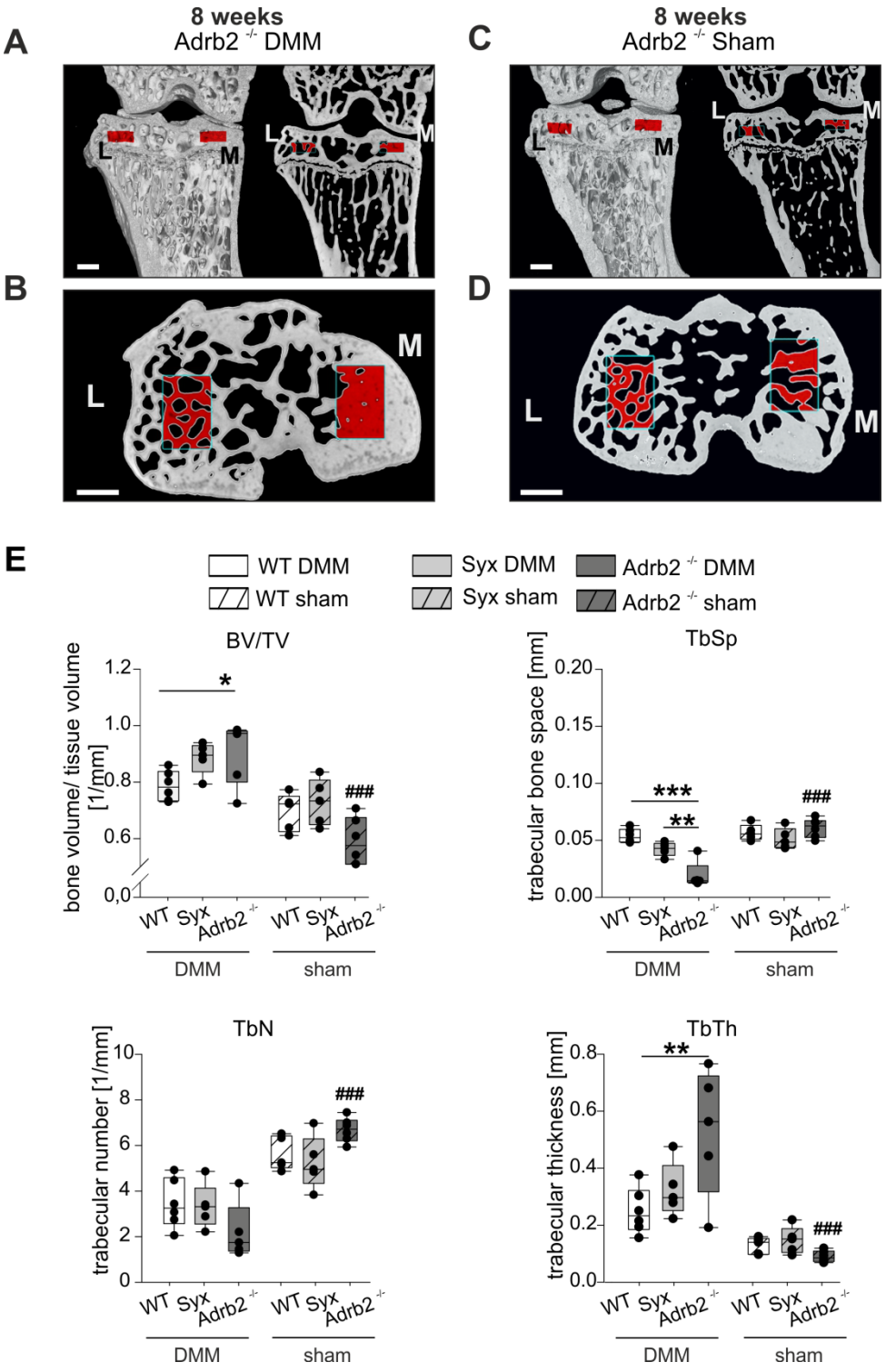

Figure 45 Micro-CT analysis of the subchondral bone architecture of Adrb2-/- mice after DMM and sham surgery.

(A) Representative micro-Ct images of the frontal knee joint and (B) top view of the tibia plateau showing the volume of interest (VOI, indicated by red rectangles) in the subchondral bone in Adrb2$^{-/-}$ mice 8 weeks after DMM or sham surgery (C-D). (E) Quantitative 3D analysis of BV/TV, TbSp, TbN, and TbTh within the VOI in WT and Syx and Adrb2$^{-/-}$ mice 8 weeks after DMM or sham surgery. (Adrb2$^{-/-}$ DMM compared to Syx DMM: TbSp p=0.002; Adrb2$^{-/-}$ DMM compared to WT DMM: BV/TV p=0.018, TbSp p<0.001, TbTh p=0.002; Adrb2$^{-/-}$ DMM compared to Adrb2$^{-/-}$ sham: BV/TV p<0.001, TbSp p<0.001,TbTh p<0.001, TbN p<0.001. Data are presented as box plots, where the boxes represent the 25th to 75th percentiles, the lines within the boxes represent the median, and the lines outside the boxes represent the 10th and 90th percentiles. Each black circle represents an individual mouse (n=5 per group). Significant p-values p≤ 0.05 between treatment groups are indicated by "*", or p≤ 0.01 as "**" or p≤ 0.001 as "***". Significant p-values between Adrb2$^{-/-}$ DMM compared to Adrb2$^{-/-}$ sham were indicated by ###. Bars: 0.45 mm.

4 Discussion

The SNS is involved in many different disorders. During the past decades, the contribution of the SNS in the musculoskeletal system such as bone homeostasis has been confirmed (Grässel, Straub, and Jenei-Lanzl 2017). Furthermore, the contribution of the SNS in musculoskeletal pathologies such as musculoskeletal pain in fibromyalgia was also reported (McEwen and Stellar 1993; Malpas 2010; Martínez-Martínez et al. 2014). However, little is known about its involvement in OA manifestation and progression. Although several joint tissues in the knee are innervated by sympathetic nerves, their role in OA development still remains unclear (Hukkanen et al. 1992; Eitner et al. 2013). The SNS is acting in the periphery mainly through the neurotransmitter NE, that is released by sympathetic nerve fibers. In the synovial fluid of OA and knee-trauma patients, a considerable amount of the sympathetic neurotransmitter NE was detected (Jenei-Lanzl et al. 2014; Miller et al. 2000) but its influences on the regenerative potential of joint-resident MSC or on multiple joint-tissues during OA progression is not known. The current study investigated these aspects and demonstrates for the first time the effects of NE on the chondrogenic potential of sASCs *in vitro* and the contribution of SNS to OA pathogenesis *in vivo*.

4.1 NE influences the regenerative potential of sASCs

Damaged articular cartilage has a limited ability to self-repair due to a lack of vascularity, and due to poor proliferation and matrix synthesis of chondrocytes (Tuan, Chen, and Klatt 2013). Recent studies have emphasized that joint-resident MSC might be involved in cartilage regeneration processes (Huang et al. 2017). A great number of MSC were detected in OA articular cartilage compared to healthy cartilage, but these MSC show an insufficient chondrogenic potential and are not able to fully regenerate the damaged cartilage (Grogan et al. 2009; Fickert, Fiedler, and Brenner 2004; Su et al. 2015). The reasons for the increase of MSC numbers and the insufficient repair of degenerative OA cartilage are not completely understood.

Furthermore, in the last decades, the interest in MSC-based therapy for OA has increased. Especially ASCs are of great interest, which have been shown to prevent OA development in rats (Zare et al. 2020) and to reduce pain and regenerate cartilage in OA patients after intraarticular injection (Freitag et al. 2020). In order to repair the damaged cartilage, the highly proliferative sASCs with greater chondrogenic capacity in producing ECM molecules would be advantageous compared with the limited proliferative and chondrogenic function of mature chondrocytes (McGonagle, Baboolal, and Jones 2017). There is strong evidence from *in vivo* and *in vitro* models that sASCs can migrate to damaged cartilage areas and to contribute to

cartilage repair (To et al. 2019; Ogata et al. 2015). However, it is not clear if their proliferation and ability to differentiate to chondrocyte phenotype are influenced by NE, which was detected in the synovial fluid and released by sympathetic nerves in joint-tissues (Grässel, Straub, and Jenei-Lanzl 2017). Therefore, this study investigated the proliferation and chondrogenic capacity of sASCs in presence of NE.

4.1.1 sASCs from OA synovia can differentiate to chondrocytes

In the initial step of this study, the molecular MSC characteristics of the isolated sASCs from osteoarthritic synovium were confirmed as MSC are able to differentiate into chondrocytes and other cell types (Dominici et al. 2006; Fan et al. 2016). In our study, sASCs expressed MSC-specific surface marker. Furthermore, the ability of OA sASCs to differentiate to chondrocyte was shown. ASCs from osteoarthritic synovium were able to condensate and develop characteristic chondrogenic pellets. Moreover, after chondrogenic differentiation, the cells expressed cartilage-specific markers and ECM molecules as described in healthy sASCs (Ogata et al. 2015). Our study therefore suggests that ASCs from osteoarthritic joint are able to differentiate to chondrocytic phenotype.

4.1.2 AR expression in sASCs

In the present study, the expression of several AR subtypes in sASCs was confirmed, indicating that sASCs are target cells of the SNS. AR gene expression in ASCs derived from OA synovial tissue was not demonstrated before, while ARs have been detected in OA BMSC (Hedderich et al. 2020). In general, studies regarding AR expression in ASCs are sparse. Only two studies have reported the expression of AR subtypes such as α2A-AR and β2-AR on RNA and protein level in ASCs from abdominal subcutaneous fat tissue (Kotova et al. 2014; Tyurin-Kuzmin et al. 2018). Interestingly, in line with our results, an expression profile of AR at the RNA level was described in chondrocytes from osteoarthritic cartilage (Speichert et al. 2019; Lorenz et al. 2016). Other cells such as osteoblasts (Huang et al. 2009), smooth muscle cells and renal cells (Carney 2016), which are from the same embryonal mesoderm origin as chondrocytes express several subtypes of α-AR or β-ARs (Motiejunaite, Amar, and Vidal-Petiot 2020) .

Furthermore, the expression of different AR subtypes might be tissue-specific and also influenced by the pathophysiological situation. This can be caused by a catabolic microenvironment with increased NE concentrations that might influence the expression level of ARs (Speichert et al. 2019; Tyurin-Kuzmin et al. 2018). *In vitro* studies regarding

chondrogenic potential of differentiated MSC and chondrocytes have shown that NE influenced cartilage physiology and pathophysiology in a catabolic manner, that was mainly by α2A-AR and β2-AR signal transmission (Jenei-Lanzl et al. 2014; Lorenz et al. 2016). Both α2A-AR and β2-AR were strongly expressed on protein level during chondrogenic differentiation of sASCs in the current study, suggesting that NE could act through both of these receptors.

Furthermore, autocrine and paracrine effects of sASCs can be excluded because TH was neither detected in monolayer nor in chondrogenic sASCs cultures. This is in agreement with previous findings in OA chondrocytes (Speichert et al. 2019) or BMSC derived from trauma or OA patients that did not express TH (Jenei-Lanzl et al. 2014; Hedderich et al. 2020). Since joint resident MSC and chondrocytes express AR, an interaction between these cells with neurotransmitters including NE was proposed, which is also supported by other studies (Takarada et al. 2009; Mitchell et al. 2011).

4.1.3 Proliferation of sASCs in presence of NE

In the last decades, it has been confirmed that MSC are present in healthy and arthritic cartilage. However, in OA cartilage the number of MSC is increased compared to that in healthy cartilage (Grogan et al. 2009; Fickert, Fiedler, and Brenner 2004; Su et al. 2015). This increase might be a result of migration of MSC from the surrounding joint tissues or the proliferation of resident MSC for matrix repair. While the increased number of MSC suggests an increased regeneration capacity, they however show reduced proliferative and chondrogenic potential (Grogan et al. 2009). NE, which is released from sympathetic nerves in the joint, might be one factor that influences the proliferation of MSC. This study, demonstrated that the treatment with NE was not toxic in any of the tested concentrations and did not influence cell proliferation, indicating that NE in the knee-joint might not influence the proliferation or viability of sASCs. This is in line with another study showing that NE did not affect the viability of human OA chondrocytes (Speichert et al. 2019) Interestingly, the proliferation of both OA and trauma BMSC was inhibited dose-dependently by NE without affecting cell viability (Hedderich et al. 2020). Treatment with the highest concentration of 10^{-6} M NE reduced the proliferation of OA BMSC significantly through the activity of β2-AR signalling pathway. This confirms another study reporting the G1-phase cell cycle arrest of human OA chondrocytes after treatment with 10^{-6} M NE, which was reversed by the beta2-AR antagonist (Lorenz et al. 2016). Altogether, these interesting data strongly imply that regenerative MSC or chondrocytes in the knee-joint are differently affected in their proliferation by NE, potentially due to a different AR expression profile. These data suggest that compared to the proliferation of MSC, their potential to differentiate and to produce ECM molecules is crucial for cartilage repair.

4.1.4 NE-effects on the chondrogenic potential of sASCs

In this study, NE suppressed sASCs chondrogenesis dose-dependently. This finding is corroborated by recent work, demonstrating decreased sGAG and type II collagen synthesis of BMSC during chondrogenic differentiation under NE influence (Jenei-Lanzl et al. 2014). This effect was caused by the acceleration of the hypertrophic pathway, where the expression of hypertrophic markers such as *MMP-13* and *COL10* was reversed by a specific β2-AR antagonist. However, in the current study, hypertrophic differentiation characterized by increased RUNX2 or MMP-13 expression was not observed, potentially due to physioxic cell culture conditions (2% O_2) in this study that promotes chondrogenesis as demonstrated previously (Portron et al. 2015; Pattappa et al. 2019). Compared to normoxic conditions, the low oxygen concentration stimulated the chondrogenic differentiation by increased expression of chondrogenic markers and downregulated the expression of hypertrophic markers of chondrocytes and MSC (Portron et al. 2015; Pattappa et al. 2019). Altogether, it can be excluded that the reduced chondrogenic potential of sASCs is due to hypertrophic differentiation or a decreased cell number after NE treatment. Furthermore, the treatment with NE followed by activation of AR signaling indicated by elevated ERK1/2 levels, downregulated the expression of type II collagen and sGAG. These results are in line with a recent study showing the inhibition of type II collagen protein expression in murine chondrocytes after stimulation with an β2-AR agonist and increased phosphorylation of ERK1/2 (Mitchell et al. 2011).

Our data revealed that a high NE concentration (10^{-6} M) reduces the chondrogenic potential, indicating the contribution of the β2-AR signaling (Pongratz and Straub 2014), as supported by previous studies (Mitchell et al. 2011; Jenei-Lanzl et al. 2014) (Pongratz and Straub 2014). Contrary to expectations, the β2-AR antagonist propranolol neutralized the NE effects only in tendency, while the α2A-AR antagonist yohimbine significantly reversed the inhibitory effect of NE on the pellet volume and synthesis of type II collagen and sGAG, indicating that NE is acting through the α2A-AR. These mixed α2A-/β2-AR-mediated effects might be due to the instability of NE under cell culture conditions, as demonstrated in this study. The initial NE concentration was reduced to less than 40% after one to two days. Similar to our results, NE-mediated α2A-AR signaling has been described in chondrocytes of the temporomandibular joint (Jiao et al. 2016). In that study, NE in a concentration of 10^{-8} M led to the increased expression of catabolic markers such as MMP-13 in monolayer culture, which was abolished by α2A-AR antagonist yohimbine. In the present study, the α1-AR was not involved in NE-induced effects, as described in other studies regarding α1-AR-induced influences on chondrogenesis. This study demonstrated that sASCs from osteoarthritic synovia have the ability to differentiate into chondrogenic phenotype, which is reduced by NE mainly through the

α2A-AR signaling. However, the underlying mechanisms of NE inhibitory effects in sASC via ERK1/2 activation and its influence on matrix synthesis, remain unclear.

4.1.5 NE-induced activation of intracellular signaling pathways

In the current study, treatment with high NE concentrations led to the activation of the downstream intracellular ERK1/2 signaling pathway, without influencing the alternative PKA pathway. ERK1/2 are two mitogen-activated protein kinases (MAPK), that are considered to play a role at the beginning of chondrogenesis and also in the synthesis of matrix proteins. At the beginning of chondrogenesis, ERK1/2 negatively regulate chondrogenesis by repressing the cell-cell adhesion in the initial MSC condensation step (Stanton, Underhill, and Beier 2003). In agreement with this, ERK 1/2 inhibition was shown to increase chondrogenesis of chick mesenchymal stem cells from chick limb bud, while ERK 1/2 phosphorylation decreased the chondrogenesis in the same system (Oh et al. 2000). Another MAP kinase, p38, was reported to show opposing effects compared to ERK1/2. The inhibition of p38 reduced the chondrogenesis of MSC (Oh et al. 2000). As ERK 1/2 can be activated by AR mediated signalling (Blesen et al. 1995; Bogoyevitch et al. 1996; Alblas et al. 1993), it was analysed in the present study. *In vitro*, ERK1/2 phosphorylation affects the chondrogenic nodule formation at the beginning of chondrogenesis by downregulating the expression of cell adhesion molecules such as cadherins and integrins that play an initial role in condensation (Oh et al. 2000; Oberlender and Tuan 1994; Tavella et al. 1997; Yoon et al. 2000). It can be therefore be speculated that the ERK 1/2 activation by NE and α2A-AR signalling might affect also the expression of adhesion molecules including cadherins and integrins. In the current study, NE treatment influenced matrix protein synthesis but not chondrogenic nodule formation. ERK 1/2 plays a pivotal role not only in the chondrogenesis of MSC but also in the expression of type II collagen by chondrocytes. Several studies showed that ERK 1/2 phosphorylation inhibits the expression of type II collagen in murine or rat articular chondrocytes, which was reversed by an ERK 1/2 inhibitor (Eo, Choi, and Kim 2016; Mitchell et al. 2011). This is in line with our present study which demonstrated that NE stimulation and subsequent activation of α2A-AR signalling indicated by ERK 1/2 phosphorylation, mediated the reduction of type II collagen. Our data are consistent with one study that investigated the dose-dependent inhibitory effects of NE in chondrocytes temporomandibular joint (Jiao et al. 2016). The authors demonstrated that α2A-AR mediated catabolic effects of NE by decreasing aggrecan and increasing MMP-13, which were attenuated by yohimbine. Furthermore, they also reported that NE-mediated effects were suppressed by an ERK1/2 inhibitor. Another previous study showed the involvement of β2-AR in the inhibition of type II collagen of murine chondrocytes (Mitchell et al. 2011). A specific β2-AR agonist activated ERK 1/2 signalling, leading to increased

expression of the downstream activator protein 1 (AP-1) factor Jun-B, that was mainly responsible for the inhibition of Col II gene expression in mice chondrocytes (Mitchell et al. 2011). In summary, our *in vitro* study has demonstrated that NE mediated α2-AR signalling inhibits the expression of type II collagen and sGAG and therefore the chondrogenic potential of sASCs. These data suggest that the release of NE by sympathetic nerves in the knee-joint might influence synovium-resident ASC in their regeneration capacity and therefore the cartilage damage, thus contributing to the development of OA (Grogan et al. 2009). Overall, these results suggest that inhibition of the α2-AR signaling might be a promising new therapeutic approach in OA treatment.

4.2 Novel insights into sympathectomy effects in OA development

Peripheral sympathetic nerves are selectively destroyed by chemical sympathectomy using 6-OHDA, leading to drastically reduced concentration of NE and other catecholamines in the tissue (Thoenen and Tranzer 1968). The partial blockage of signal transmission by the SNS using sympathectomy has been previously reported in a murine arthritis model (Jenei-Lanzl et al. 2015; Härle et al. 2008), in which, sympathectomy with 6-OHDA had anti-inflammatory effects. The contribution of the SNS in OA is however unclear. The present study investigated contribution of the SNS in OA pathogenesis using sympathectomy in a murine OA model and demonstrated that sympathectomy affects several aspects of OA.

4.2.1 Elevated splenic NE levels after OA induction by DMM

The present study demonstrated that chemical sympathectomy destroyed sympathetic nerves in the synovium. This is in line with other studies showing approximately 80% reduction of sympathetic nerve fibers in the periphery (Härle et al. 2008). The spleen is innervated by sympathetic nerve fibers that release a great amount of catecholamines (Felten et al. 1987). In addition to the reduction of sympathetic nerves, splenic NE levels were rapidly depleted after sympathectomy as reported in a previous study analyzing collagen-induced arthritis in mice (Jenei-Lanzl et al. 2015; Härle et al. 2008).

Surprisingly, elevated NE levels were detected in the spleen of WT mice with OA induced by DMM surgery, suggesting an increased sympathetic activity compared to sham or healthy WT mice. A local inflammation post OA induction might be one reason for the elevated NE levels as inflammation can be associated with increased activity of the SNS (Pongratz and Straub 2014). The increased sympathetic activity due to DMM could also induce an increased NE outflow from lymphoid organs such as the spleen, as already shown in humans with rheumatoid arthritis (Grässel, Straub, and Jenei-Lanzl 2017; Pongratz and Straub 2014). Another explanation for the elevated sympathetic tone could be the mechanical stress caused by DMM (Marenzara and Chenu 2008). Increased NE serum level and sympathetic nerve distribution in the bone have been reported to result from an SNS response to mechanical stress in rats with OA in the temporomandibular joints after abnormal loading (Jiao, Niu, Xu, et al. 2015). In that study, sympathectomy in mice with 6-OHDA reduced the NE level in the condylar subchondral bone after aberrant mechanical loading in the temporomandibular joint. Interestingly, the present work demonstrated a reduced splenic NE level after DMM or sham surgery in β2-AR deficient mice, an effect similar to Syx mice. However, the link between β2-AR expression and NE synthesis remains unclear.

In brief, OA induction leads to increased NE level in WT mice but not in Syx or β2-AR deficient mice. Compared to WT mice, both Syx and β2-AR deficient mice had less pronounced progression of OA induced by DMM surgery, implying a role of the sympathetic tone in OA pathogenesis.

4.2.2 The protective effect of sympathectomy in OA cartilage

OA induction by DMM causes joint instability and an abnormal mechanical loading resulting in cartilage degeneration (Glasson, Blanchet, and Morris 2007). Sympathectomy led to less pronounced cartilage degeneration indicated by lower OARSI scores. Additionally, sympathectomy reduced the degradation of type II collagen as indicated by reduced serum CTX-II levels compared to WT DMM mice. CTX-II was also demonstrated to be higher in spontaneous osteoarthritic mice (Watari et al. 2011) and in knee-OA patients compared to healthy ones (Arunrukthavon et al. 2020). The increased CTX-II level in WT mice after 4 weeks suggests that type II collagen degradation begins at the early stage of OA development. Furthermore, CTX-II is metabolized by liver or kidney and therefore might not be detectable anymore at later time points (Garnero 2007) .

The metalloprotease MMP-13 is implicated in proteolytic cleavage of type II collagen and the release of CTX-II fragment (Zhen et al. 2008). Since cartilage degradation was reduced in Syx mice compared to WT, it has been hypothesized that MMP-13 expression might also be decreased in Syx mice compared to WT. While there was a decrease in MMP-13 expression after DMM in both Syx and WT mice, there was no difference between them post DMM. Only hypertrophic chondrocytes which are increased in OA (Mackie, Tatarczuch, and Mirams 2011) were expressing MMP-13 in WT and Syx mice after DMM. By contrast sham-operated WT and Syx mice showed a strong MMP-13 expression. The expression of MMP-13 in chondrocytes of sham-operated mice was also shown in previous studies (Lorenz et al. 2014). The reduced MMP-13 expression in the present study might be due to overloading after DMM (Almonte-Becerril et al. 2010) resulting in damaged cartilage with a loss of MMP-13 expressing chondrocytes due to apoptosis. Healthy chondrocytes express certain level of MMP-13 (Yamamoto et al. 2016), which is required for a physiological cartilage ECM turnover and thus essential for cartilage homeostasis (Goldring et al. 2008). Contrary to our hypothesis, the present study indicates that sympathectomy had no impact on MMP-13 expression in the cartilage and that increased cartilage degeneration is most likely not a result of MMP-13 derived from cartilage.

Apart from the effect of increased catabolic activity in OA, the increased chondrocyte death in DMM cartilage potentially results from an increased expression of inflammatory mediators and

reactive oxygen species (ROS) released upon cartilage injury (Goldring and Otero 2011; Goodwin et al. 2010).

The present study also demonstrated that articular chondrocytes can be target cells of the SNS based on their expression of α2A-AR and β2-AR. Along this line, it has been reported that chondrocytes in murine articular cartilage express both α2A-AR and β2-AR (Mitchell et al. 2011; Lai and Mitchell 2008) and that signalling by the latter receptor inhibits type II collagen secretion of articular chondrocytes *in vitro* (Mitchell et al. 2011). Furthermore, the SNS has been reported to regulate chondrocyte growth and activity through the β2-AR receptor (Mitchell et al. 2011). The data presented here show a greater number of β2-AR expressing cells in cartilage compared to α2A-AR expressing cells. However, a decreased expression of both receptors was detected in several areas in DMM damaged cartilage compared to healthy controls, which is most likely due to the decreased number of cells in those areas. By contrast, other studies reported an upregulation of α2A-AR and β2-AR in chondrocytes after OA induction in the condylar cartilage in temporomandibular joints of rats (Jiao et al. 2016; Jiao, Niu, Li, et al. 2015). However, in those studies AR expression was assessed in areas with few cartilage lesions and defects, compared to the present study. In brief, the data showing less severe cartilage damage in β2-AR knockout than in WT strengthens the hypothesis that β2-AR signal transmission plays a major role in cartilage degeneration. Overall, these data provide strong evidence that the SNS contributes to the progression of cartilage degeneration in OA and that NE via the β2-AR-signaling plays a pivotal role in these processes.

4.2.3 Reduced synovial inflammation in OA after sympathectomy

In line with a previous report, the α2A-AR and β2-AR were expressed in the synovium from WT and Syx mice (Miller et al. 2002). Interestingly, DMM enhanced α2A-AR expression in the synovium, potentially due to increased inflammation of the synovium. Since the synovium is a major inflammatory contributor in OA pathogenesis, the influence of Syx on the DMM-induced synovitis was explored. As shown in the present study, WT animals developed pronounced synovitis after DMM which is in agreement with previous findings (Lewis et al. 2011). Interestingly, a slight increase of the synovitis score was observed already 2 weeks after DMM, suggesting that the DMM surgery leads to an early inflammatory response in the synovium. This is in line with a previous study, showing that DMM surgery leads to synovitis in mice at early stages postoperatively (Jackson et al. 2014). Inflammation of the synovium and elevated cytokine production was also observed in the synovium of patients at early stages of OA (Smith et al. 1997).

At later time points, synovitis scores in DMM-operated mice were significantly higher when compared with sham-operated mice. Notably, sympathectomy resulted in significantly lower

synovitis scores compared to WT mice, suggesting that reduced sympathetic activity attenuates synovitis. It is unclear whether synovitis in this study leads to the initiation of cartilage degeneration or results from it. Cartilage damage can lead to the release of degrading enzymes, matrix protein fragments, and cytokines into the synovial fluid (Loeser et al. 2012). The activation of synovial immune cells such as macrophages causes increased MMP production and release that might influence cartilage degeneration (Blom and Berg 2007). In the current study, synovial inflammation was shown to be linked to cartilage degeneration by a moderate correlation of OARSI and synovitis score in WT mice post DMM. These results were consistent with previous work showing that pathological changes in both tissues are linked to each other (Blom and Berg 2007).

Therefore, it was of interest to explore if synovitis is accompanied by the expression of MMP-13 because MMP-13 secreted and released from the synovium is considered to be involved in cartilage degradation during OA progression (Blom et al. 2004; Marini et al. 2003). Interestingly, at earlier time points, MMP-13 was highly expressed in the synovium of WT mice in contrast to Syx mice after DMM, likely resulting from acute local inflammation after DMM induction. The enhanced MMP-13 expression in WT mice after DMM observed in the current study might contribute to the accelerated degradation of cartilage in these animals as reported previously (Shlopov et al. 1999).

Furthermore, synovitis is promoted by the infiltration of immune cells that express pro-inflammatory mediators, including IL-1 and tumor necrosis factor-alpha (TNF-α) (Wenham and Conaghan 2010). The SNS influences the response of immune cells, which is dependent on their AR expression profile and the catecholamine concentration (Nance and Sanders 2007; Pongratz and Straub 2014). Previous reports showed an increase of pro-inflammatory cytokine production in OA synoviocytes after treatment with 10^{-6} and 10^{-7} M NE (Miller et al. 2000). These studies suggest that increased SNS activity via NE might increase inflammation and the release of cytokines into the synovial fluid, thus promoting cartilage degeneration.

The data presented here demonstrate that sympathectomy resulted in a deprivation of sympathetic nerves in the synovium. In a compensatory response for this loss, production of neurotransmitters is initiated by resident cells (Capellino et al., 2010), demonstrated by the presence of single TH-positive cells in Syx mice in the current study. The TH-positive cells were more evident in the strongly inflamed synovium after DMM in WT animals compared to the synovium of Syx animals. AR expression observed at all time points in the animals analyzed suggests that catecholamines such as NE synthesized locally by TH-positive cells, potentially stimulate nearby cells expressing the ARs in the synovium. Capellino et al. described a loss of sympathetic nerves in the synovium during inflammation in rheumatoid

arthritis, a chronic inflammatory disorder that affects many joint tissues. However, new TH expressing cells were observed in the inflamed synovium, considered to have anti-inflammatory effects by inhibiting innate immune cells early in the inflammation process. NE is known to mediate anti-inflammatory effects in RA in a concentration dependent manner via the targeted β2-AR (Pongratz and Straub 2014; Lorton and Bellinger 2015). It was also reported that the released NE from the synovium reduced the joint inflammation in RA (Capellino et al. 2010; Harle et al. 2005; Jenei-Lanzl et al. 2015). The production of NE by TH-positive synoviocytes has been shown to correlate with the degree of synovitis in RA (Miller et al. 2002). The anti-inflammatory character of these TH-positive cells has been demonstrated so far only in RA models *in vivo*. *In vitro* studies have described the anti-inflammatory effects of TH-positive cells in the synovium by inhibition of TNF in OA and RA synovial cells (Herrmann et al. 2018). However, no *in vivo* studies exist regarding the anti-inflammatory character of TH expressing cells in the synovium in OA, that may have a role in the suppression of synovitis. It can be therefore speculated that the synovitis in WT mice is due to the progressive cartilage damage and not due to the increased expression of TH-positive cells in the synovium (Miller et al. 2002).

4.2.4 Aggravation of subchondral bone changes after sympathectomy

Emerging evidence indicates that bone remodelling is increased in OA, leading to subchondral bone changes such as elevated subchondral bone density, volume and mineralization (Adebayo et al. 2017; Radin, Paul, and Tolkoff 1970). The DMM model used in the present study resulted in characteristic OA changes of the subchondral bone. This is in line with many reports, describing the subchondral bone changes in surgically induced and spontaneous OA animal models, (Brandt et al. 1997; Hayami et al. 2004) and particularly in DMM induced OA studies (Fang et al. 2018; Das Neves Borges, Vincent, and Marenzana 2017).

Recent studies addressed the involvement of SNS and especially NE in the regulation of bone remodelling (Ma et al. 2013). Based on the presence of sympathetic nerves in the subchondral bone (Hukkanen et al. 1992) and the expression ARs in osteoblasts and osteoclast (Huang et al. 2009; Mlakar et al. 2015), studies suggested that the SNS participates in bone metabolism (Franquinho et al. 2010; Lerner and Persson 2008). The two major receptors for NE, the α2-AR and β2-AR were detectable in the area of osteophyte formation in the present study. Furthermore, a higher expression of these receptors and TH was observed at an early stage after OA induction, indicating SNS contribution in OA related subchondral bone changes.

The present study clearly demonstrated that a partial blockage of the SNS by sympathectomy aggravates the OA-specific changes in mice such as the increase of the subchondral bone

volume, and the thickness of the subchondral bone plate after DMM compared to WT animals after DMM. These novel data strongly indicate that signal transmission of the SNS via neurotransmitters affects bone remodelling during OA development. This finding is in agreement with a previous study that described a similar phenotype in mice deficient in dopamine β-hydroxylase, an enzyme which converts dopamine to NE. Knockout of this enzyme resulted in increased bone density, indicating that reduced SNS activity increased bone formation (Takeda et al. 2002). Furthermore, chemical sympathectomy with 6-OHDA in adult rats without additional OA induction inhibited bone resorption (Hu et al. 2010). In the same study, rats without sympathectomy that were stressed by unpredictable footshock, had higher NE levels in serum and increased bone resorption, (Hu et al. 2010). The increased subchondral bone volume observed after sympathectomy in the present study in Syx mice compared to WT mice after OA induction could therefore be explained by decreased bone resorption on the one hand, and reduced osteoclast activity on the other hand. These results imply that decreased NE level and signal transmission of the SNS decreased osteoclast activity, leading to higher bone volume. Consistent with these results, sympathectomy with 6-OHDA decreased bone NE level and prevented bone loss after abnormal loading of the temporomandibular joint in mice (Jiao, Niu, Xu, et al. 2015).

In Syx mice, the SNS in partially blocked by a reduction in the release of catecholamines leading to a destruction of the peripheral sympathetic nerves. In β2-AR deficient mice, the β2-signaling is completely blocked, while sympathetic nerves are present, that release catecholamines. This implies that signal transmission through the β2-AR plays a major role in OA specific increased subchondral bone volume. As the knockout of β2-AR caused more bone formation then the blockage of the SNS signaling by sympathectomy, it can be inferred that the β2-AR signaling plays a pivotal role in sympathetic activity in OA.

Recent studies report that chronic stress with elevated NE levels leads to compromised fracture healing in mice and that leptin, a hormone regulating body weight inhibits bone formation and induced osteoporosis by targeting the β2-AR (Takeda et al. 2002). There is evidence that SNS activity causes bone loss through an increase of bone resorption and a decrease in bone formation mainly by the β2-AR signaling (Elefteriou 2018; Elefteriou et al. 2005). While more studies provide evidence of the β2-AR contribution in bone metabolism, a few also report the involvement of α2-AR (Jiao et al. 2016). It was reported in animal studies without OA induction that the SNS promotes bone resorption through the β2-AR by increasing RANKL which in turn stimulates osteoclasts (Elefteriou et al. 2005; Ducy et al. 2000). In osteoclasts *in vitro*, NE acting through the β2-AR signaling was shown to promote osteoclast differentiation and activity (Jiao, Niu, Li, et al. 2015; Kondo et al. 2013; Muschter et al. 2019).

Overall, these data suggest that the SNS promotes osteoclast differentiation via β2-AR signaling. The involvement of the β2-AR in subchondral bone during knee-OA progression was never investigated before. However, a few studies demonstrated the subchondral bone loss which occurs at the early OA, was reversed by the treatment of a specific β2-AR antagonist in the temporomandibular joint of rats, indicating that the β2-AR promote degenerative bone remodelling (Elefteriou et al. 2005; Jiao, Niu, Li, et al. 2015).

Since previous studies demonstrated that the β2-AR signalling leads to bone resorption, it was surprising in the current study that β2-AR deficient mice had pronounced bone volume after DMM but not after sham surgery compared to WT. This indicates that the deletion of β2-AR might induce enhanced bone formation not only systemically, but also in response to the mechanical loading, that is more excessive in DMM than in sham-operated mice (Marenzana and Chenu 2008. In this regard, the role of β2-AR signalling in the regulation of bone remodelling in healthy mice in response to mechanical loading needs to be investigated. OA induction of the β2-AR knockout mice in the current study thus reveals new insights into OA pathogenesis.

Based on the similar effects of the β2-AR deficiency in the prevention of OA progression as sympathectomy, the current data suggest a critical role for the β2-AR signaling in sympathetic activity during OA. Moreover, a similar amount of NE was detected in the spleen of β2-AR deficient and Syx mice. These data indicate that both, the decreased NE and the β2-AR levels, lower OA progression after DMM in β2-AR knockout mice. However, sympathectomy reduced only the peripheral NE release but not the central NE level, as 6-OHDA does not cross the blood-brain barrier (Laverty, Sharman, and Vogt 1965; Kostrzewa and Jacobowitz 1974). Therefore, the synthesis of catecholamines and their release from the central nervous system are not affected in the current study.

Clinical studies regarding the use of AR-blockers in OA are sparse. Previous reports indicate an association between OA and cardiovascular disease, such as hypertension that is caused by vasoconstriction of blood vessels (Ribeiro-da-Silva et al. 2018; Morović-Vergles et al. 2013). Both OA and cardiovascular disease share the same risk factors such as age and obesity (Ledford et al. 1998). The use of α-AR or β2-AR antagonists for hypertension was shown to reduce knee OA symptoms and knee OA pain (Valdes et al. 2017; Driban et al. 2016). However, the effect of drugs targeting the SNS on OA progression is not known. The long-term use of β2-AR agonists together with corticosteroids in asthma are known to reduce bone mineral density and lead to osteoporosis. However, this side effect is considered to be a result of corticosteroids and not of β2-AR agonists (Ledford et al. 1998). The effects of activated ARs vary in different tissues. α-AR or β-AR agonists have an anti-inflammatory effect in the lung (Bosmann et al. 2012), while β2-AR antagonist causes anti-inflammatory effects in

autoimmune myocarditis of rats by decreasing the serum level of IL-1β and TNF-α (Liu et al. 2010). Thus, the underlying mechanism of the SNS differs with the AR expression profile and with the disease and tissue involved. The SNS can thus be considered to be an important pathophysiological feature in OA. As joint-tissues such as cartilage, synovium and bone express ARs, therapeutic targeting with α-AR or β-AR antagonist might therefore be a promising option in reducing OA progression.

5 Conclusion

In conclusion, the present study demonstrates for the first time that the SNS contributes to OA progression and manifestation. The data suggest catabolic effects of SNS in cartilage as sympathectomy was protective in OA. Furthermore, the current study suggests the increased synovial inflammation accompanied by an enhanced MMP-13 expression in the synovium, might contribute to cartilage degeneration. The synovitis grade was enhanced by sympathetic activity, which was accompanied by an increased number of TH-expressing cells that produce catecholamines. Further investigation is needed to elaborate if sympathetic activity affects the production of cytokines by synoviocytes, or macrophages in the synovium, leading to proinflammatory processes. In contrast to effects in cartilage and synovium, sympathectomy aggravated OA-specific changes in the subchondral bone, such as increased bone volume and thickness. With respect to SNS in OA, this study demonstrated that a reduced sympathetic activity is protective overall in the knee joint by ignoring the minimal aggravating effects in the subchondral bone. The data on DMM induction in β2-AR knockout mice reveal that the β2-AR signalling is mainly involved in cartilage degeneration and the aggravated subchondral bone changes. It needs to be however investigated whether the MSC are involved in the pathologic changes during OA in β2-AR knockout mice, as suggested by the *in vitro* data showing inhibition of the chondrogenic potential of sASCs through NE mediated α2-AR signalling.

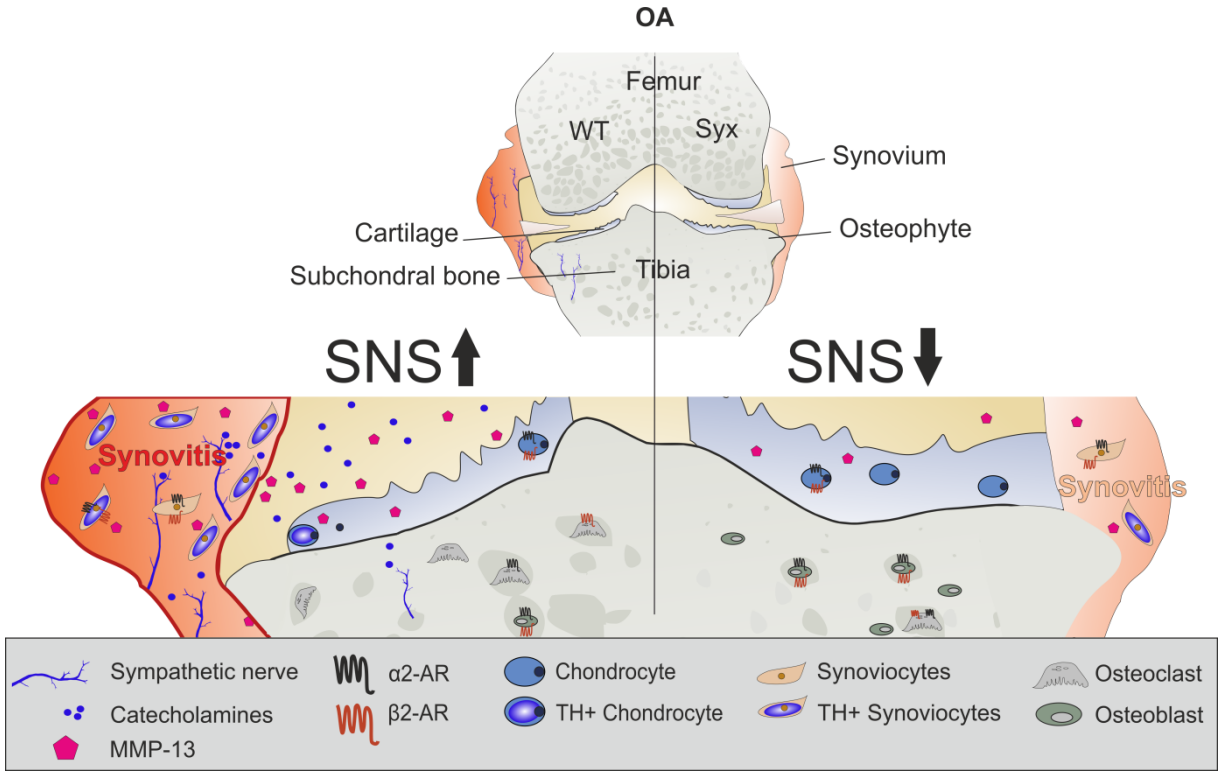

Figure 46 Hypothetic illustration of the SNS effects during OA progression.
Schematic illustration shows cells of the joint tissues expressing the α2-AR and β2-Ars with sympathetic TH-positive (TH+) nerves invading the synovium and subchondral bone. In OA, the sympathetic nerves invade the surrounding cartilage and release catecholamines. The increased SNS activity in OA, leads to increased catecholamine levels such as NE, leading to inhibitory effects on regenerative MSC and hence reduced cartilage regeneration. The sympathectomy results in less pronounced synovitis and less MMP-13 expression in the synovium compared to the WT joint tissue, where the enhanced MMP-13 expression might contribute to cartilage degradation (Shlopov et al. 1999). The TH expressing cells are increased in the synovium of WT mice, indicating catecholamines production locally. The decreased SNS activity in Syx mice decreases the osteoclast activity leading to increased subchondral bone volume. Illustration was made using CorelDraw software.

Therapeutically, the opposing SNS effects in the joint tissues analyzed suggest a tissue-specific treatment of β2-AR antagonists during OA progression. It can only be speculated if the increased subchondral bone thickness after a β2-AR antagonist treatment can be tolerated if the cartilage degeneration and synovitis are attenuated. Thus, future experiments are required to understand how the sympathetic system can be modulated in patients with OA or post-traumatic knee injury to prevent the disease progression, thus paving way for novel therapeutic options targeting the SNS in OA.

6 References

Adebayo, O. O., F. C. Ko, P. T. Wan, S. R. Goldring, M. B. Goldring, T. M. Wright, and M. C. H. van der Meulen. 2017. 'Role of subchondral bone properties and changes in development of load-induced osteoarthritis in mice', *Osteoarthritis Cartilage*, 25: 2108-18.

Aguilar M.I., M. T. Hearn. 1996. 'High-resolution reversed-phase high-performance liquid chromatography of peptides and proteins', *Methods Enzymol*, 270:3-26.

Aigner, T., and J. Stöve. 2003. 'Collagens--major component of the physiological cartilage matrix, major target of cartilage degeneration, major tool in cartilage repair', *Adv Drug Deliv Rev*, 55: 1569-93.

Alblas, J., E. J. van Corven, P. L. Hordijk, G. Milligan, and W. H. Moolenaar. 1993. 'Gi-mediated activation of the p21ras-mitogen-activated protein kinase pathway by alpha 2-adrenergic receptors expressed in fibroblasts', *J Biol Chem*, 268: 22235-8.

Almonte-Becerril, M., F. Navarro-Garcia, A. Gonzalez-Robles, M. A. Vega-Lopez, C. Lavalle, and J. B. Kouri. 2010. 'Cell death of chondrocytes is a combination between apoptosis and autophagy during the pathogenesis of Osteoarthritis within an experimental model', *Apoptosis*, 15: 631-8.

Arner, E. C. 2002. 'Aggrecanase-mediated cartilage degradation', *Curr Opin Pharmacol*, 2: 322-9.

Arunrukthavon, P., D. Heebthamai, P. Benchasiriluck, S. Chaluay, T. Chotanaphuti, and S. Khuangsirikul. 2020. 'Can urinary CTX-II be a biomarker for knee osteoarthritis?', *Arthroplasty*, 2: 6.

Bapat, Santul, Daniel Hubbard, Akul Munjal, Monte Hunter, and Sadanand Fulzele. 2018. 'Pros and cons of mouse models for studying osteoarthritis', *Clinical and translational medicine*, 7: 36-36.

Bau, B., P. M. Gebhard, J. Haag, T. Knorr, E. Bartnik, and T. Aigner. 2002. 'Relative messenger RNA expression profiling of collagenases and aggrecanases in human articular chondrocytes in vivo and in vitro', *Arthritis Rheum*, 46: 2648-57.

Bay-Jensen, A. C., E. Slagboom, P. Chen-An, P. Alexandersen, P. Qvist, C. Christiansen, I. Meulenbelt, and M. A. Karsdal. 2013. 'Role of hormones in cartilage and joint metabolism: understanding an unhealthy metabolic phenotype in osteoarthritis', *Menopause*, 20: 578-86.

Becerra, J., J. A. Andrades, E. Guerado, P. Zamora-Navas, J. M. López-Puertas, and A. H. Reddi. 2010. 'Articular cartilage: structure and regeneration', *Tissue Eng Part B Rev*, 16: 617-27.

Bijlsma, J. W., F. Berenbaum, and F. P. Lafeber. 2011. 'Osteoarthritis: an update with relevance for clinical practice', *Lancet*, 377: 2115-26.

Blesen, T. V., B. E. Hawes, D. K. Luttrell, K. M. Krueger, K. Touhara, E. Porfflri, M. Sakaue, L. M. Luttrell, and R. J. Lefkowitz. 1995. 'Receptor-tyrosine-kinase- and Gβγ-mediated MAP kinase activation by a common signalling pathway', *Nature*, 376: 781.

Blom, A. B., and W.B. Berg. 2007. 'The Synovium and Its Role in Osteoarthritis.' in Farach-Carson M.C. Bronner F. (ed.), *Bone and Osteoarthritis. Topics in Bone Biology* (Springer, London).

Blom, A. B., P. L. van Lent, A. E. Holthuysen, P. M. van der Kraan, J. Roth, N. van Rooijen, and W. B. van den Berg. 2004. 'Synovial lining macrophages mediate osteophyte formation during experimental osteoarthritis', *Osteoarthritis Cartilage*, 12: 627-35.

Blumer, M. J., B. Hausott, C. Schwarzer, A. R. Hayman, J. Stempel, and H. Fritsch. 2012. 'Role of tartrate-resistant acid phosphatase (TRAP) in long bone development', *Mech Dev*, 129: 162-76.

Bogoyevitch, M. A., M. B. Andersson, J. Gillespie-Brown, A. Clerk, P. E. Glennon, S. J. Fuller, and P. H. Sugden. 1996. 'Adrenergic receptor stimulation of the mitogen-activated protein kinase cascade and cardiac hypertrophy', *The Biochemical journal*, 314 (Pt 1): 115-21.

Bonner W.A., H.R. Hulett, R.G. Sweet, L.A. Herzenberg.1972. 'Fluorescence activated cell sorting', *Rev Sci Instrum*, Mar;43(3):404-9.
Bonnet, C. S., and D. A. Walsh. 2005. 'Osteoarthritis, angiogenesis and inflammation', *Rheumatology (Oxford)*, 44: 7-16.
Bosmann, M., J. J. Grailer, K. Zhu, M. A. Matthay, J. V. Sarma, F. S. Zetoune, and P. A. Ward. 2012. 'Anti-inflammatory effects of β2 adrenergic receptor agonists in experimental acute lung injury', *Faseb j*, 26: 2137-44.
Brandt, K. D., D. S. Schauwecker, S. Dansereau, J. Meyer, B. O'Connor, and S. L. Myers. 1997. 'Bone scintigraphy in the canine cruciate deficiency model of osteoarthritis. Comparison of the unstable and contralateral knee', *J Rheumatol*, 24: 140-5.
Buckland-Wright, C. 2004. 'Subchondral bone changes in hand and knee osteoarthritis detected by radiography', *Osteoarthritis Cartilage*, 12 Suppl A: S10-9.
Buckwalter, J. A., and H. J. Mankin. 1998. 'Articular cartilage: tissue design and chondrocyte-matrix interactions', *Instr Course Lect*, 47: 477-86.
Buckwalter, J. A., V. C. Mow, and A. Ratcliffe. 1994. 'Restoration of Injured or Degenerated Articular Cartilage', *J Am Acad Orthop Surg*, 2: 192-201.
Busija, L., L. Bridgett, S. R. Williams, R. H. Osborne, R. Buchbinder, L. March, and M. Fransen. 2010. 'Osteoarthritis', *Best Pract Res Clin Rheumatol*, 24: 757-68.
Campbell, T. M., S. M. Churchman, A. Gomez, D. McGonagle, P. G. Conaghan, F. Ponchel, and E. Jones. 2016. 'Mesenchymal Stem Cell Alterations in Bone Marrow Lesions in Patients With Hip Osteoarthritis', *Arthritis Rheumatol*, 68: 1648-59.
Capellino, S., M. Cosentino, C. Wolff, M. Schmidt, J. Grifka, and R. H. Straub. 2010. 'Catecholamine-producing cells in the synovial tissue during arthritis: modulation of sympathetic neurotransmitters as new therapeutic target', *Ann Rheum Dis*, 69: 1853-60.
Carney, E. 2016. 'Role of the β3 adrenergic receptor in renal function', *Nature Reviews Nephrology*, 12: 378-78.
Chaganti, R. K., and N. E. Lane. 2011. 'Risk factors for incident osteoarthritis of the hip and knee', *Curr Rev Musculoskelet Med*, 4: 99-104.
Chandrasekhar, S., M. A. Esterman, and H. A. Hoffman. 1987. 'Microdetermination of proteoglycans and glycosaminoglycans in the presence of guanidine hydrochloride', *Anal Biochem*, 161: 103-8.
Charni-Ben Tabassi, N., S. Desmarais, A. C. Bay-Jensen, J. M. Delaissé, M. D. Percival, and P. Garnero. 2008. 'The type II collagen fragments Helix-II and CTX-II reveal different enzymatic pathways of human cartilage collagen degradation', *Osteoarthritis Cartilage*, 16: 1183-91.
Clements, K. M., J. K. Flannelly, J. Tart, S. M. Brockbank, J. Wardale, J. Freeth, A. E. Parker, and P. Newham. 2011. 'Matrix metalloproteinase 17 is necessary for cartilage aggrecan degradation in an inflammatory environment', *Ann Rheum Dis*, 70: 683-9.
Courties, A., J. Sellam, and F. Berenbaum. 2017. 'Role of the autonomic nervous system in osteoarthritis', *Best Pract Res Clin Rheumatol*, 31: 661-75.
Cross, M., E. Smith, D. Hoy, S. Nolte, I. Ackerman, M. Fransen, L. Bridgett, S. Williams, F. Guillemin, C. L. Hill, L. L. Laslett, G. Jones, F. Cicuttini, R. Osborne, T. Vos, R. Buchbinder, A. Woolf, and L. March. 2014. 'The global burden of hip and knee osteoarthritis: estimates from the global burden of disease 2010 study', *Ann Rheum Dis*, 73: 1323-30.
D'Lima, D. D., B. J. Fregly, S. Patil, N. Steklov, and C. W. Colwell, Jr. 2012. 'Knee joint forces: prediction, measurement, and significance', *Proc Inst Mech Eng H*, 226: 95-102.
Das Neves Borges, P., T. L. Vincent, and M. Marenzana. 2017. 'Automated assessment of bone changes in cross-sectional micro-CT studies of murine experimental osteoarthritis', *PLOS ONE*, 12: e0174294.
De Bari, C., F. Dell'Accio, P. Tylzanowski, and F. P. Luyten. 2001. 'Multipotent mesenchymal stem cells from adult human synovial membrane', *Arthritis Rheum*, 44: 1928-42.
Dean, D. D., J. Martel-Pelletier, J. P. Pelletier, D. S. Howell, and J. F. Woessner, Jr. 1989. 'Evidence for metalloproteinase and metalloproteinase inhibitor imbalance in human osteoarthritic cartilage', *J Clin Invest*, 84: 678-85.

Decker, T., and M. L. Lohmann-Matthes. 1988. 'A quick and simple method for the quantitation of lactate dehydrogenase release in measurements of cellular cytotoxicity and tumor necrosis factor (TNF) activity', *J Immunol Methods*, 115: 61-9.

Demoor, M., D. Ollitrault, T. Gomez-Leduc, M. Bouyoucef, M. Hervieu, H. Fabre, J. Lafont, J. M. Denoix, F. Audigié, F. Mallein-Gerin, F. Legendre, and P. Galera. 2014. 'Cartilage tissue engineering: molecular control of chondrocyte differentiation for proper cartilage matrix reconstruction', *Biochim Biophys Acta*, 1840: 2414-40.

DePhillipo, N. N., G. Moatshe, J. Chahla, Z. S. Aman, H. W. Storaci, E. R. Morris, C. M. Robbins, L. Engebretsen, and R. F. LaPrade. 2019. 'Quantitative and Qualitative Assessment of the Posterior Medial Meniscus Anatomy: Defining Meniscal Ramp Lesions', *Am J Sports Med*, 47: 372-78.

Diekman, B. O., and F. Guilak. 2013. 'Stem cell-based therapies for osteoarthritis: challenges and opportunities', *Curr Opin Rheumatol*, 25: 119-26.

Ding, C., J. Martel-Pelletier, J. P. Pelletier, F. Abram, J. P. Raynauld, F. Cicuttini, and G. Jones. 2007. 'Meniscal tear as an osteoarthritis risk factor in a largely non-osteoarthritic cohort: a cross-sectional study', *J Rheumatol*, 34: 776-84.

Dominici, M., K. Le Blanc, I. Mueller, I. Slaper-Cortenbach, F. Marini, D. Krause, R. Deans, A. Keating, Dj Prockop, and E. Horwitz. 2006. 'Minimal criteria for defining multipotent mesenchymal stromal cells. The International Society for Cellular Therapy position statement', *Cytotherapy*, 8: 315-7.

Driban, J. B., G. H. Lo, C. B. Eaton, K. L. Lapane, M. Nevitt, W. F. Harvey, C. E. McCulloch, and T. E. McAlindon. 2016. 'Exploratory analysis of osteoarthritis progression among medication users: data from the Osteoarthritis Initiative', *Ther Adv Musculoskelet Dis*, 8: 207-19.

Ducy, P., M. Amling, S. Takeda, M. Priemel, A. F. Schilling, F. T. Beil, J. Shen, C. Vinson, J. M. Rueger, and G. Karsenty. 2000. 'Leptin inhibits bone formation through a hypothalamic relay: a central control of bone mass', *Cell*, 100: 197-207.

Duke, J. 2011. ' Autonomic Nervous System.' in James Duke (ed.), *Anesthesia Secrets (Fourth Edition)* (Mosby: Philadelphia).

Eckstein, F., Maximilian Reiser, Karl-Hans Englmeier, and Reinhard Putz. 2001. 'In vivo morphometry and functional analysis of human articular cartilage with quantitative magnetic resonance imaging – from image to data, from data to theory', *Anatomy and Embryology*, 203: 147-73.

Eitner, A., J. Pester, S. Nietzsche, G. O. Hofmann, and H. G. Schaible. 2013. 'The innervation of synovium of human osteoarthritic joints in comparison with normal rat and sheep synovium', *Osteoarthritis Cartilage*, 21: 1383-91.

El Bagdadi, K., F. Zaucke, A. Meurer, R. H. Straub, and Z. Jenei-Lanzl. 2019. 'Norepinephrine Inhibits Synovial Adipose Stem Cell Chondrogenesis via α2a-Adrenoceptor-Mediated ERK1/2 Activation', *Int J Mol Sci*, 20: 3127.

Elefteriou, F. 2018. 'Impact of the Autonomic Nervous System on the Skeleton', *Physiol Rev*, 98: 1083-112.

Elefteriou, F., J. D. Ahn, S. Takeda, M. Starbuck, X. Yang, X. Liu, H. Kondo, W. G. Richards, T. W. Bannon, M. Noda, K. Clement, C. Vaisse, and G. Karsenty. 2005. 'Leptin regulation of bone resorption by the sympathetic nervous system and CART', *Nature*, 434: 514-20.

Elefteriou, F., P. Campbell, and Y. Ma. 2014. 'Control of bone remodeling by the peripheral sympathetic nervous system', *Calcified tissue international*, 94: 140-51.

Eo, S. H., S. Y. Choi, and S. J. Kim. 2016. 'PEP-1-SIRT2-induced matrix metalloproteinase-1 and -13 modulates type II collagen expression via ERK signaling in rabbit articular chondrocytes', *Exp Cell Res*, 348: 201-08.

Estes, B. T., B. O. Diekman, and F. Guilak. 2008. 'Monolayer cell expansion conditions affect the chondrogenic potential of adipose-derived stem cells', *Biotechnol Bioeng*, 99: 986-95.

Evans, C. H., V. B. Kraus, and L. A. Setton. 2014. 'Progress in intra-articular therapy', *Nat Rev Rheumatol*, 10: 11-22.

Fan, W., J. Li, Y. Wang, J. Pan, S. Li, L. Zhu, C. Guo, and Z. Yan. 2016. 'CD105 promotes chondrogenesis of synovium-derived mesenchymal stem cells through Smad2 signaling', *Biochem Biophys Res Commun*, 474: 338-44.
Fang, H., L. Huang, I. Welch, C. Norley, D. W. Holdsworth, F. Beier, and D. Cai. 2018. 'Early Changes of Articular Cartilage and Subchondral Bone in The DMM Mouse Model of Osteoarthritis', *Sci Rep*, 8: 2855.
Farndale, R. W., D. J. Buttle, and A. J. Barrett. 1986. 'Improved quantitation and discrimination of sulphated glycosaminoglycans by use of dimethylmethylene blue', *Biochim Biophys Acta*, 883: 173-7.
Fazzalari, N. L., and I. H. Parkinson. 1997. 'Fractal properties of subchondral cancellous bone in severe osteoarthritis of the hip', *J Bone Miner Res*, 12: 632-40.
Fellows, C.R., R. Williams, I.R. Davies, K. Gohil, D. M. Baird, J. Fairclough, P. Rooney, C.W. Archer, and I. M. Khan. 2017. 'Characterisation of a divergent progenitor cell sub-populations in human osteoarthritic cartilage: the role of telomere erosion and replicative senescence', *Sci Rep*, 7: 41421-21.
Felson, D. T. 2006. 'Clinical practice. Osteoarthritis of the knee', *N Engl J Med*, 354: 841-8.
Felten, D. L., K. D. Ackerman, S. J. Wiegand, and S. Y. Felten. 1987. 'Noradrenergic sympathetic innervation of the spleen: I. Nerve fibers associate with lymphocytes and macrophages in specific compartments of the splenic white pulp', *J Neurosci Res*, 18: 28-36, 118-21.
Fickert, S., J. Fiedler, and R. E. Brenner. 2004. 'Identification of subpopulations with characteristics of mesenchymal progenitor cells from human osteoarthritic cartilage using triple staining for cell surface markers', *Arthritis Res Ther*, 6: R422-32.
Findlay, D. M., and G. J. Atkins. 2014. 'Osteoblast-chondrocyte interactions in osteoarthritis', *Curr Osteoporos Rep*, 12: 127-34.
Fox, S. A. J., A. Bedi, and S. A. Rodeo. 2009. 'The basic science of articular cartilage: structure, composition, and function', *Sports health*, 1: 461-68.
Franquinho, F., M. A. Liz, A. F. Nunes, E. Neto, M. Lamghari, and M. M. Sousa. 2010. 'Neuropeptide Y and osteoblast differentiation--the balance between the neuro-osteogenic network and local control', *Febs j*, 277: 3664-74.
Freitag, J., K. Shah, J. Wickham, D. Li, C. Norsworthy, and A. Tenen. 2020. 'Evaluation of autologous adipose-derived mesenchymal stem cell therapy in focal chondral defects of the knee: a pilot case series', *Regen Med*.
Fuerst, M., J. Bertrand, L. Lammers, R. Dreier, F. Echtermeyer, Y. Nitschke, F. Rutsch, F. K. Schäfer, O. Niggemeyer, J. Steinhagen, C. H. Lohmann, T. Pap, and W. Rüther. 2009. 'Calcification of articular cartilage in human osteoarthritis', *Arthritis Rheum*, 60: 2694-703.
Gadjanski, I., K. Spiller, and G. Vunjak-Novakovic. 2012. 'Time-dependent processes in stem cell-based tissue engineering of articular cartilage', *Stem Cell Rev Rep*, 8: 863-81.
Garnero, P. 2007. 'New Biochemical Markers of Cartilage Turnover in Osteoarthritis: Recent Developments and Remaining Challenges', *International Bone and Mineral Society Knowledge Environment*, 4: 7-18.
Garnero, P., and P. D. Delmas. 2003. 'Biomarkers in osteoarthritis', *Curr Opin Rheumatol*, 15: 641-6.
Glasson, S. S., T. J. Blanchet, and E. A. Morris. 2007. 'The surgical destabilization of the medial meniscus (DMM) model of osteoarthritis in the 129/SvEv mouse', *Osteoarthritis Cartilage*, 15: 1061-9.
Goldring, M. B., and K. B. Marcu. 2009. 'Cartilage homeostasis in health and rheumatic diseases', *Arthritis Res Ther*, 11: 224.
Goldring, M. B., and M. Otero. 2011. 'Inflammation in osteoarthritis', *Curr Opin Rheumatol*, 23: 471-78.
Goldring, M. B., M. Otero, K. Tsuchimochi, K. Ijiri, and Y. Li. 2008. 'Defining the roles of inflammatory and anabolic cytokines in cartilage metabolism', *Ann Rheum Dis*, 67 Suppl 3: iii75-82.
Goldring, M. B., K. Tsuchimochi, and K. Ijiri. 2006. 'The control of chondrogenesis', *J Cell Biochem*, 97: 33-44.

Goodwin, W., D. McCabe, E. Sauter, E. Reese, M. Walter, J. A. Buckwalter, and J. A. Martin. 2010. 'Rotenone prevents impact-induced chondrocyte death', *J Orthop Res*, 28: 1057-63.

Grässel, S., R. H. Straub, and Z. Jenei-Lanzl. 2017. 'The Sensory and Sympathetic Nervous System in Cartilage Physiology and Pathophysiology.' in Susanne Grässel and Attila Aszódi (eds.), *Cartilage: Volume 2: Pathophysiology* (Springer International Publishing: Cham).

Greenwood, C., J. Clement, A. Dicken, P. Evans, I. Lyburn, R. M. Martin, N. Stone, P. Zioupos, and K. Rogers. 2018. 'Age-Related Changes in Femoral Head Trabecular Microarchitecture', *Aging and disease*, 9: 976-87.

Grogan, S. P., S. Miyaki, H. Asahara, D. D. D'Lima, and M. K. Lotz. 2009. 'Mesenchymal progenitor cell markers in human articular cartilage: normal distribution and changes in osteoarthritis', *Arthritis Res Ther*, 11: R85.

Hannan, M. T., J. J. Anderson, Y. Zhang, D. Levy, and D. T. Felson. 1993. 'Bone mineral density and knee osteoarthritis in elderly men and women. The Framingham Study', *Arthritis Rheum*, 36: 1671-80.

Harle, P., D. Mobius, D. J. Carr, J. Scholmerich, and R. H. Straub. 2005. 'An opposing time-dependent immune-modulating effect of the sympathetic nervous system conferred by altering the cytokine profile in the local lymph nodes and spleen of mice with type II collagen-induced arthritis', *Arthritis Rheum*, 52: 1305-13.

Härle, P., G. Pongratz, J. Albrecht, I. H. Tarner, and R. H. Straub. 2008. 'An early sympathetic nervous system influence exacerbates collagen-induced arthritis via CD4+CD25+ cells', *Arthritis & Rheumatism*, 58: 2347-55.

Hayami, T., M. Pickarski, G. A. Wesolowski, J. McLane, A. Bone, J. Destefano, G. A. Rodan, and L. T. Duong. 2004. 'The role of subchondral bone remodeling in osteoarthritis: reduction of cartilage degeneration and prevention of osteophyte formation by alendronate in the rat anterior cruciate ligament transection model', *Arthritis Rheum*, 50: 1193-206.

Hayman, A. R. 2008. 'Tartrate-resistant acid phosphatase (TRAP) and the osteoclast/immune cell dichotomy', *Autoimmunity*, 41: 218-23.

Hedderich, J., K. El Bagdadi, P. Angele, S. Grässel, A. Meurer, R. H. Straub, F. Zaucke, and Z. Jenei-Lanzl. 2020. 'Norepinephrine Inhibits the Proliferation of Human Bone Marrow-Derived Mesenchymal Stem Cells via β2-Adrenoceptor-Mediated ERK1/2 and PKA Phosphorylation', *Int J Mol Sci*, 21.

Heinegård, D. . 2007. 'Cartilage Matrix Destruction.' in Farach-Carson M.C. Bronner F. (ed.), *Bone and Osteoarthritis* (Springer, London: London).

Hennig, T., H. Lorenz, A. Thiel, K. Goetzke, A. Dickhut, F. Geiger, and W. Richter. 2007. 'Reduced chondrogenic potential of adipose tissue derived stromal cells correlates with an altered TGFbeta receptor and BMP profile and is overcome by BMP-6', *J Cell Physiol*, 211: 682-91.

Herman, B. C., L. Cardoso, R. J. Majeska, K. J. Jepsen, and M. B. Schaffler. 2010. 'Activation of bone remodeling after fatigue: differential response to linear microcracks and diffuse damage', *Bone*, 47: 766-72.

Hermann, W., S. Lambova, and U. Muller-Ladner. 2018. 'Current Treatment Options for Osteoarthritis', *Curr Rheumatol Rev*, 14: 108-16.

Herrmann, M., S. Anders, R. H. Straub, and Z. Jenei-Lanzl. 2018. 'TNF inhibits catecholamine production from induced sympathetic neuron-like cells in rheumatoid arthritis and osteoarthritis in vitro', *Sci Rep*, 8: 9645.

Holmes, K.L., G. Otten and W.M. Yokoyama.2002. 'Flow Cytometry Analysis Using the Becton Dickinson FACS Calibur', *Curr Protoc Immunol*, 49: 5.4.1-5.4.22.

Hu, K., H. Zhou, G. Zhang, R. Qin, R. Hou, L. Kong, and Y. Ding. 2010. 'The effect of chemical sympathectomy and stress on bone remodeling in adult rats', *Neuro Endocrinol Lett*, 31: 807-13.

Huang, H. H., T. C. Brennan, M. M. Muir, and R. S. Mason. 2009. 'Functional alpha1- and beta2-adrenergic receptors in human osteoblasts', *J Cell Physiol*, 220: 267-75.

Huang, Y. Z., H. Q. Xie, A. Silini, O. Parolini, Y. Zhang, L. Deng, and Y. C. Huang. 2017. 'Mesenchymal Stem/Progenitor Cells Derived from Articular Cartilage, Synovial Membrane and Synovial Fluid for Cartilage Regeneration: Current Status and Future Perspectives', *Stem Cell Rev*, 13: 575-86.

Hudelmaier, M., C. Glaser, J. Hohe, K. H. Englmeier, M. Reiser, R. Putz, and F. Eckstein. 2001. 'Age-related changes in the morphology and deformational behavior of knee joint cartilage', *Arthritis Rheum*, 44: 2556-61.

Hukkanen, M., Y. T. Konttinen, R. G. Rees, S. Santavirta, G. Terenghi, and J. M. Polak. 1992. 'Distribution of nerve endings and sensory neuropeptides in rat synovium, meniscus and bone', *Int J Tissue React*, 14: 1-10.

Hunter, D. J., and D. T. Felson. 2006. 'Osteoarthritis', *Bmj*, 332: 639-42.

Imhof, H., I. Sulzbacher, S. Grampp, C. Czerny, S. Youssefzadeh, and F. Kainberger. 2000. 'Subchondral bone and cartilage disease: a rediscovered functional unit', *Invest Radiol*, 35: 581-8.

Inada, M., T. Yasui, S. Nomura, S. Miyake, K. Deguchi, M. Himeno, M. Sato, H. Yamagiwa, T. Kimura, N. Yasui, T. Ochi, N. Endo, Y. Kitamura, T. Kishimoto, and T. Komori. 1999. 'Maturational disturbance of chondrocytes in Cbfa1-deficient mice', *Dev Dyn*, 214: 279-90.

Intemann, J., D. J. J. De Gorter, A. J. Naylor, B. Dankbar, and C. Wehmeyer. 2020. 'Importance of osteocyte-mediated regulation of bone remodelling in inflammatory bone disease', *Swiss Med Wkly*, 150: w20187.

Itoh, Y., N. Ito, H. Nagase, R. D. Evans, S. A. Bird, and M. Seiki. 2006. 'Cell surface collagenolysis requires homodimerization of the membrane-bound collagenase MT1-MMP', *Mol Biol Cell*, 17: 5390-9.

Jackson, M. T., B. Moradi, S. Zaki, M. M. Smith, S. McCracken, S. M. Smith, C. J. Jackson, and C. B. Little. 2014. 'Depletion of protease-activated receptor 2 but not protease-activated receptor 1 may confer protection against osteoarthritis in mice through extracartilaginous mechanisms', *Arthritis Rheumatol*, 66: 3337-48.

Jenei-Lanzl, Z., S. Capellino, F. Kees, M. Fleck, T. Lowin, and R. H Straub. 2015. 'Anti-inflammatory effects of cell-based therapy with tyrosine hydroxylase-positive catecholaminergic cells in experimental arthritis', *Ann Rheum Dis*, 74: 444-51.

Jenei-Lanzl, Z., S. Grassel, G. Pongratz, F. Kees, N. Miosge, P. Angele, and R. H. Straub. 2014. 'Norepinephrine inhibition of mesenchymal stem cell and chondrogenic progenitor cell chondrogenesis and acceleration of chondrogenic hypertrophy', *Arthritis Rheumatol*, 66: 2472-81.

Jenei-Lanzl Z., R.H. Straub, T. Dienstknecht, M. Huber, M. Hager, S. Grassel, R. Kujat, M.K. Angele, P. Angele. 2010. 'Estradiol inhibits chondrogenic differentiation of mesenchymal stem cells via nonclassic signaling', *Arthritis Rheum*, 62: 1088– 96.

Jiao, K., L. N. Niu, Q. H. Li, G. T. Ren, C. M. Zhao, Y. D. Liu, F. R. Tay, and M. Q. Wang. 2015. 'beta2-Adrenergic signal transduction plays a detrimental role in subchondral bone loss of temporomandibular joint in osteoarthritis', *Sci Rep*, 5: 12593.

Jiao, K., L. Niu, X. Xu, Y. Liu, X. Li, F. R. Tay, and M. Wang. 2015. 'Norepinephrine Regulates Condylar Bone Loss via Comorbid Factors', *J Dent Res*, 94: 813-20.

Jiao, K., G. Zeng, L. N. Niu, H. X. Yang, G. T. Ren, X. Y. Xu, F. F. Li, F. R. Tay, and M. Q. Wang. 2016. 'Activation of alpha2A-adrenergic signal transduction in chondrocytes promotes degenerative remodelling of temporomandibular joint', *Scientific reports*, 6: 30085.

Johnstone, B., T. M. Hering, A. I. Caplan, V. M. Goldberg, and J. U. Yoo. 1998. 'In vitro chondrogenesis of bone marrow-derived mesenchymal progenitor cells', *Exp Cell Res*, 238: 265-72.

Kajimura, D., E. Hinoi, M. Ferron, A. Kode, K. J. Riley, B. Zhou, X. E. Guo, and G. Karsenty. 2011. 'Genetic determination of the cellular basis of the sympathetic regulation of bone mass accrual', *J Exp Med*, 208: 841-51.

Karemaker, J. M. 2017. 'An introduction into autonomic nervous function', *Physiol Meas*, 38: R89-r118.

Kees, M. G., G. Pongratz, F. Kees, J. Scholmerich, and R. H. Straub. 2003. 'Via beta-adrenoceptors, stimulation of extrasplenic sympathetic nerve fibers inhibits lipopolysaccharide-induced TNF secretion in perfused rat spleen', *J Neuroimmunol*, 145: 77-85.

Kemeny D.M. 1994. ' ELISA: Anwendung des Enzyme Linked Immunosorbent Assay im biologisch/medizinischen Labor', *G Fischer.*

Knudson, C. B., and W. Knudson. 2001. 'Cartilage proteoglycans', *Semin Cell Dev Biol*, 12: 69-78.

Kondo, M., H. Kondo, K. Miyazawa, S. Goto, and A. Togari. 2013. 'Experimental tooth movement-induced osteoclast activation is regulated by sympathetic signaling', *Bone*, 52: 39-47.

Kostrzewa, R. M., and D. M. Jacobowitz. 1974. 'Pharmacological actions of 6-hydroxydopamine', *Pharmacol Rev*, 26: 199-288.

Kotova, P. D., V. Y. Sysoeva, O. A. Rogachevskaja, M. F. Bystrova, A. S. Kolesnikova, P. A. Tyurin-Kuzmin, J. I. Fadeeva, V. A. Tkachuk, and S. S. Kolesnikov. 2014. 'Functional expression of adrenoreceptors in mesenchymal stromal cells derived from the human adipose tissue', *Biochim Biophys Acta*, 1843: 1899-908.

Krenn, V., L. Morawietz, G. R. Burmester, R. W. Kinne, U. Mueller-Ladner, B. Muller, and T. Haupl. 2006. 'Synovitis score: discrimination between chronic low-grade and high-grade synovitis', *Histopathology*, 49: 358-64.

Lafont, J. E. 2010. 'Lack of oxygen in articular cartilage: consequences for chondrocyte biology', *Int J Exp Pathol*, 91: 99-106.

Laemmli U.K.1970. 'Cleavage of structural proteins during the assembly of the head of bacteriophage T4', *Nature* 227: 680–685.

Lai, L. P., and J. Mitchell. 2008. 'Beta2-adrenergic receptors expressed on murine chondrocytes stimulate cellular growth and inhibit the expression of Indian hedgehog and collagen type X', *J Cell Biochem*, 104: 545-53.

Laverty, R., D. F. Sharman, and M. Vogt. 1965. 'Action of 2, 4, 5-trihydroxyphenylethylamine on the storgae an release of noradrenaline', *Br J Pharmacol Chemother*, 24: 549-60.

Ledford, D., A. Apter, A. M. Brenner, K. Rubin, K. Prestwood, M. Frieri, and B. Lukert. 1998. 'Osteoporosis in the corticosteroid-treated patient with asthma', *Journal of Allergy and Clinical Immunology*, 102: 353-62.

Lefebvre, V., and M. Dvir-Ginzberg. 2017. 'SOX9 and the many facets of its regulation in the chondrocyte lineage', *Connect Tissue Res*, 58: 2-14.

Lerner, U. H., and E. Persson. 2008. 'Osteotropic effects by the neuropeptides calcitonin gene-related peptide, substance P and vasoactive intestinal peptide', *J Musculoskelet Neuronal Interact*, 8: 154-65.

Lewis, J. S., W. C. Hembree, B. D. Furman, L. Tippets, D. Cattel, J. L. Huebner, D. Little, L. E. DeFrate, V. B. Kraus, F. Guilak, and S. A. Olson. 2011. 'Acute joint pathology and synovial inflammation is associated with increased intra-articular fracture severity in the mouse knee', *Osteoarthritis Cartilage*, 19: 864-73.

Li, G., J. Yin, J. Gao, T. S. Cheng, N. J. Pavlos, C. Zhang, and M. H. Zheng. 2013. 'Subchondral bone in osteoarthritis: insight into risk factors and microstructural changes', *Arthritis Res Ther*, 15: 223.

Li, H., D. Wang, Y. Yuan, and J. Min. 2017. 'New insights on the MMP-13 regulatory network in the pathogenesis of early osteoarthritis', *Arthritis Res Ther*, 19: 248.

Li, N., J. Gao, L. Mi, G. Zhang, L. Zhang, N. Zhang, R. Huo, J. Hu, and K. Xu. 2020. 'Synovial membrane mesenchymal stem cells: past life, current situation, and application in bone and joint diseases', *Stem Cell Res Ther*, 11: 381.

Lilly, G. D. 1966. 'Effect of sympathectomy on development of chronic osteoarthritis: case report', *Ann Surg*, 163: 856-8.

Liu, C., C. Liu, L. Si, H. Shen, Q. Wang, and W. Yao. 2018. 'Relationship between subchondral bone microstructure and articular cartilage in the osteoarthritic knee using 3T MRI', *Journal of Magnetic Resonance Imaging*, 48: 669-79.

Liu, H., W. Li, W. Gu, Y. Kong, N. Yang, and L. Chen. 2010. 'Immunoregulatory effects of carvedilol on rat experimental autoimmune myocarditis', *Scand J Immunol*, 71: 38-44.

Livak K.J., T.D. Schmittgen. 2001. 'Analysis of relative gene expression data using real-time quantitative PCR and the 2(-Delta Delta C(T)) Method', *Methods,* 25(4):402-8.
Loeser, R. F., S. R. Goldring, C. R. Scanzello, and M. B. Goldring. 2012. 'Osteoarthritis: a disease of the joint as an organ', *Arthritis Rheum*, 64: 1697-707.
Loeuille, D., I. Chary-Valckenaere, J. Champigneulle, A. C. Rat, F. Toussaint, A. Pinzano-Watrin, J. C. Goebel, D. Mainard, A. Blum, J. Pourel, P. Netter, and P. Gillet. 2005. 'Macroscopic and microscopic features of synovial membrane inflammation in the osteoarthritic knee: correlating magnetic resonance imaging findings with disease severity', *Arthritis Rheum*, 52: 3492-501.
Lohmander, L. S., L. M. Atley, T. A. Pietka, and D. R. Eyre. 2003. 'The release of crosslinked peptides from type II collagen into human synovial fluid is increased soon after joint injury and in osteoarthritis', *Arthritis Rheum*, 48: 3130-9.
Lorenz, J., and S. Grässel. 2014. 'Experimental osteoarthritis models in mice', *Methods Mol Biol*, 1194: 401-19.
Lorenz, J., N. Schafer, R. Bauer, Z. Jenei-Lanzl, R. H. Springorum, and S. Grassel. 2016. 'Norepinephrine modulates osteoarthritic chondrocyte metabolism and inflammatory responses', *Osteoarthritis Cartilage*, 24: 325-34.
Lorenz, J., E. Seebach, G. Hackmayer, C. Greth, R.J. Bauer, K. Kleinschmidt, D. Bettenworth, M. Böhm, J. Grifka, and S. Grässel. 2014. 'Melanocortin 1 receptor-signaling deficiency results in an articular cartilage phenotype and accelerates pathogenesis of surgically induced murine osteoarthritis', *PLOS ONE*, 9: e105858-e58.
Lorton, D., and D. L. Bellinger. 2015. 'Molecular mechanisms underlying β-adrenergic receptor-mediated cross-talk between sympathetic neurons and immune cells', *Int J Mol Sci*, 16: 5635-65.
Ma, Yun, Jessica J. Krueger, Sara N. Redmon, Sasidhar Uppuganti, Jeffry S. Nyman, Maureen K. Hahn, and Florent Elefteriou. 2013. 'Extracellular norepinephrine clearance by the norepinephrine transporter is required for skeletal homeostasis', *J Biol Chem*, 288: 30105-13.
Mackie, E. J., L. Tatarczuch, and M. Mirams. 2011. 'The skeleton: a multi-functional complex organ: the growth plate chondrocyte and endochondral ossification', *J Endocrinol*, 211: 109-21.
Magnusson, K., A. Turkiewicz, and M. Englund. 2019. 'Nature vs nurture in knee osteoarthritis - the importance of age, sex and body mass index', *Osteoarthritis Cartilage*, 27: 586-92.
Malpas, S. C. 2010. 'Sympathetic nervous system overactivity and its role in the development of cardiovascular disease', *Physiol Rev*, 90: 513-57.
Marini, S., G. F. Fasciglione, G. Monteleone, M. Maiotti, U. Tarantino, and M. Coletta. 2003. 'A correlation between knee cartilage degradation observed by arthroscopy and synovial proteinases activities', *Clin Biochem*, 36: 295-304.
Marenzana M, C. Chenu.2008. 'Sympathetic nervous system and bone adaptive response to its mechanical environment', *J Musculoskelet Neuronal Interact,* 8(2):111-20.
Martínez-Martínez, L. A., T. Mora, A. Vargas, M. Fuentes-Iniestra, and M. Martínez-Lavín. 2014. 'Sympathetic nervous system dysfunction in fibromyalgia, chronic fatigue syndrome, irritable bowel syndrome, and interstitial cystitis: a review of case-control studies', *J Clin Rheumatol*, 20: 146-50.
Mathiessen, A., and P. G. Conaghan. 2017. 'Synovitis in osteoarthritis: current understanding with therapeutic implications', *Arthritis Res Ther*, 19: 18.
McErlain, D. D., V. Ulici, M. Darling, J. S. Gati, V. Pitelka, F. Beier, and D. W. Holdsworth. 2012. 'An in vivo investigation of the initiation and progression of subchondral cysts in a rodent model of secondary osteoarthritis', *Arthritis Res Ther*, 14: R26.
McEwen, B. S., and E. Stellar. 1993. 'Stress and the individual. Mechanisms leading to disease', *Arch Intern Med*, 153: 2093-101.
McGonagle, D., T. G. Baboolal, and E. Jones. 2017. 'Native joint-resident mesenchymal stem cells for cartilage repair in osteoarthritis', *Nat Rev Rheumatol*, 13: 719-30.

McIlvaine TC. 1921. '*A buffer solution for colorimetric comparison*'. *J. Biol. Chem,* 49, Nr.1, 183–186.
Medvedeva, E. V., E. A. Grebenik, S. N. Gornostaeva, V. I. Telpuhov, A. V. Lychagin, P. S. Timashev, and A. S. Chagin. 2018. 'Repair of Damaged Articular Cartilage: Current Approaches and Future Directions', *Int J Mol Sci*, 19.
Mikos, A. G., S. W. Herring, P. Ochareon, J. Elisseeff, H. H. Lu, R. Kandel, F. J. Schoen, M. Toner, D. Mooney, A. Atala, M. E. Van Dyke, D. Kaplan, and G. Vunjak-Novakovic. 2006. 'Engineering complex tissues', *Tissue Eng*, 12: 3307-39.
Miller, L. E., J. Grifka, J. Schölmerich, and R. H. Straub. 2002. 'Norepinephrine from synovial tyrosine hydroxylase positive cells is a strong indicator of synovial inflammation in rheumatoid arthritis', *J Rheumatol*, 29: 427-35.
Miller, L. E., H. P. Jüsten, J. Schölmerich, and R. H. Straub. 2000. 'The loss of sympathetic nerve fibers in the synovial tissue of patients with rheumatoid arthritis is accompanied by increased norepinephrine release from synovial macrophages', *Faseb j*, 14: 2097-107.
Mitchell, J., L. P. Lai, F. Peralta, Y. Xu, and K. Sugamori. 2011. 'beta2-adrenergic receptors inhibit the expression of collagen type II in growth plate chondrocytes by stimulating the AP-1 factor Jun-B', *Am J Physiol Endocrinol Metab*, 300: E633-9.
Mlakar, V., S. Jurkovic M., J. Zupan, R. Komadina, J. Prezelj, and J. Marc. 2015. 'ADRA2A is involved in neuro-endocrine regulation of bone resorption', *Journal of Cellular and Molecular Medicine*, 19: 1520-29.
Molinoff, P. B. 1984. 'Alpha- and beta-adrenergic receptor subtypes properties, distribution and regulation', *Drugs*, 28 Suppl 2: 1-15.
Morović-Vergles, J., L. Salamon, D. Marasović-Krstulović, T. Kehler, D. Sakić, O. Badovinac, T. Vlak, S. Novak, N. Stiglić-Rogoznica, M. Hanih, D. Bedeković, S. Grazio, M. Kadojić, J. Milas-Ahić, V. Prus, D. Stamenković, D. Sošo, B. Anić, D. Babić-Naglić, and S. Gamulin. 2013. 'Is the prevalence of arterial hypertension in rheumatoid arthritis and osteoarthritis associated with disease?', *Rheumatol Int*, 33: 1185-92.
Motiejunaite, J., L. Amar, and E. Vidal-Petiot. 2020. 'Adrenergic receptors and cardiovascular effects of catecholamines', *Ann Endocrinol (Paris)*.
Murphy, J. M., K. Dixon, S. Beck, D. Fabian, A. Feldman, and F. Barry. 2002. 'Reduced chondrogenic and adipogenic activity of mesenchymal stem cells from patients with advanced osteoarthritis', *Arthritis Rheum*, 46: 704-13.
Muschter D., Fleischhauer L, Taheri S., Schillinge A.F., Clausen-Schaumann H, Grässel S. 2020. 'Sensory neuropeptides are required for bone and cartilage homeostasis in a murine destabilization-induced osteoarthritis model ', *Bone*,133:115181.
Muschter, D., A. S. Beiderbeck, T. Spath, C. Kirschneck, A. Schroder, and S. Grassel. 2019. 'Sensory Neuropeptides and their Receptors Participate in Mechano-Regulation of Murine Macrophages', *Int J Mol Sci*, 20.
Nachlas, M. M., S. I. Margulies, J. D. Goldberg, and A. M. Seligman. 1960. 'The determination of lactic dehydrogenase with a tetrazolium salt', *Anal Biochem*, 1: 317-26.
Nagatsu, T., M. Levitt, and S. Udenfriend. 1964. 'Tyrosin hydroxylase. The initial step in norepinephrine biosynthesis', *J Biol Chem*, 239: 2910-7.
Nakasa, T., N. Adachi, T. Kato, and M. Ochi. 2014. 'Correlation between subchondral bone plate thickness and cartilage degeneration in osteoarthritis of the ankle', *Foot Ankle Int*, 35: 1341-9.
Nance, D. M., and V. M. Sanders. 2007. 'Autonomic innervation and regulation of the immune system (1987-2007)', *Brain Behav Immun*, 21: 736-45.
Ng, L. J., S. Wheatley, G. E. Muscat, J. Conway-Campbell, J. Bowles, E. Wright, D. M. Bell, P. P. Tam, K. S. Cheah, and P. Koopman. 1997. 'SOX9 binds DNA, activates transcription, and coexpresses with type II collagen during chondrogenesis in the mouse', *Dev Biol*, 183: 108-21.
O'Neill, T. W., P. S. McCabe, and J. McBeth. 2018. 'Update on the epidemiology, risk factors and disease outcomes of osteoarthritis', *Best Pract Res Clin Rheumatol*, 32: 312-26.
Oberlender, S.A., and R.S. Tuan. 1994. 'Expression and functional involvement of N-cadherin in embryonic limb chondrogenesis', *Development*, 120: 177-87.

Ogata, Y., Y. Mabuchi, M. Yoshida, E. G. Suto, N. Suzuki, T. Muneta, I. Sekiya, and C. Akazawa. 2015. 'Purified Human Synovium Mesenchymal Stem Cells as a Good Resource for Cartilage Regeneration', *PLOS ONE*, 10: e0129096-e96.

Oh, C. D., S. H. Chang, Y. M. Yoon, S. J. Lee, Y. S. Lee, S. S. Kang, and J. S. Chun. 2000. 'Opposing role of mitogen-activated protein kinase subtypes, erk-1/2 and p38, in the regulation of chondrogenesis of mesenchymes', *J Biol Chem*, 275: 5613-9.

Palo, N., S. S. Chandel, S. K. Dash, G. Arora, M. Kumar, and M. R. Biswal. 2015. 'Effects of Osteoarthritis on Quality of life in Elderly Population of Bhubaneswar, India: A Prospective Multicenter Screening and Therapeutic Study of 2854 Patients', *Geriatr Orthop Surg Rehabil*, 6: 269-75.

Pattappa, G., B. Johnstone, J. Zellner, D. Docheva, and P. Angele. 2019. 'The Importance of Physioxia in Mesenchymal Stem Cell Chondrogenesis and the Mechanisms Controlling Its Response', *Int J Mol Sci*, 20.

Pelletier, J. P., J. Martel-Pelletier, and S. B. Abramson. 2001. 'Osteoarthritis, an inflammatory disease: potential implication for the selection of new therapeutic targets', *Arthritis Rheum*, 44: 1237-47.

Pongratz, G., and R. H. Straub. 2014. 'The sympathetic nervous response in inflammation', *Arthritis Res Ther*, 16: 504.

Portron, S., V. Hivernaud, C. Merceron, J. Lesoeur, M. Masson, O. Gauthier, C. Vinatier, L. Beck, and J. Guicheux. 2015. 'Inverse regulation of early and late chondrogenic differentiation by oxygen tension provides cues for stem cell-based cartilage tissue engineering', *Cell Physiol Biochem*, 35: 841-57.

Pottenger, L. A., F. M. Phillips, and L. F. Draganich. 1990. 'The effect of marginal osteophytes on reduction of varus-valgus instability in osteoarthritic knees', *Arthritis Rheum*, 33: 853-8.

Prasadam, I., S. Farnaghi, J. Q. Feng, W. Gu, S. Perry, R. Crawford, and Y. Xiao. 2013. 'Impact of extracellular matrix derived from osteoarthritis subchondral bone osteoblasts on osteocytes: role of integrinβ1 and focal adhesion kinase signaling cues', *Arthritis Res Ther*, 15: R150.

Prasadam, I., S. van Gennip, T. Friis, W. Shi, R. Crawford, and Y. Xiao. 2010. 'ERK-1/2 and p38 in the regulation of hypertrophic changes of normal articular cartilage chondrocytes induced by osteoarthritic subchondral osteoblasts', *Arthritis & Rheumatism*, 62: 1349-60.

Prieto-Potin, I., R. Largo, J. A. Roman-Blas, G. Herrero-Beaumont, and D. A. Walsh. 2015. 'Characterization of multinucleated giant cells in synovium and subchondral bone in knee osteoarthritis and rheumatoid arthritis', *BMC musculoskeletal disorders*, 16: 226-26.

Pritzker, K. P., S. Gay, S. A. Jimenez, K. Ostergaard, J. P. Pelletier, P. A. Revell, D. Salter, and W. B. van den Berg. 2006. 'Osteoarthritis cartilage histopathology: grading and staging', *Osteoarthritis Cartilage*, 14: 13-29.

Radin, E. L., I. L. Paul, and M. J. Tolkoff. 1970. 'Subchondral bone changes in patients with early degenerative joint disease', *Arthritis Rheum*, 13: 400-5.

Rehm H., T. Letzel. 2006. 'Der Experimentator: Proteinbiochemie/Proteomics', *Spektrum Akademischer Verlag*, 37-113.

Reid, I. R. 2008. 'Effects of beta-blockers on fracture risk', *J Musculoskelet Neuronal Interact*, 8: 105-10.

Ribeiro-da-Silva, M., D. M. Vasconcelos, I. S. Alencastre, M. J. Oliveira, D. Linhares, N. Neves, G. Costa, R. Henrique, M. Lamghari, and C. J. Alves. 2018. 'Interplay between sympathetic nervous system and inflammation in aseptic loosening of hip joint replacement', *Sci Rep*, 8: 16044.

Roughley, P. J., Q. Nguyen, and J. S. Mort. 1991. 'Mechanisms of proteoglycan degradation in human articular cartilage', *J Rheumatol Suppl*, 27: 52-4.

Sambrook J., D.W. Russell.2000. 'Molecular cloning: a laboratory manual. 3 Volume ', Cold Spring Harbor Laborat.

Scanzello, C. R., and S. R. Goldring. 2012. 'The role of synovitis in osteoarthritis pathogenesis', *Bone*, 51: 249-57.

Schmitz S., 2011.'Der Experimentator: Zellkultur', *Spektrum akademischer Verlag.*

Sekiya, I., T. Muneta, M. Horie, and H. Koga. 2015. 'Arthroscopic Transplantation of Synovial Stem Cells Improves Clinical Outcomes in Knees With Cartilage Defects', *Clin Orthop Relat Res*, 473: 2316-26.

Sekiya, I., M. Ojima, S. Suzuki, M. Yamaga, M. Horie, H. Koga, K. Tsuji, K. Miyaguchi, S. Ogishima, H. Tanaka, and T. Muneta. 2012. 'Human mesenchymal stem cells in synovial fluid increase in the knee with degenerated cartilage and osteoarthritis', *J Orthop Res*, 30: 943-9.

Sellam, J., and F. Berenbaum. 2010. 'The role of synovitis in pathophysiology and clinical symptoms of osteoarthritis', *Nat Rev Rheumatol*, 6: 625-35.

Sepriano, A., J. A. Roman-Blas, R. D. Little, F. Pimentel-Santos, J. María Arribas, R. Largo, J. C. Branco, and G. Herrero-Beaumont. 2015. 'DXA in the assessment of subchondral bone mineral density in knee osteoarthritis—A semi-standardized protocol after systematic review', *Semin Arthritis Rheum*, 45: 275-83.

Shepherd, D. E. T., and B. B. Seedhom. 1999. 'Thickness of human articular cartilage in joints of the lower limb', *Ann Rheum Dis*, 58: 27.

Shlopov, B. V., G. N. Smith, Jr., A. A. Cole, and K. A. Hasty. 1999. 'Differential patterns of response to doxycycline and transforming growth factor beta1 in the down-regulation of collagenases in osteoarthritic and normal human chondrocytes', *Arthritis Rheum*, 42: 719-27.

Smith, M. D. 2011. 'The normal synovium', *Open Rheumatol J*, 5: 100-6.

Smith, M. D., S. Triantafillou, A. Parker, P. P. Youssef, and M. Coleman. 1997. 'Synovial membrane inflammation and cytokine production in patients with early osteoarthritis', *J Rheumatol*, 24: 365-71.

Spector, T. D., F. Cicuttini, J. Baker, J. Loughlin, and D. Hart. 1996. 'Genetic influences on osteoarthritis in women: a twin study', *Bmj*, 312: 940-3.

Speichert, S., N. Molotkov, K. El Bagdadi, A. Meurer, F. Zaucke, and Z. Jenei-Lanzl. 2019. 'Role of Norepinephrine in IL-1beta-Induced Chondrocyte Dedifferentiation under Physioxia', *Int J Mol Sci*, 20.

Stanton, L. A., T. M. Underhill, and F. Beier. 2003. 'MAP kinases in chondrocyte differentiation', *Dev Biol*, 263: 165-75.

Stoker, D. J. . 1980. *Anatomy of the knee joint* (Springer: Knee Arthrography).

Stöve, J., L. Lehmann, S. Fickert, T. Aigner, and R. Brenner. 2007. 'Artificial organs: a new option for treating osteoarthritis', *Curr Drug Deliv*, 4: 77-88.

Su, X., W. Zuo, Z. Wu, J. Chen, N. Wu, P. Ma, Z. Xia, C. Jiang, Z. Ye, S. Liu, J. Liu, G. Zhou, C. Wan, and G. Qiu. 2015. 'CD146 as a new marker for an increased chondroprogenitor cell sub-population in the later stages of osteoarthritis', *J Orthop Res*, 33: 84-91.

Suri, S., S. E. Gill, S. Massena de Camin, D. Wilson, D. F. McWilliams, and D. A. Walsh. 2007. 'Neurovascular invasion at the osteochondral junction and in osteophytes in osteoarthritis', *Ann Rheum Dis*, 66: 1423-8.

Swingler, T. E., J. G. Waters, R. K. Davidson, C. J. Pennington, X. S. Puente, C. Darrah, A. Cooper, S. T. Donell, G. R. Guile, W. Wang, and I. M. Clark. 2009. 'Degradome expression profiling in human articular cartilage', *Arthritis Res Ther*, 11: R96.

Takarada, T., H. Hojo, M. Iemata, K. Sahara, A. Kodama, N. Nakamura, E. Hinoi, and Y. Yoneda. 2009. 'Interference by adrenaline with chondrogenic differentiation through suppression of gene transactivation mediated by Sox9 family members', *Bone*, 45: 568-78.

Takeda, S., F. Elefteriou, R. Levasseur, X. Liu, L. Zhao, K. L. Parker, D. Armstrong, P. Ducy, and G. Karsenty. 2002. 'Leptin regulates bone formation via the sympathetic nervous system', *Cell*, 111: 305-17.

Tanamas, S. K., A. E. Wluka, J. P. Pelletier, J. Martel-Pelletier, F. Abram, Y. Wang, and F. M. Cicuttini. 2010. 'The association between subchondral bone cysts and tibial cartilage volume and risk of joint replacement in people with knee osteoarthritis: a longitudinal study', *Arthritis Res Ther*, 12: R58-R58.

Tavella, S., G. Bellese, P. Castagnola, I. Martin, D. Piccini, R. Doliana, A. Colombatti, R. Cancedda, and C. Tacchetti. 1997. 'Regulated expression of fibronectin, laminin and related integrin receptors during the early chondrocyte differentiation', *Journal of Cell Science*, 110: 2261-70.

Tetlow, L. C., D. J. Adlam, and D. E. Woolley. 2001. 'Matrix metalloproteinase and proinflammatory cytokine production by chondrocytes of human osteoarthritic cartilage: associations with degenerative changes', *Arthritis Rheum*, 44: 585-94.

Thoenen, H., and J. P. Tranzer. 1968. 'Chemical sympathectomy by selective destruction of adrenergic nerve endings with 6-Hydroxydopamine', *Naunyn Schmiedebergs Arch Exp Pathol Pharmakol*, 261: 271-88.

To, K., B. Zhang, K. Romain, C. Mak, and W. Khan. 2019. 'Synovium-Derived Mesenchymal Stem Cell Transplantation in Cartilage Regeneration: A PRISMA Review of in vivo Studies', *Front Bioeng Biotechnol*, 7.

Towbin H.,Staehelin T.,Gordon J. 1979. 'Electrophoretic transfer of proteins from polyacrylamide gels to nitrocellulose sheets: procedure and some applications ' *Proc Natl Acad Sci U S A,* 76(9):4350-4.

Tuan, R. S., A. F. Chen, and B. A. Klatt. 2013. 'Cartilage regeneration', *J Am Acad Orthop Surg*, 21: 303-11.

Tyurin-Kuzmin, P. A., D. T. Dyikanov, J. I. Fadeeva, V. Y. Sysoeva, and N. I. Kalinina. 2018. 'Flow cytometry analysis of adrenoceptors expression in human adipose-derived mesenchymal stem/stromal cells', *Sci Data*, 5: 180196.

Ulrich-Vinther, M., M. D. Maloney, E. M. Schwarz, R. Rosier, and R. J. O'Keefe. 2003. 'Articular cartilage biology', *J Am Acad Orthop Surg*, 11: 421-30.

Valdes, A. M., A. Abhishek, K. Muir, W. Zhang, R. A. Maciewicz, and M. Doherty. 2017. 'Association of Beta-Blocker Use With Less Prevalent Joint Pain and Lower Opioid Requirement in People With Osteoarthritis', *Arthritis Care Res (Hoboken)*, 69: 1076-81.

Venkatakrishnan, A. J., X. Deupi, G. Lebon, C. G. Tate, G. F. Schertler, and M. M. Babu. 2013. 'Molecular signatures of G-protein-coupled receptors', *Nature*, 494: 185.

Vos, T. et al. 2017. 'Global, regional, and national incidence, prevalence, and years lived with disability for 328 diseases and injuries for 195 countries, 1990-2016: a systematic analysis for the Global Burden of Disease Study 2016', *The Lancet*, 390: 1211-59.

Watari, T., K. Naito, K. Sakamoto, H. Kurosawa, I. Nagaoka, and K. Kaneko. 2011. 'Evaluation of the effect of oxidative stress on articular cartilage in spontaneously osteoarthritic STR/OrtCrlj mice by measuring the biomarkers for oxidative stress and type II collagen degradation/synthesis', *Exp Ther Med*, 2: 245-50.

Wenham, C. Y., and P. G. Conaghan. 2010. 'The role of synovitis in osteoarthritis', *Ther Adv Musculoskelet Dis*, 2: 349-59.

Wolfstadt, J. I., B. J. Cole, D. J. Ogilvie-Harris, S. Viswanathan, and J. Chahal. 2015. 'Current concepts: the role of mesenchymal stem cells in the management of knee osteoarthritis', *Sports health*, 7: 38-44.

Wuelling, M., and A. Vortkamp. 2011. 'Chondrocyte proliferation and differentiation', *Endocr Dev*, 21: 1-11.

Yamamoto, K., T. Okano, W. Miyagawa, R. Visse, Y. Shitomi, S. Santamaria, J. Dudhia, L. Troeberg, D. K. Strickland, S. Hirohata, and H. Nagase. 2016. 'MMP-13 is constitutively produced in human chondrocytes and co-endocytosed with ADAMTS-5 and TIMP-3 by the endocytic receptor LRP1', *Matrix biology : journal of the International Society for Matrix Biology*, 56: 57-73.

Yamamoto, T., and K. Ishihara. 1994. 'Stability of Glutathione in Solution.' in Toshimasa Yano, Ryuichi Matsuno and Kozo Nakamura (eds.), *Developments in Food Engineering: Proceedings of the 6th International Congress on Engineering and Food* (Springer US: Boston, MA).

Yang, X., J. Zheng, Y. Xiong, H. Shen, L. Sun, Y. Huang, C. Sun, Y. Li, and J. He. 2010. 'Beta-2 adrenergic receptor mediated ERK activation is regulated by interaction with MAGI-3', *FEBS Lett*, 584: 2207-12.

Yirmiya, R., I. Goshen, A. Bajayo, T. Kreisel, S. Feldman, J. Tam, V. Trembovler, V. Csernus, E. Shohami, and I. Bab. 2006. 'Depression induces bone loss through stimulation of the sympathetic nervous system', *Proc Natl Acad Sci U S A*, 103: 16876-81.

Yoon, Y. M., C. Oh, D. Y. Kim, Yun-Sil Lee, J. Park, T. Huh, Shin-Sung Kang, and J. Chun. 2000. 'Epidermal growth factor negatively regulates chondrogenesis of mesenchymal cells by modulating the protein kinase C-α, Erk-1, and p38 MAPK signaling pathways', *J Biol Chem*, 275: 12353-9.

Yuan, X. L., H. Y. Meng, Y. C. Wang, J. Peng, Q. Y. Guo, A. Y. Wang, and S. B. Lu. 2014. 'Bone-cartilage interface crosstalk in osteoarthritis: potential pathways and future therapeutic strategies', *Osteoarthritis Cartilage*, 22: 1077-89.

Zare, R., N. Tanideh, B. Nikahval, M. S. Mirtalebi, N. Ahmadi, S. Zarea, O. K. Hosseinabadi, R. Bhimani, and S. Ashkani-Esfahani. 2020. 'Are Stem Cells Derived from Synovium and Fat Pad Able to Treat Induced Knee Osteoarthritis in Rats?', *International Journal of Rheumatology*, 2020: 9610261.

Zhen, E. Y., I. J. Brittain, D. A. Laska, P. G. Mitchell, E. U. Sumer, M. A. Karsdal, and K. L. Duffin. 2008. 'Characterization of metalloprotease cleavage products of human articular cartilage', *Arthritis Rheum*, 58: 2420-31.

Zheng, C. H., and M. E. Levenston. 2015. 'Fact versus artifact: avoiding erroneous estimates of sulfated glycosaminoglycan content using the dimethylmethylene blue colorimetric assay for tissue-engineered constructs', *Eur Cell Mater*, 29: 224-36; discussion 36.

Zhou, L., C. K. Kwoh, D. Ran, E. L. Ashbeck, and W. H. Lo-Ciganic. 2020. 'Lack of evidence that beta blocker use reduces knee pain, areas of joint pain, or analgesic use among individuals with symptomatic knee osteoarthritis', *Osteoarthritis Cartilage*, 28: 53-61.

7 Danksagung

An dieser Stelle möchte ich mich herzlich bei all den Menschen bedanken, die mir mit Rat und Tat zur Seite standen und zum Gelingen dieser Arbeit beigetragen haben.

An erster Stelle möchte ich mich bei Zsuzsa Jenei-Lanzl bedanken für das entgegengebrachte Vertrauen und die Unterstützung bei der Bearbeitung dieses hochinteressanten Forschungsthemas. Vielen Dank für die Ratschläge und auch für die stets offene Tür bei Fragen.

Weiterhin möchte ich mich bei Prof. Frank Zaucke für die Bearbeitung dieses Themas in seiner Forschungsgruppe bedanken. Ich danke ihm für seinen Einfallsreichtum und seiner Unterstützung. Vielen Dank für die hervorragenden Arbeitsbedingungen.

Besonderer Dank gilt meinem Doktorvater Prof. Enrico Schleiff, dessen Bemühungen und Unterstützung weit über das übliche Maß hinaus gingen. Vielen Dank für die hervorragende und bedeutende Betreuung, die besonderen wissenschaftlichen Diskussionen die in hohem Maße die Weiterentwicklung meines Themas ermöglicht haben.

Ein ganz besonderer Dank gilt Frau Prof. Meurer, die sie sich dazu bereit erklärt hat, als Zweitgutachterin meiner Doktorarbeit zu fungieren. Vielen Dank für die Unterstützung, der interessanten Forschungstreffen und Diskussionen.

Danke auch an meine Kooperationspartnern, Shahed Taheri und Birgit Striegl, für die Durchführung der Micro-CT Messungen sowie der Arbeitsgruppe von Frau Prof. Grässel für die Mithilfe bei der Tierzucht und der Tieroperationen. Ebenso bedanke ich mich bei Dr. Christoph Dorn und der Arbeitsgruppe von Prof. Dr. Rainer H. Straub für die Durchführung der HPLC-Messungen. Danken möchte ich auch meinem Lektor Dr. Kavi Devraj, der sich bereit erklärt hat diese Dissertation zu prüfen.

Danke an alle Kollegen und Freunde, die immer an mich geglaubt haben. Besonderer Dank gilt Liudmila Leppik, die mich in schwierigen Zeiten nicht nur fachlich, sondern auch mental gestärkt hat. Danken möchte ich auch Khyati Keswani für die abwechslungsreichen und aufbauenden Kaffeepausen, ihrer fachlichen Unterstützung im Labor und ihrer Freundschaft.

An wichtigster Stelle möchte ich mich bei meinen Eltern bedanken, für ihre unermüdliche Unterstützung während meines Studiums und der Promotion. Ich danke Ihnen für Ihre wertvolle Liebe und der Ermutigung zum Weitergehen dieses Bildungsweges und das Vertrauen in mir. Ihre enorme Unterstützung und Fürsorge haben mir immer geholfen Rückschläge zu überwinden und die Welt außerhalb des Labors zu schätzen.

Vielen Dank an meine Schwestern Fatiha, Sanaa, Samya, Saliha und Najat, die immer ein offenes Ohr für mich hatten und die mir stets mit Rat und Tat zur Seite standen.

Ein ganz besonderer Dank gilt meinem liebevollen Ehemann Nabil für seine Geduld und Liebe in den anstrengenden Zeiten. Du hast die ein oder andere schlechte Laune ausgehalten, gabst mir Motivation und hast mich immer wieder aufgebaut. Ich konnte mich immer auf Dich verlassen.

8 Erklärung

Erklärung Ich erkläre hiermit, dass ich mich bisher keiner Doktorprüfung im Mathematisch-Naturwissenschaftlichen Bereich unterzogen habe.

Frankfurt am Main, den..... .....
Karima El Bagdadi

9 Versicherung

Versicherung Ich erkläre hiermit, dass ich die vorgelegte Dissertation über

„Sympathetic Influences on Articular Cartilage Regeneration Capacity and Osteoarthritis Manifestation"

selbständig angefertigt und mich anderer Hilfsmittel als der in ihr angegebenen nicht bedient habe, insbesondere, dass alle Entlehnungen aus anderen Schriften mit Angabe der betreffenden Schrift gekennzeichnet sind.

Ich versichere, die Grundsätze der guten wissenschaftlichen Praxis beachtet, und nicht die Hilfe einer kommerziellen Promotionsvermittlung in Anspruch genommen zu haben.

Frankfurt am Main, den..... .....
Karima El Bagdadi